PCI-based Targeted Therapy for Treatment Resistant Sarcoma

Abriel Czachorowski

Master's thesis

Department of Biosciences

The Faculty of Mathematics and Natural Sciences

UNIVERSITY OF OSLO

June 2019

PCI-based Targeted Therapy for Treatment Resistant Sarcoma

Abriel Czachorowski

Supervisors

Dr. Anette Weyergang

Dr. Susanne Lorenz

and professor Winnie Eskild

Department of Radiation Biology

Institute for Cancer Research – The Norwegian Radium Hospital

Oslo University Hospital

2019

PCI-based targeted therapy for treatment resistant sarcoma

Abriel Czachorowski

http://www.duo.uio.no/

Print: Reprosentralen, University of Oslo

Abstract

Sarcomas arise in patients of all ages and account for approximately 1% of new cancer diagnoses in Norway and the United States. Osteosarcoma is a subtype of sarcoma that typically affects children and adolescents and accounts for 8.9% of cancer-related deaths in children worldwide. Even though osteosarcoma is relatively rare, the low 5-year survival rate of 60-70% and the occurrence in children is the reason why novel approaches are necessary for this aggressive disease. Surgery and chemotherapy are the two main treatments for patients and ionizing radiation is included as an adjuvant with the attempt to control local recurrence as well as metastases, which is the major cause of mortality. Osteosarcomas frequently exhibit numerous mutations and aneuploidies which contribute to the aggression of the disease. Intrinsic or treatment-acquired resistance to chemotherapy and ionizing radiation is common in osteosarcoma patients and this contributes to the pressing need of developing novel therapeutic approaches for this disease.

The present project evaluated photochemical internalization (PCI), a method for intracellular drug delivery, as an approach to osteosarcoma treatment. The project included patient derived osteosarcoma cell lines, OSA and MG-63, which were subjected to numerous rounds of chemotherapy and radiation in order to generate resistant forms. Ionizing radiation-resistant cell lines, OSA/IR and MG-63/IR, were generated by biweekly exposure of 7.5 Gy for 2.5 weeks and 5 Gy for 2 weeks, respectively. One doxorubicin-resistant cell line, MG-63/DR, was established by continuous exposure to 0.5 µM doxorubicin for 3 weeks. MG-63/IR and MG-63/DR were both found moderately resistant to ionizing radiation and doxorubicin, respectively, when compared to the parental cells. No ionizing radiation-resistance was, however, obtained in the OSA/IR cell line. RNA sequencing was applied to the nontreated parental cells as well as the resistant cells. The sequencing data was assessed to evaluate mechanisms of resistance as well as possible targets for therapy to be used alongside PCI. Overall, the RNA sequencing indicated the resistant cell lines to be more aggressive compared to the parental cell lines. Western blotting confirmed that both parental cell lines highly expressed the epidermal growth factor receptor (EGFR). An EGFR-targeted toxin, EGF/rGel/rGel, was therefore tested on the cell lines in combination with PCI. A strong treatment response of PCI-EGF/rGel/rGel was observed in all parental and resistant cell lines, in contrast to PCI-rGel, indicating PCI-EGF/rGel/rGel as a promising treatment approach for EGFR expressing, treatment resistant osteosarcoma.

Acknowledgements

The work presented in this thesis was carried out at the Department of Radiation Biology, Institute for Cancer Research at the Norwegian Radium Hospital, Oslo University Hospital in the time period of January 2018 to June 2019. This is a thesis for the master's degree in Molecular Biology at the Department of Biosciences, Faculty of Mathematics and Natural Sciences, University of Oslo. This chapter of my life, my education and my career has been demanding, inspiring and enriching. I have learned so much, both personally and scientifically. Numerous individuals have helped and supported me throughout this period.

First and foremost, I would like to wholeheartedly thank my supervisors Anette Weyergang and Susanne Lorenz. Anette for being a great role model and for her patience, compassion, extensive knowledge and helpful guidance in every moment. You are the definition of an excellent supervisor and thank you for giving me this opportunity. Susanne for teaching me to look at biology in a different light and to further develop my scientific background. Special thanks to Ane Sofie Viset Fremstedal for her patience with me during training, her uplifting presence and always being there for me if I needed help in the laboratory. I would also like to thank Ane Longva for teaching me so many valid skills in the laboratory and for her constantly kind demeanor. Also, to Maria Elisabeth Brandal Berstad for her warm guidance and for supplying me with her "miracle drug", EGF/rGel/rGel.

My sincere thanks go to everyone in the PCI group for creating an exceedingly supportive and welcoming working environment. Also, to everyone in the Department of Radiation Biology for always being friendly, patient and helpful. I would like to thank the other students in the department that I have met for always providing encouragement or guidance if necessary.

My good friends Eoin, Steph and Amanda for the constant support, reassurance and for making me laugh when I truly needed it. A very special thank you to my mom, my dad, Morgan and Eirik for the constant love and support in everything I do. Without you all, I would not be where I am today, and I owe all my success to you.

I would like to dedicate this thesis in memoriam of my Uncle Tony, who unfortunately passed away during this thesis in April 2018. He was my role model and taught me how to live and love life to the fullest. He encouraged me to go into the science field and would have been very proud of this accomplishment.

Oslo, June 2019

Table of Contents

Abbreviations

$^1O_2$	singlet oxygen
CBX5	chromobox protein homolog 5
cDNA	complementary DNA
CSCs	cancer stem cells
ddH_2O	double distilled water
DMSO	dimethyl sulfoxide
DSBs	double stranded breaks in DNA
EGF	epidermal growth factor
EGFR	epidermal growth factor receptor
EGFR/rGel/rGel	EGF genetically fused to two molecules of recombinant gelonin
FBS	fetal bovine serum
gDNA	genomic DNA
gy	gray (standard unit of ionizing radiation)
HIF1A	hypoxia inducible factor 1 alpha
HR	homologous recombination
IR	ionizing radiation
LD_{50}	lethal dose at 50% viability
LD_{95}	lethal dose reducing 95% viability
MDR	multidrug resistance
NGS	next-generation sequencing
NHEJ	non-homologous end joining
O_2	molecular oxygen
PBS	phosphate buffered saline
PCI	photochemical internalization
PDT	photodynamic therapy
PFA	paraformaldehyde
P-gp	P-glycoprotein 1 / multidrug resistance protein 1
PS	photosensitizer
RB	retinoblastoma gene
rGel	recombinant gelonin
RIPA	radioimmunoprecipitation assay buffer
RIPs	type I ribosome-inactivating proteins
RNA seq	RNA sequencing
ROS	reactive oxygen species
RT	room temperature
RTase	reverse transcriptase
RTK	receptor tyrosine kinase
SDS-PAGE	sodium dodecyl sulfate-polyacrylamide gel electrophoresis
SSBs	single stranded breaks in DNA
TGFB1	transforming growth factor beta 1
$TPCS_{2a}$	meso-tetraphenyl chlorin disulfonate (Amphinex®)
VEGFA	vascular endothelial growth factor A

1. Introduction:

1.1 Sarcoma:

Sarcoma is a heterogeneous group of malignancies that originates in connective tissue including fibrous tissue, bone, cartilage and striated muscle [1]. There are approximately 15,000 new sarcoma cases arising every year in the United States [2] and 138 new cases every year in Norway [3], and these account for about 1% of new cancer diagnoses in these countries [4]. Sarcomas may be divided into two extensive groups dependent on how they arise: (1) translocation associated sarcomas and (2) sarcomas with highly aberrant and complex genomes [4]. The former involves mutations of tumor suppressors and occurs most frequent in young adults and children [4]. The latter is associated with accumulation of several mutations and aberrations and is usually seen in mid-adulthood between 50 and 60 years of age [4]. Furthermore, sarcomas may also be divided into two main groups dependent on where they arise; osteosarcoma and soft tissue sarcoma. The present studies have been focusing on osteosarcoma.

1.1.1 WHAT IS OSTEOSARCOMA?

Osteosarcoma originates in tissue that produces osteoid [5]. It is usually found in the metaphyseal regions of long bones (Figure 1) like the distal femur, proximal tibia, and proximal humerus [5]. Osteosarcoma typically affects children and adolescents (10-25 years), but it can also appear in late adulthood [5]. The rapid cell division in these long bones during growth has been associated with the predominance of osteosarcomas in children and adolescents [6]. Osteosarcoma is a rare type of cancer with an incidence of 4.8 cases per million people worldwide per year [6]. It is, however, the third most common cancer found in children and adolescents and it accounts for 8.9% of cancer-related deaths in children worldwide [6]. Presently, there is an overall 5-year survival rate of 60-70% for osteosarcoma patients in the United States [6, 7].

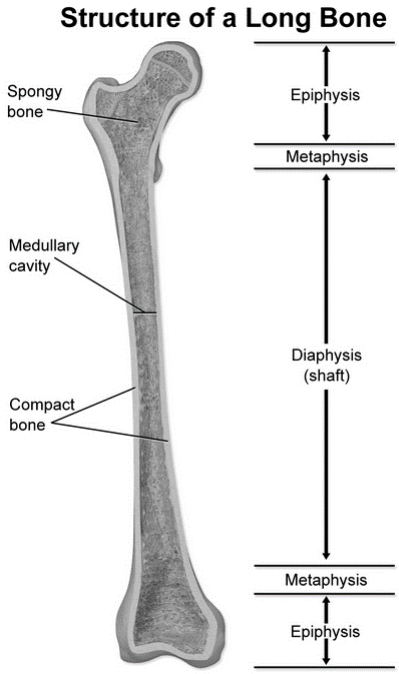

Figure 1: The structure of a long bone. Retrieved from https://en.wikipedia.org/wiki/Metaphysis.

There are currently three main histologic subtypes of osteosarcomas dependent on the matrix in which the cancer has arose: osteoblastic, fibroblastic and chondroblastic [6]. Studies have shown that patients diagnosed with the osteoblastic or chondroblastic subtype suffer from poorer prognosis compared to the fibroblastic subtype [6].

Independent on subtype, most osteosarcomas exhibit aneuploidies, in which the cells have an abnormal number of chromosomes [5]. Structural chromosomal abnormalities are, in addition, a result of their highly unstable genome [8]. The most common chromosomal alterations in osteosarcoma involve amplifications of the chromosomes 6p21, 8q24 and 12q14 [6]. Several osteosarcomas are due to mutations of tumor suppressor genes [5], such as the retinoblastoma gene (RB gene) which function is to control the transition from the G_0- to G_1/S phase of the cell cycle. Thus, people with inherited retinoblastoma have a 500 times increased risk of developing osteosarcoma [5]. Mutations in the tumor suppressor p53 have also been associated with increased risk of sarcoma, such as in Li-Fraumeni syndrome. P53, which is responsible for controlling the progression of the cell cycle when the DNA is damaged, is found mutated in 50% of all cancers and 22% of osteosarcomas [6].

1.1.2 Past and present treatments for osteosarcoma

During the 1900s, amputation was the predominant treatment for osteosarcoma despite the lack of inadequate conditions, equipment, and techniques [5]. The development of roentgenograms (X-ray images) during the 1900s was a huge improvement for surgeons in diagnosing and amputation of the cancerous limb [5]. In the 1930s, Dallas Phemister invented allografts and bone grafts which were used with the attempt to save the cancerous limb [5]. Also, during this time, there were further advances in orthopedic methods for the treatment of osteosarcoma including surgical implants. These advantages had, however, little effect on overall survival of osteosarcoma patients [5]. A significant improvement came 40 years later, in the 1970s, when chemotherapy was invented [5]. Chemotherapy became the main treatment for osteosarcoma patients and it caused a massive increase in patient survival rates from 30% to 70% [5]. Still to this day, combinations of different chemotherapies and surgery are considered the two standard treatments for osteosarcoma. Within the past few decades, surgical techniques have become more advanced and improved, and amputations are to a large extent replaced by limb preservation surgery [5]. The prognosis for patients with metastasis, however, are still low with a 5-year survival between 20 and 40% [5]. Although chemotherapy and surgery have been successful for some patients with metastatic disease, the prognosis for this patient group is no longer increasing. Novel therapeutic modalities are therefore still highly warranted for osteosarcoma, especially in cases with advanced disease.

1.2 Chemotherapy

Chemotherapy has become first line treatment for many types of cancer, including osteosarcoma. Chemotherapy covers a broad class of drugs with different chemical structures and mechanism of action, which are administrated to kill the parenchymal cancer cells during cell growth and division. Chemotherapy exerts cancer selectivity through its higher efficacy in fast dividing cells, one of the hallmarks of cancer [9]. Chemotherapeutic drugs kill cancer cells by using one or a combination of the following means: necrosis, activation of the host immune response, inhibition of proliferation in tumor cells and induction of apoptosis [10]. Furthermore, these drugs can be categorized into alkylating agents, antimetabolites, antitumor antibiotics, topoisomerase inhibitors, mitotic inhibitors, corticosteroids, hormones and antagonists, and many more [10]. Adverse effects caused by the targeting of normal cells, such as hair loss, fatigue, nausea and vomiting, anemia, infertility, and nervous

system problems, are however a recognized limitation for chemotherapy [11]. Chemotherapy is usually administrated as a systemic treatment and is used in the treatment of metastatic disease including osteosarcoma. The most frequently used chemotherapeutic drugs in osteosarcomas are high-dose methotrexate, doxorubicin, cisplatin, ifosfamide, vincristine, bleomycin and cyclophosphamide [5, 12]. The present studies focus on doxorubicin as a drug of choice for osteosarcoma treatment.

1.2.1 DOXORUBICIN

Doxorubicin (Figure 2) is one of the most commonly used chemotherapeutic drugs to treat osteosarcoma. It belongs to the anthracycline class of drugs which refers to chemotherapeutic drugs isolated from *Streptomyces* bacterium [13] and doxorubicin, specifically, is harvested from a modified strain of *Streptomyces peucetius* [14]. Doxorubicin has been on the market for four decades and has been used in the treatment of breast, lung, gastric, ovarian, thyroid, lymphomas, multiple myeloma and many more cancers [13]. Cardiotoxicity is recognized as the most severe side effect by doxorubicin [13]. Other adverse effects include nausea, vomiting, gastrointestinal problems, alopecia, neurological disturbances and bone marrow aplasia [15].

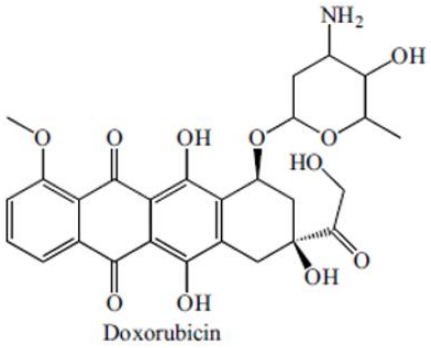

Figure 2: Structure of doxorubicin, an anthracycline isolated from *Streptomyces peucetius*.

Like all anthracyclines, doxorubicin has two main mechanisms of toxicity. First, doxorubicin embeds itself in DNA where it disturbs the function of the topoisomerase-II protein. This protein functions to eliminate supercoiling during replication and transcription, create double stranded breaks during recombination and organize tangled DNA during mitosis [16]. When topoisomerase-II is disturbed by doxorubicin, the cells cannot perform these necessary tasks, and this leads to growth arrest and subsequent cell death [14]. The second mechanism of toxicity involves the development of free radicals which harm the cell's membrane, proteins and DNA [13]. In short, reactive oxygen species (ROS) are formed when doxorubicin enters the mitochondria and becomes oxidized to semiquinone which is quickly converted back into doxorubicin [13]. This buildup of ROS causes lipid peroxidation which leads to collapse of the cell membrane, damage of the DNA and oxidative stress [13]. These instances all signal apoptosis to occur in the cells [13]. A more detailed description of doxorubicin's mechanism of action is displayed in Figure 3.

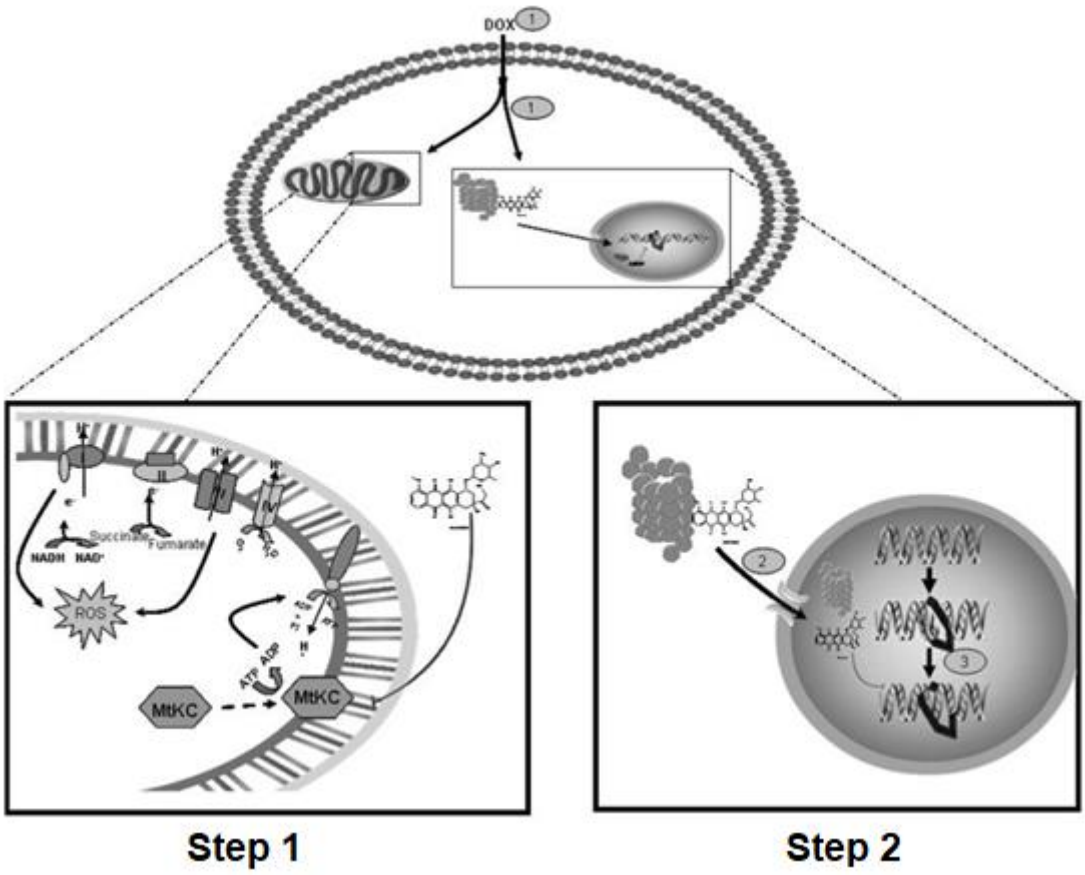

Figure 3: Doxorubicin enters the cell by passive diffusion through the cell membrane. It then binds to the proteosome with high affinity (Step 1). Doxorubicin binds to the 20S proteasomal subunit and forms a complex that moves towards the nucleus and enters the nuclear pores (Step 2). Inside the nucleolus, doxorubicin binds DNA and inhibits topoisomerase-II function (Step 3). In addition to its effect in the nucleolus, doxorubicin can also access the mitochondria where it binds to cardiolipin and this event prevents the mitochondrial creatine kinase (MtCK) protein from binding to the membrane of the mitochondria. MtCK provides the ATP necessary to catalyze creatine into phosphocreatine which is an important energy storage molecule involved in oxidative phosphorylation. Instead of phosphocreatine, doxorubicin is cycled by complex I of the mitochondrial respiratory chain and this causes a buildup of ROS in the mitochondria. Modified from [15].

1.3 Radiation therapy

Radiation therapy is one of the cornerstones of cancer treatment and more than 50% of solid cancers worldwide, undergo radiation therapy as part of their treatment plan [17, 18]. Radiation therapy is often an alternative for chemotherapy-resistant solid tumors and for solid tumors not accessible by surgical removal [19]. In sarcoma patients, radiation therapy can be used both before or after surgery and the modality has been shown to decrease the frequency of amputations [20]. Radiation therapy is often prescribed alongside chemotherapy and the combination may result in a synergistic effect where the cancer cells become more sensitive to both treatments [18, 19]. As compared to chemotherapy, radiation therapy is more selective as it is directed specifically towards the tumor [19]. The adverse effects of radiation therapy are highly dependent on the localization of the tumor, but includes skin

reactions, fatigue, decreased heart and lung function, infertility, nervous system dysfunction and increased risk of developing new cancer [17]. High doses of radiation therapy have been indicated as the main environmental factor for the development of secondary osteosarcoma [5]. Radiation-induced secondary cancer is likely caused by treatment induced mutations in normal cells [21]. Radiation therapy usually refers to ionizing radiation including X-rays, gamma rays, alpha particles and beta particles which all consist of wavelengths less than 10^{-11} meters [22].

For therapy, ionizing radiation (IR) can be given internally via alpha and beta particles injected into the body or externally via X-rays and gamma rays directed to the cancerous tissue [23]. The energy of ionizing radiation is enough to liberate electrons from atoms which then form ions [23]. DNA is the main intracellular target of radiation therapy. DNA may be damaged directly by the formation of single and double stranded breaks or indirectly via the production of free radicals [17]. These free radicals form ROS which can lead to crosslinking, depolymerization and base modification, damage and ejection [17].

The introduction of DNA damage employed by ionizing radiation initiates a variety of repair mechanisms. These repair mechanisms are mainly initiated during the two checkpoints within the cell cycle, the G_1 restriction point and the G_2 checkpoint [17]. These checkpoints function to ensure that DNA damage is repaired before the cell can replicate and divide. When a cell reaches a checkpoint, the DNA is sensed and scanned for damage. If damage is detected, the cell cycle pauses and repair proteins are recruited to the damage site. If the damage is successfully repaired, the cell is released to proceed through the cell cycle. If the damage cannot be repaired, the cell is destined for death, and this is the main mechanism of radiation therapy. However, these repair mechanisms are not completely error-proof and sometimes the cell cycle progresses, even when there is damage present. This leads to mutations in the DNA that become permanent and are carried on through cell division to be passed down to cell progeny [17]. In short, failed DNA repair can issue apoptosis or continuous growth where mutations are accumulated [19]. A schematic map of this process as well as an illustration of the cell cycle is displayed in Figure 4.

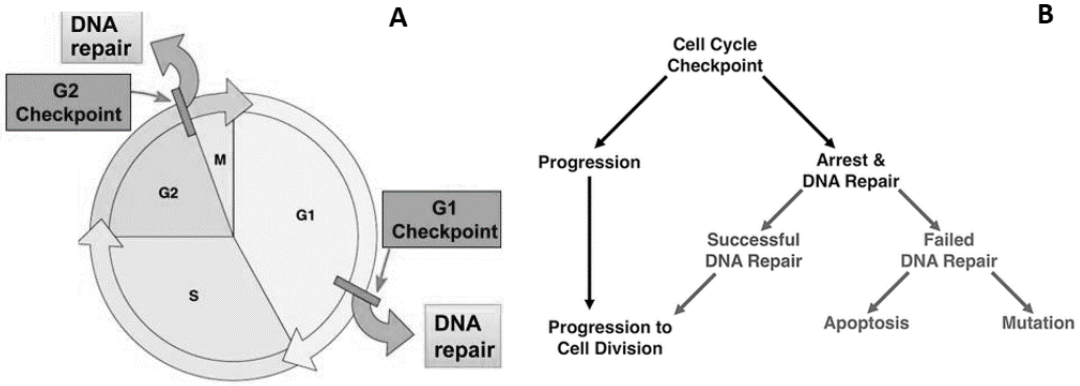

Figure 4A: The cell cycle including the synthesis (S) and mitotic (M) phases in addition to the G_1 and G_2 checkpoints. **4B:** Possible outcomes after entering a cell cycle checkpoint. The cell is released for cell cycle progression if no DNA damage is detected. In case of damage, the cell is arrested, and repair mechanisms are activated. Successful repair releases the cell to proceed with the cell cycle. Failed repair is a signal to initiate apoptosis. Cells may, however, progress into the cell cycle with gained mutations. Retrieved from [24].

Ionizing radiation can directly damage DNA by producing single or double stranded breaks. There are special series of repair mechanisms that are initiated when these breaks are detected in the DNA. They involve the recruitment of specific proteins to the break site that all work together to repair the damage including ATM and RAD3-related kinase (ATR), which is recruited in the presence of single stranded

breaks, and ataxia telangiectasia mutated kinase (ATM), which is recruited in the presence of double stranded breaks [17, 25]. Several proteins are simultaneously recruited and facilitate the complete activation of ATR kinase and ATM kinase [26]. Specifically, ATR kinase forms a complex with (1) replication protein A (RPA), (2) cell cycle checkpoint protein Rad17, (3) Rad9, Hus1 and Rad1 (9-1-1 complex) and (4) DNA topoisomerase 2-binding protein 1 (TopBP1) [26]. ATM kinase associates with the MRN complex, which consists of Mre11, Rad50 and Nbs1 proteins [26].

Double stranded breaks in the DNA are the most toxic effect generated by ionizing radiation and they can be repaired either by homologous recombination (HR) or non-homologous end joining (NHEJ) [19]. The choice between which mechanism is related to the cell cycle phase in which the damage occurred. NHEJ may be initiated in all phases of the cell cycle, while HR generally operates in S and G_2 [19]. HR involves the exchange of DNA sequences located on homologous chromosomes where the damaged DNA sequence is replaced with an intact, complementary sequence [19]. NHEJ is a process that directly pieces together the broken DNA strands [19]. HR is more accurate than NHEJ since identical DNA sequences are exchanged, whereas NHEJ can lead to errors due to the accidental loss of genetic material from the damaged ends of DNA [19]. However, it is assumed that NHEJ is the more frequently occurring pathway since most damage is detected during the G_1 phase [19]. A more detailed illustration of the DNA damage response upon ionizing radiation is outlined in Figure 5.

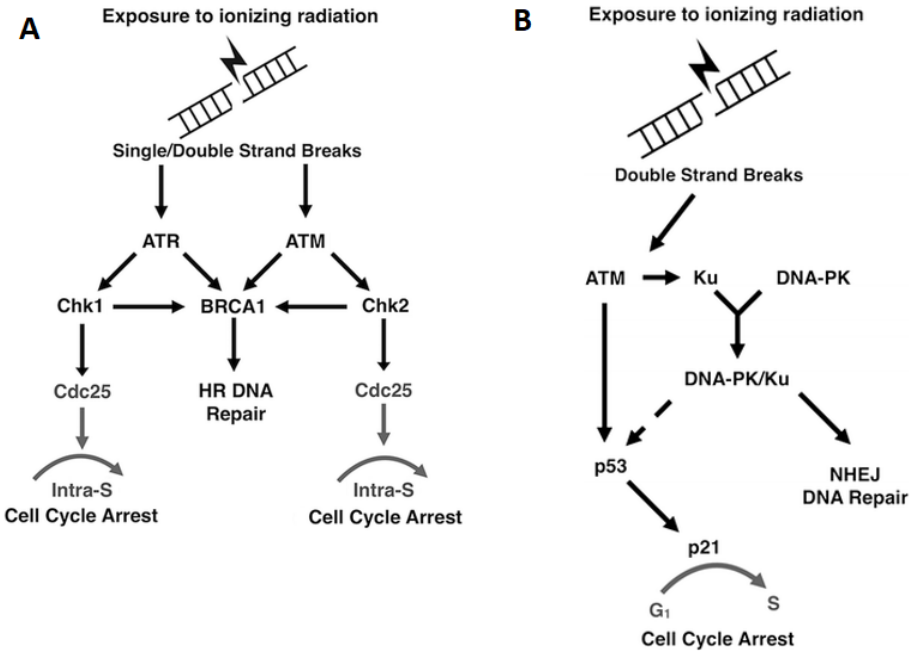

Figure 5: Mechanisms of the DNA damage response
A: The pathway of homologous recombination. Once a break in sensed in the DNA, ATR kinase (SSBs) and ATM kinase (DSBs) are activated. ATR and ATM phosphorylate Chk1 and Chk2 which signal intra-S cell cycle arrest via activation of Cdc25. BRCA1, a tumor suppressor, is also phosphorylated by ATM/ATR kinase and this protein initiates homologous recombination. Retrieved from [17].
B: The pathway of non-homologous end joining. Once a DSB is recognized, ATM kinase is activated and phosphorylates p53 and Ku. Ku becomes activated and recruits DNA-PK to the break site. These two form a complex and initiate non-homologous end joining by making the broken ends more easily accessible by other enzymes. The DNA-PK/Ku complex also plays a role in the initiation of the p53- and p21- pathways which leads to cell cycle arrest at the G1/S checkpoint. Retrieved from [17].

1.4 Photodynamic therapy

Photodynamic therapy (PDT) is a treatment modality for both cancerous and benign diseases. PDT involves a photosensitizer, light at the appropriate wavelength and oxygen which together produce a photochemical reaction which generates reactive oxygen species [27]. Singlet oxygen ($^1O_2$) is indicated as the most important ROS generated by PDT [28]. The reactive oxygen species formed initiates a cascade of oxidation reactions which eventually lead to cell death, mainly through apoptosis or necrosis [27]. The anticancer properties of PDT may be divided in three: direct cytotoxicity towards tumor cells, damage of the tumor vasculature and activation of anticancer immunity (Figure 6) [27].

PDT is comprised of 2 steps: distribution of a photosensitizer and irradiation of the tumor with light in the visible part of the specter. Photosensitizers are light-sensitive molecules that selectively accumulate in cancerous tissues prior to light exposure [27]. PDT has mainly been recognized as a local treatment, since the light exposure is localized to the tumor site. In the last decades, advances in PDT-induced anticancer immunity has, however, indicated PDT as a systemic treatment which might be efficient also in metastatic disease [27]. PDT can be prescribed either before or after surgery, chemotherapy or radiation therapy without weakening the effect of any of these treatments [27]. Another advantage of PDT is the profile of adverse effects which is better than observed for chemotherapy or radiation therapy [27]. Common side effects of PDT are light sensitivity, pain and inflammation in the treated area [29].

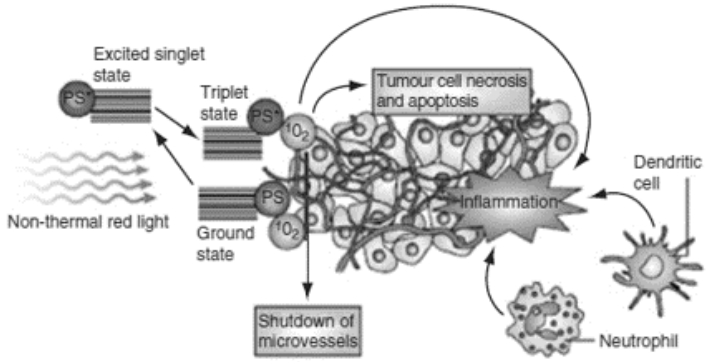

Figure 6: Antitumor properties of PDT. Singlet oxygen ($^1O_2$) is generated through a photochemical reaction. Cancer cells are targeted directly by induction of apoptosis and necrosis. The tumor cells are also targeted indirectly by damage of the tumor vasculature and by the activation of antitumor immunity. Retrieved from [30].

1.4.1 PHOTOSENSITIZER AND LIGHT CHARACTERISTICS

The photosensitizers used in PDT can be divided into three groups: porphyrins, chlorins and other dyes [31]. All these structural types allow for the acceptance of light energy to generate a triplet-state electron [31]. Most photosensitizers have a tetrapyrrole structure which contain four pyrrole rings [27]. The most successful photosensitizers are pure compounds that are easily cleared from the body, cheap to produce and have good storing capabilities [27]. The intracellular distribution of a photosensitizer is highly dependent on its physiochemical characteristics and different photosensitizers may accumulate in different cellular organelles [31].

Photosensitizers are activated at a specific wavelength of light dependent on the photosensitizer [31]. In cancer therapy, light absorption at 600-800 nm is usually preferred. Light at longer wavelengths do not have the energy to form the singlet oxygen, while light at shorter wavelengths cannot penetrate sufficiently through tissue [27].

1.4.2 PHOTODYNAMIC REACTION

At ground state, photosensitizers are at a stable state with 2 electrons at opposite spin in a preferred molecular orbital. When light is absorbed, one of the electrons is transferred to an orbital with higher energy and the photosensitizer is excited. The photosensitizer then has two possible fates: either it can emit the additional energy as heat or fluorescence or it can form a more stable triplet state [27]. The photosensitizer in triplet state can further react with molecular oxygen (O_2) through a type II reaction producing the highly reactive $^1O_2$. The photosensitizer in triplet state may also react through a type I reaction with another photosensitizer in triplet state or another substrate to produce other ROS [27]. A schematic illustration of the activation of a photosensitizer and subsequent photochemical reactions are included in Figure 7.

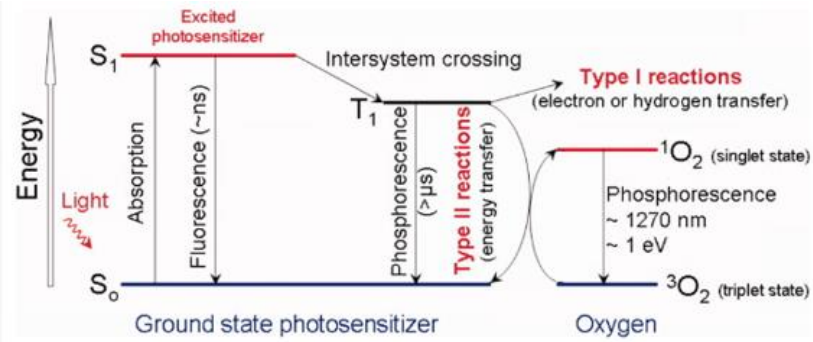

Figure 7: The figure illustrates a simplified Jablonski diagram. The photosensitizer absorbs light and is transferred from its ground state (S_0) to an excited singlet state (S_1). The photosensitizer then may emit the excess energy as fluorescence or it can go through intersystem crossing where it forms an excited triplet state (T_1). The photosensitizer in the triplet state can decay back to the ground state via phosphorescence or it can transfer its energy to O_2 in a type II reaction forming singlet state oxygen ($^1O_2$). Another option is the type I reaction in which the photosensitizer reacts with another photosensitizer or an organic molecule to generate other ROS. Retrieved from [27].

1.5 Photochemical internalization

Photochemical internalization (PCI) is a modality for intracellular release of membrane-impermeable therapeutic drugs entrapped in vesicles [32-34]. It is based on the foundations of photodynamic therapy where photosensitizers, light and oxygen are combined to create reactive oxygen species which allows for destabilization of the endo/lysosomal membrane. Specifically, the therapeutic drug/compound concentrates alongside a photosensitizer in endocytic vesicles. Light exposure activates the photosensitizer which induces the formation of reactive oxygen species that destabilize the endosomal

and lysosomal membranes and the therapeutic drug of interest is released into the cytosol where it can reach its target (Figure 8) [32].

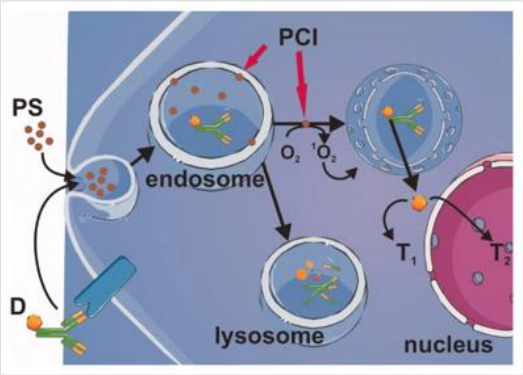

Figure 8: Principles of photochemical internalization. The photosensitizer (PS) and therapeutic drug (D) enter the cell through endocytosis since they cannot penetrate the plasma membrane. They eventually end up in endosomes with the amphiphilic photosensitizer in the endosomal membrane and with the hydrophilic therapeutic drug in the lumen. Light exposure causes activation of the photosensitizer that leads to endocytic membrane destabilization and release of the therapeutic drug into the cytosol where it can reach its therapeutic target (T1 and T2). Retrieved from [27].

Several macromolecules with intracellular targets have high potency as cancer therapeutics but are lacking an efficient mechanism to enter through the plasma membrane (Figure 9). These compounds are endocytosed into the cell and end up in endocytic compartments before they are subjected to lysosomal degradation. Photochemical internalization combats this by damaging the endosomal membrane prior to lysosomal degradation of the therapeutic drug of interest [35]. The therapeutic compound can then be released into the cytosol and exert its effect [34, 35]. PCI has been shown to enhance the therapeutic effect of several different drugs. The ideal drug for PCI delivery should (1) be taken up only in cancer cells, (2) have an intracellular target, (3) not readily cross the plasma membrane, (4) use endocytosis to enter the cell, and (5) not leak from endocytic compartments without the aid of PCI [36]. Several types of macromolecules that meet these characteristics have been considered for PCI, including type I ribosome-inactivating proteins (RIPs), immunotoxins, gene-encoding plasmids, adenovirus, oligonucleotides and bleomycin [36, 37]. PCI is also a highly selective cancer treatment since the photosensitizer molecules are preferentially concentrated in tumor tissue and since light exposure is applied only to the cancerous regions [38]. Another advantage of PCI is that it is a minimally invasive procedure since singlet oxygen has a short lifespan and affects only a small surrounding cellular region (10-100 nm), so distant structures and molecules will be unaltered [39].

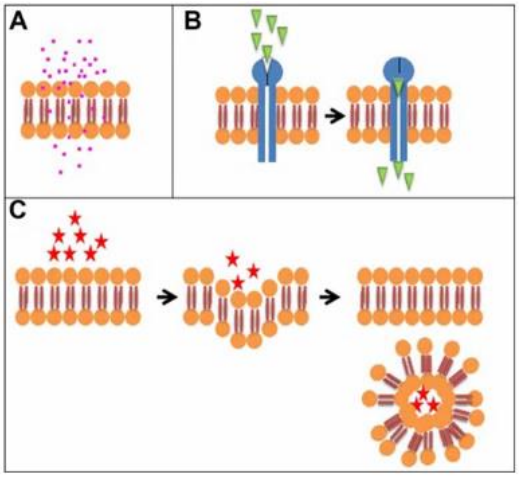

Figure 9: Cellular processes for drug uptake. The type of process the cell adopts to take up a molecule depends on the physiochemical characteristics of the compound. **A.** Passive diffusion (small and lipophilic molecules) **B.** Specific uptake channels (large and polar molecules—sugars, amino acids, ions) **C.** Endocytosis (very large and hydrophilic molecules). Retrieved from [36].

1.5.1 CHARACTERISTICS OF PCI-PHOTOSENSITIZERS

Photosensitizers used for photochemical internalization differ from those used in photodynamic therapy. Whereas photosensitizers used for tumor targeted PDT usually are lipophilic, the photosensitizers used in PCI are amphiphilic [40]. This is because the photosensitizers must be able to intercalate, not penetrate, the plasma membrane, and then localize in the membranes of endosomes or lysosomes [37]. PCI-photosensitizers therefore contain a hydrophilic region, usually composed of two sulfonate groups in cis position that prevents them from complete penetration [37]. The most commonly used photosensitizers in PCI are aluminum phthalocyanine disulfonate ($AlPcS_{2a}$), meso-tetraphenyl porphyrin disulfonate ($TPPS_{2a}$) and meso-tetraphenyl chlorin disulfonate ($TPCS_{2a}$) (Figure 10) [39, 40]. $TPCS_{2a}$, is approved for clinical trials on PCI and is the photosensitizer used in the present studies.

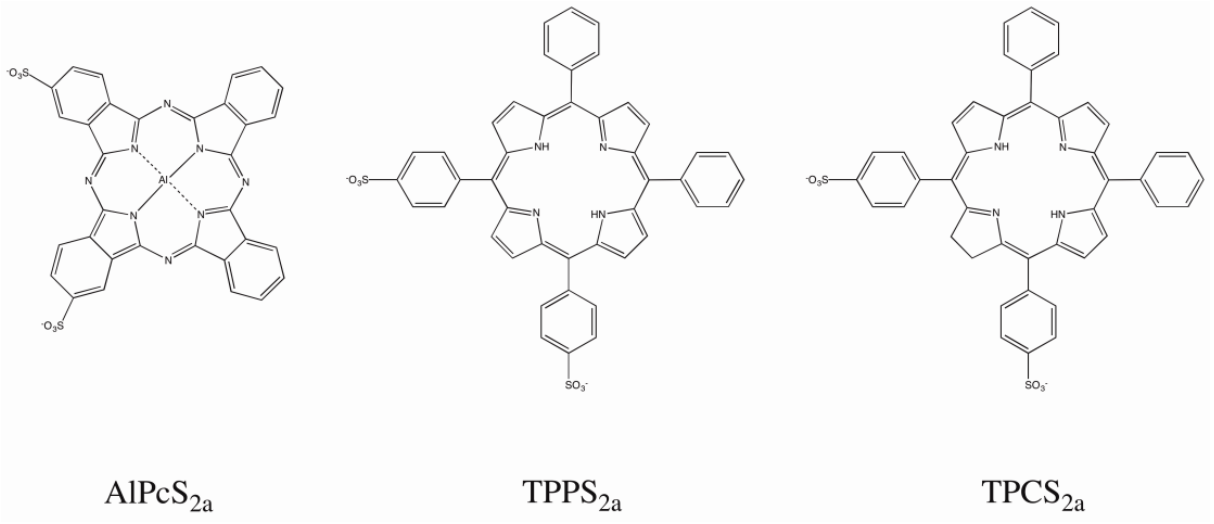

Figure 10: Chemical structures of common photosensitizers used in PCI. $AlPcS_{2a}$: aluminum phthalocyanine disulfonate, $TPPS_{2a}$: meso-tetraphenyl porphyrin disulfonate, $TPCS_{2a}$: meso-tetraphenyl chlorin disulfonate. Modified from [39, 41].

1.5.2 TYPE I RIBOSOME INACTIVATING TOXINS (RIPS)

RIPs are toxins isolated from plants such as *Ricinus communis*, *Gelonium multiflorum* and *Saponaria officinalis*. These toxins cause N-glycosidase activity of the 28S RNA unit of the 60s ribosome complex which leads to inhibition of protein synthesis and eventual cell death [36]. There are two types of RIPs: type I and type II. Type I RIPs contain a cytotoxic A-chain with N-glycosidase activity, whereas type II RIPs contain both the cytotoxic A-chain and a cell binding B-chain. Examples of type I RIPs are gelonin, agrostin and saporin and examples of type II RIPs are ricin, abrin and mistletoe lectin [36]. Both type I and type II RIPs have similar toxicity once inside the cell, but the type II RIPs have better cellular uptake due to their cell binding B chain [36]. Thus, type I RIPs are better suited for PCI since they are taken up by endocytosis and are to a large extent degraded in lysosomes. Type I RIPs are toxic only when they enter the cytoplasm and bind to the ribosome. Type I RIPs, therefore, exert little efficacy on their own, but when combined with PCI, they are highly effective [38]. Type I RIPs are also desirable for PCI since

they can be modified with cell binding moieties to form targeted protein toxins, where the cell binding moiety specifically recognizes cancer-related proteins expressed on the surface of target cells [36].

1.6 Treatment resistance in cancer:

Within the past few decades, the advancements in cancer research have vastly improved. The number of drugs invented, treatments established, and patients cured have greatly increased and we are, in general, coming closer to having a better understanding of cancer. However, despite all these developments in technology and knowledge, there are still some major challenges which limits treatment efficacy. One major problem is resistance and especially multidrug resistance (MDR), when a patient shows resistance to two or more different modes of cancer treatment [42]. Resistance may be divided in acquired resistance, which is developed during treatment, and intrinsic resistance, which is preexisting before treatment is initiated [42]. Resistance is found in all forms of cancer and is associated with drug-based treatments as well as radiotherapy [42].

1.6.1 Mechanisms of chemoresistance

Even though chemotherapy is frequently highly successful in treating cancer, treatment limiting adverse effects, as well as resistance, are major obstacles [10]. Patients undergoing chemotherapy for an extended period can also develop resistance to other types of treatment (cross resistance). Chemoresistance can be caused by several cellular mechanisms. One of these mechanisms are the expression of drug efflux pumps, such as multidrug resistance protein 1 or permeability glycoprotein (MDR1 or P-gp), multidrug resistance-associated protein 1 (MRP1) and breast cancer resistance protein (BCRP) (Figure 11). These pumps are transmembrane proteins which pump drugs from the cytosol into the extracellular environment and thereby prevent the drugs from exerting their intracellular action [10]. Several cytotoxic agents are substrates for these pumps including doxorubicin [10].

Another mechanism of chemoresistance includes enhanced DNA repair where chemotherapeutic drugs are ineffective due to overactive DNA repair proteins that prevent the cytotoxic drugs from harming the DNA (Section 1.3). Drug resistance may also be due to altered protein signal transduction, including irregular apoptosis and autophagy which prevent drug induced cell death [10].

Another mechanism of chemoresistance involves increased drug inactivation by phase I and phase II enzymes in the liver, intestines and tumor tissues [10]. Several anticancer drugs also require metabolic activation (prodrugs) and resistance may in these cases be caused by genetic mutations or inactivation of the metabolic enzymes responsible [10].

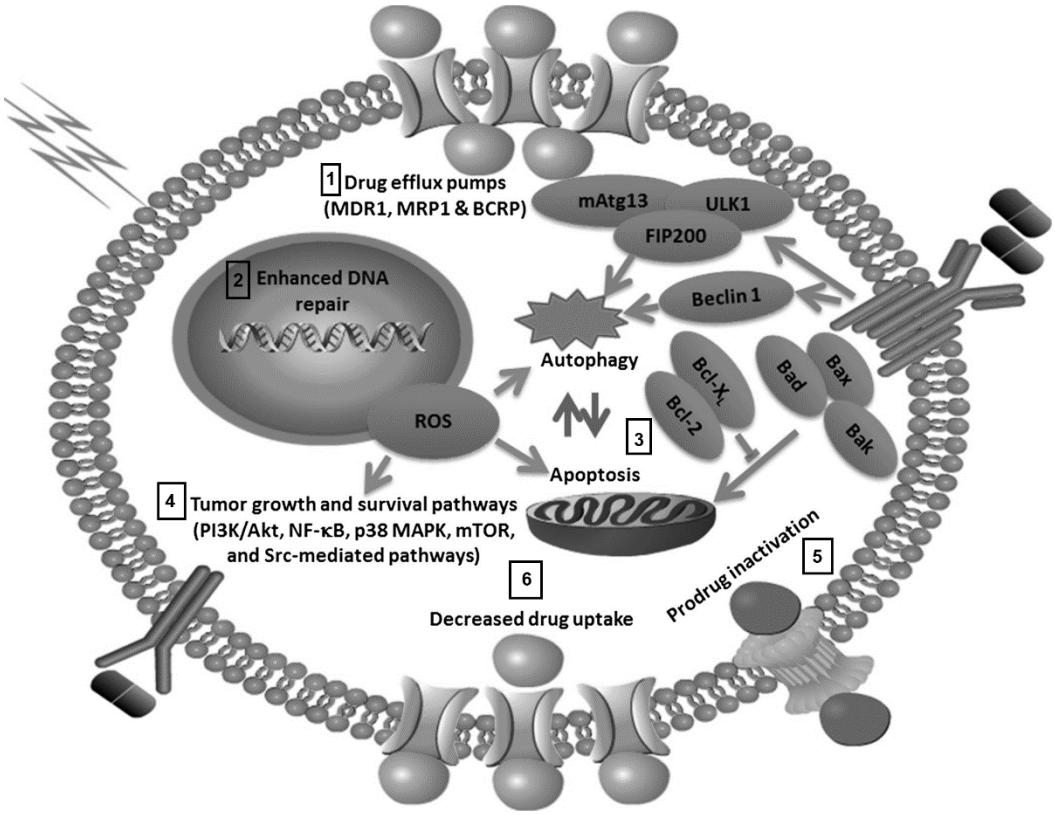

Figure 11: Mechanisms for chemoresistance. 1: drug efflux pumps, 2: enhanced DNA repair, 3: irregular apoptosis and autophagy, 4: tumor growth and survival pathways, 5: enhanced drug inactivation by phase I and II enzymes and 6: decreased drug uptake. Modified from [10].

With regards to doxorubicin, chemoresistance can be due to several mechanisms including overexpression of the ABCB1 and ABCC1 transporters and the amplification of the TOP2A gene [13]. Since doxorubicin inhibits the function of the topoisomerase-II enzyme, increased expression of topoisomerase-II may also decrease drug sensitivity [43]. Specifically, the effect of doxorubicin is dependent on the level of expression of topoisomerase-II where cells with increased expression of topoisomerase-II are more resistant to doxorubicin [43].

1.6.2 Mechanisms of radiation resistance

Radiation therapy is associated with intrinsic as well as acquired resistance. Radiotherapy resistance can be caused by several mechanisms including the adaptive pathway in which the tumor becomes resistant to high doses of radiation therapy after being exposed initially to low doses [23]. The adaptive pathway of resistance is related to ROS-induced activation of the NF-κB gene which transcribes anti-apoptotic proteins [23]. NF-κB activation also induces the production of antioxidant enzymes which further contribute to increased cell survival and reduced ionizing radiation sensitivity [23].

DNA damage repair pathways are also highly involved in radiotherapy resistance (Section 1.3). The DNA sensor DNA-dependent protein kinase (DNA-PK) promotes resistance by activation of transcription factors stimulating repair and survival. Another sensor, RAD51, is frequently overexpressed in tumor cells and facilitates the homologous recombination DSB repair pathway, contributing to IR resistance

[23]. Furthermore, RAD51 is controlled by p53 status since p53 negatively regulates RAD51 expression; so a defect in p53 would lead to RAD51 overexpression and thereby increased resistance to IR [23].

In addition, factors in the tumor surroundings, such as amount of oxygen, is of high importance for IR resistance. Hypoxic tumors, characterized by areas with low oxygen pressure, are resistant to IR [19, 23]. In well-oxygenated tumors, the free radicals induced by IR are easily formed with subsequent DNA damage. In hypoxic tumors, the formation of free radicals upon IR is inhibited by the lack of oxygen [19].

Another mechanism of IR resistance involves pathways that act through receptor tyrosine kinases (RTKs). Epidermal growth factor receptor (EGFR) is an RTK that is commonly overexpressed in many cancers and is responsible for cell proliferation, survival, invasion and angiogenesis [23]. EGFR stimulates cell survival events by activating the PI3K/Akt, STAT and Ras-Raf-MAPK pathways which all increase the cell's survivability following IR [23].

1.6.3 TUMOR HETEROGENEITY

Tumor heterogeneity is an important factor in chemotherapy and ionizing radiation-resistance. Most tumors consist of heterogenous cell populations with different sensitivity towards treatment. Relapse after treatment is therefore often likely caused by treatment resistant cell populations which survive the treatment and maintain the disease. The presence of cancer stem cells (CSCs) has also been indicated as an important reason for chemotherapy and radiation resistance. CSCs are defined as a small fraction of cancer cells which share many characteristics with normal stem cells as they can self-renew and repopulate. CSCs are thought to be treatment resistant and serve as a model on why a minor fraction of tumor cells surviving treatment can form the basis of a new tumor [44].

1.7 Targeted therapy

The treatment effect of both ionizing radiation and chemotherapy is often limited by adverse effects caused by damage to healthy cells [45]. The last decades have, however, provided a new genesis of cancer treatment with higher selectivity towards cancer cells referred to as targeted cancer therapy [45]. Targeted therapeutics are specifically designed to target unique proteins overexpressed on cancer cells [45]. Targeted cancer therapeutics may be divided in monoclonal antibodies, small molecule inhibitors and antibody linked cytotoxic compounds, including immunotoxins and antibody-drug conjugates [45]. Monoclonal antibodies act by inhibiting a specific receptor/enzyme and subsequent downstream signaling, in addition to stimulate immune-mediated cytotoxicity [45]. Immunotoxins and antibody-drug conjugates utilize an antibody to carry a toxin or chemotherapeutic drug into the cancer cell [45]. Small molecular inhibitors work intracellularly by inhibiting specific enzymes and receptors that contribute to cancer proliferation and growth [45].

1.7.1 Epidermal Growth Factor Receptor (EGFR)

Epidermal growth factor receptor (EGFR) is an RTK which refers to a group of cell surface receptors responsible for regulating several central events in the cell including growth, migration, metabolism, survival, proliferation and differentiation [46-48]. EGFR is a 170 kDa transmembrane glycoprotein expressed in many types of tissues [36, 47]. EGFR belongs to the ErbB family of RTKs which is divided into four subgroups: 1. EGFR (ErbB1, HER1), 2. ErbB2 (neu, HER2), 3. ErbB3 (HER3) and 4. ErbB4 (HER4) where human epidermal growth factor receptor (HER) is another common name for the receptors of this group [47, 49, 50]. All these receptors are structurally similar, and each contain an extracellular domain, a hydrophobic transmembrane domain and an intracellular domain with kinase activity (Figure 12) [36, 50].

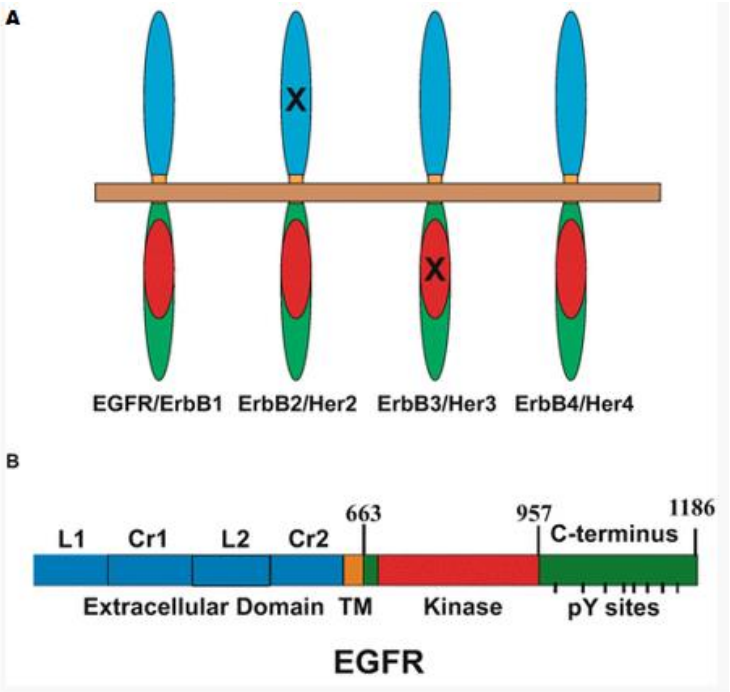

Figure 12: The ErbB family of receptor tyrosine kinases.
A. There are four types of ErbB receptors: EGFR/ErbB1/HER1, ErbB2/HER2, ErbB3/HER3 and ErbB4/HER4. There are no known ligands for ErbB2 and this receptor is argued to act as a co-receptor for other receptors in the ErbB family. ErbB3 has low kinase activity but functions as a co-receptor for other receptors in the ErbB family [74,75,76].
B. ErbB receptors contain an N-terminal extracellular domain, a single hydrophobic transmembrane helix (TM), an intracellular domain with tyrosine kinase activity and a C-terminal regulatory domain containing tyrosine residues. The extracellular domain is divided into 4 regions where L1 and L2 are ligand-binding regions while Cr1 and Cr2 are areas rich in cysteine residues that aid in receptor dimerization. The intracellular regulatory domain of the RTK is highly conserved in all 4 types of ErbB proteins. The extracellular ligand-binding domains are not conserved which allows each type to bind to different ligands Retrieved from [50, 51].

EGFR has been argued to play a large role in cancer development [46, 48, 49, 52]. Irregular expression or activity of these receptors and their associated proteins are related to cancer and shown to cause abnormal regulation of many cell processes [52, 53]. Specifically, EGF and EGFR are related to cancer development and metastasis in several ways: 1. Increasing cancer cell proliferation and migration through the Ras-ERK and PI3K-Akt pathways, 2. Localization of EGFR to the nucleus to increase cell proliferation, and 3. Activation of matrix metalloproteinases that promote cancer invasion and metastasis [47].

In many types of cancers, EGFR are found mutated or overexpressed [50]. Around 30% of solid tumors contain a gain-of-function mutation of EGFR, independent on the type of cancer [47]. The types of cancers which contain abnormal EGFR signaling include: breast (50-70%), lung (50-70%), colorectal (50-

70%), glioblastoma (37-58%) and sarcoma (16.9%) [51, 54]. Overexpression of EGFR has been related to poor prognosis including aggressive disease, metastasis and drug resistance [50, 51]. EGFR has been intensively studied as a target in cancer research and both monoclonal antibodies and small molecular inhibitors targeting EGFR have clinical approval for the treatment of cancer [51].

EGFR exerts endocytosis as a part of its mechanism of action (Figure 13). Upon activation, the receptor is internalized, via clathrin-mediated endocytosis, and subjected to endosomal trafficking prior to lysosomal degradation [51]. EGFR therefore has the ability to transport drugs into endo/lysosomal compartments which can be utilized in combination with PCI (Figure 13).

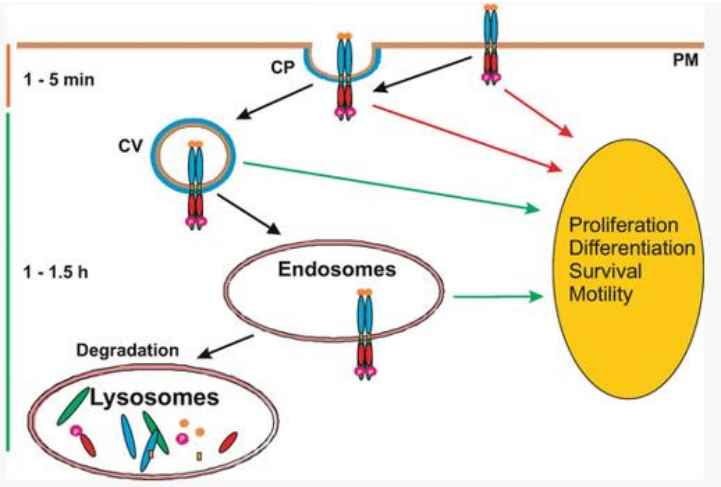

Figure 13: EGFR (blue/red receptor) is activated at the plasma membrane (PM) when it binds to EGF (orange spheres). After 1 to 5 minutes, the receptor is internalized in a clathrin-coated pit (CP) and ends up in a clathrin-coated vesicle (CV). EGFR continues to signal even while in endosomes for about 1 to 1.5 hours after it is endocytosed in the cell. EGFR signals until it is eventually degraded in lysosomes. Retrieved from [51].

2. Materials and methods

2.1 Cell lines and cultivation

The human osteosarcoma cell lines OSA (ATCC® CRL-2098™), also known as SJSA-1, and MG-63 (ATCC® CRL-1427™) were the two main cell lines used in the present studies. The human uterine sarcoma cell line MES-SA (ATCC® CRL-1976™) was used as a control cell line to compare the effects of the different treatments with the OSA and MG-63 cell lines. All cell lines were acquired from the American Type Culture Collection in Manassas, Virginia in the United States of America. The OSA and MG-63 cell lines are deficient in the p53 protein due to mutation or complete inactivation, respectively [55, 56]. The MES-SA cell line contains an intact p53 protein [57]. The OSA and MG-63 cell lines were grown in RPMI-1640 Medium #R8758 (Sigma-Aldrich, St. Louis, Mo., USA) as recommended by ATCC [55, 56], along with 100 IU/ml penicillin (Sigma-Aldrich), 100 µg/ml streptomycin (Sigma-Aldrich) and 10% fetal bovine serum (Thermo Fisher Scientific, Waltham, Wa, USA, Lot. No. 41G3930K) in a humidified incubator containing 5 % CO_2 at 37°C. The MES-SA cell lines were grown in McCoy's 5A Medium #M9309 (Sigma-Aldrich) supplied as described for RPMI-1640 above.

2.1.1 Establishment of ionizing radiation resistant cell lines

Ionizing radiation-resistant OSA and MG-63 were established as a part of the project. These cell lines will here be referred to as OSA/IR and MG-63/IR. Ionizing radiation was delivered by an X-ray generator (Faxitron CP160, Tucson, AZ, USA). The cells were grown in 75 cm^2 flasks (Nunclon™, Thermo Fisher Scientific) and irradiated twice a week with 7.5 Gy for OSA/IR and 5 Gy for MG-63/IR. The radiation dose was selected based on the 50% lethal dose (LD_{50}) in preliminary experiments. The treatment was continued 2.5 weeks for OSA/IR resulting in a total dose of 37.5 Gy and 2 weeks for MG-63/IR resulting in a total dose of 20 Gy. Parental untreated cells of both lines were grown alongside the ionizing radiation-treated cells and served as control cells during this project. The sensitivity of the OSA/IR and MG-63/IR to ionizing radiation was evaluated by the MTT assay (Section 2.4 (ionizing radiation) and Section 2.6.1 (MTT assay)).

2.1.2 Establishment of doxorubicin resistant cell lines

Doxorubicin-resistant cell lines of MG-63 were established as part of the project. This cell line will here be referred to as MG-63/DR. MG-63/DR was established by 3 weeks of continuous exposure to 0.5 µM doxorubicin. The doxorubicin dose was selected based on the 50% lethal dose (LD_{50}) in preliminary experiments. The cells were grown in 75 cm^2 flasks (Nunclon™, Thermo Fisher Scientific) and doxorubicin was added alongside the culture medium twice a week. Doxorubicin at a concentration of 2 mg/ml was purchased from Nycomed Pharma AS (Asker, Norway) and stored at -20 °C. The doxorubicin was aliquoted to prevent too many freeze-thaw cycles and each aliquot did not endure more than three freeze-thaw cycles. Parental untreated cells were grown alongside the doxorubicin-treated cells and served as control cells during this project. Determination of decreased sensitivity to doxorubicin was distinguished by the MTT assay (Procedure 2.6.1), where the parental cell lines and the

doxorubicin-resistant cell lines were exposed to increasing concentrations of doxorubicin. There were multiple attempts at making an OSA/DR cell line. Generation of OSA/DR cells was, however, not successful due to severe toxicity of continuous doxorubicin exposure to OSA/PAR cells.

2.2 Standard procedures

2.2.1 Subcultivation

All cell lines were grown in 75 cm^2 flasks and subcultured at 50-80% confluency. The cell passage numbers never exceeded passage 42. All cell lines were tested for mycoplasma before they were allowed into the cell lab. Both OSA, MG-63 and their variant cell lines were subcultured 2-3 times per week. The MES-SA cell line was subcultured 1-2 times per week. OSA/PAR cells were subcultured at a ratio between 1:5 and 1:15. OSA/IR cells were subcultured at a ratio between 1:3 and 1:9. MG-63/PAR cells were subcultured at a ratio between 1:4 and 1:12. MG-63/IR cells were subcultured at a ratio between 1:3 and 1:10. MG-63/DR cells were subcultured at a ratio between 1:3 and 1:10. MES-SA cells were subcultured at a ratio between 1:3 and 1:15. The split ratio of the resistant cells was regularly adjusted since their growth rate was slow during the first 2-3 weeks following treatment and then increased. All cell lines were closely monitored and never reached confluency.

Procedure:

1. Old culture medium was removed from the culture flask using vacuum suction
2. Cells were washed with 2 ml of 37° C phosphate buffered saline (PBS) without calcium or magnesium (Sigma-Aldrich, Cat. No. D8537) (This prepared the cells for trypsination by removing any leftover medium which inhibits trypsin activity).
3. 2-3 ml of 37° C trypsin-EDTA solution (Sigma-Aldrich, Cat. No. T3924) was added. (Trypsin is a protease that interacts with the cell-cell and cell-substratum interactions by cleaving peptide bonds. This action releases the cells from the bottom of the flask. The trypsin was allowed to work for 6-8 minutes while the culture flask was placed in an incubator at 37 °C).
4. The cells were observed under a microscope to determine if they detached from the flask. The flask was lightly tapped to detach all cells from the flask.
5. 7-8 ml of culture medium was added once the cells were detached to neutralize trypsin. A fraction of the cell suspension (split ratio) was moved to a new culture flask that contained 15 – 18 ml of 37° C fresh culture medium.

2.2.2 Cryopreservation

All cell lines were cryopreserved 1 month after the resistant cell lines were produced. Dimethyl sulfoxide (DMSO) was included in the freezing medium since it is a cryoprotectant that prevents ice crystal formation that can injure the cells and cause death.

Procedure:

1. The cells were trypsinated as explained in Section 2.2.1 and culture medium was added to neutralize the enzyme. The cells were centrifuged for 3 minutes at room temperature (RT) in order to pellet the cells.
2. The supernatant was cautiously removed and the freezing medium containing 50% fetal bovine serum, 40% culture medium and 10% DMSO from Sigma-Aldrich (Cat. No. D8418) was added slowly for 2 minutes while resuspending the pellet.
3. The cell suspension was transferred into cryogenic vials (Nunc® CryoTubes®, Sigma-Aldrich). The vials were placed inside the Mr. Frosty™ Freezing Container containing isopropanol (Sigma-Aldrich) which provides the vials with an optimal rate of cooling (-1°C/minute) for cell preservation.
4. Mr. Frosty™ was transferred to a -80°C freezer and left overnight.
5. The vials were then removed from the container and stored in a nitrogen freezer.

2.2.3 THAWING AND PROPAGATION OF CELLS

Procedure:

1. Cryogenic vials containing the cell line of interest were thawed in a water bath at 37°C for 1 minute.
2. 5 ml of prewarmed medium was added to the thawed cells and the cells were centrifuged for 3 minutes at RT.
3. The supernatant (containing the DMSO which is cytotoxic) was removed cautiously using vacuum suction and the cell pellet was resuspended in 5 ml culture medium.
4. The cell suspension was transferred to a 175 cm^2 culture flask with 40 ml of prewarmed culture medium. The cells were closely monitored the following days and the cells were subcultured when the cells were reaching 80% confluency. The cells were used for experiments following one week.

2.2.4 CELL COUNTING AND SEEDING

The number of cells in a suspension following trypsination was counted using Glasstic® Slides from KOVA (Cat. No. 87144/87144E, Garden Grove, CA, USA) that contain a hemocytometer counting grid. 10 µl of the cell suspension was added to the counting chamber. The grid contains nine squares where three squares that are aligned in a diagonal were counted and an average number of cells was calculated per square. The average was multiplied by 10^4 since the volume of one square in the grid is 0.1 µl. This number gave the number of cells/ml. The formula below was used to determine how many cells needed to be seeded out:

$$c1v1 = c2v2$$

Where:

c1: the initial number of cells/ml in the suspension
v1: the volume (ml) needed in the cell suspension
c2: the number of cells/ml needed for the whole experiment
v2: the volume (ml) needed for the whole experiment

The appropriate seeding density for PDT, PCI, ionizing radiation and chemotherapy experiments was based on the growth curves in Section 3.1 (Figure 17). These seeding densities were used to ensure that the cells did not become confluent and were growing in the log-phase throughout the duration of all experiments; the densities are displayed in Table 2 (Section 3.1). The difference in seeding densities per experiment was due to the size of the plates used; 96-well plates for PCI and chemotherapy experiments and 60 mm cell culture dishes for ionizing radiation.

2.3 PDT and PCI treatment of cells

2.3.1 LIGHT SOURCE AND PHOTOSENSITIZER

The photosensitizer $TPCS_{2a}$ (Amphinex®) was provided by PCI Biotech AS (Oslo, Norway) and stored at a concentration of 0.35 mg/ml in the refrigerator at 4 °C protected from light. All experiments involving $TPCS_{2a}$ were performed under subdued light. A LumiSource™ lamp (PCI Biotech AS) was used as the light source in PDT and PCI experiments. This lamp consists of 4 light tubes (Osram 18W/67) which emits blue light with a λmax = 435nm and a fluence rate of 11.7 mW/cm^2 [58]. The lamp was turned on 15-20 minutes before illumination to certify that the light strength was consistent over the duration of the experiments.

2.3.2 PDT AND PCI PROCEDURES

PDT and PCI experiments were accomplished in 96 well plates (Nunc 96 MicroWell® with Nunclon® Delta Surface, Thermo Fisher Scientific). Refer to Table 2 for seeding densities. After seeding, the cells were left in an incubator overnight for attachment to the substratum. Cells were then incubated with 0.35 µg/ml $TPCS_{2a}$ (photosensitizer) for 18 hours before they were washed once with drug free medium and incubated 3 hours with recombinant gelonin (rGel) (produced in the project group) or EGF/rGel/rGel (produced in the project group) at indicated concentrations. After 3 hours of drug incubation, the medium was replaced with drug free medium and the cells exposed to light using LumiSource at indicated light exposure times. Cell viability was measured with the MTT assay (Procedure 2.6.1) 48 hours post light exposure. A timeline of the PCI procedure is displayed in Figure 14.

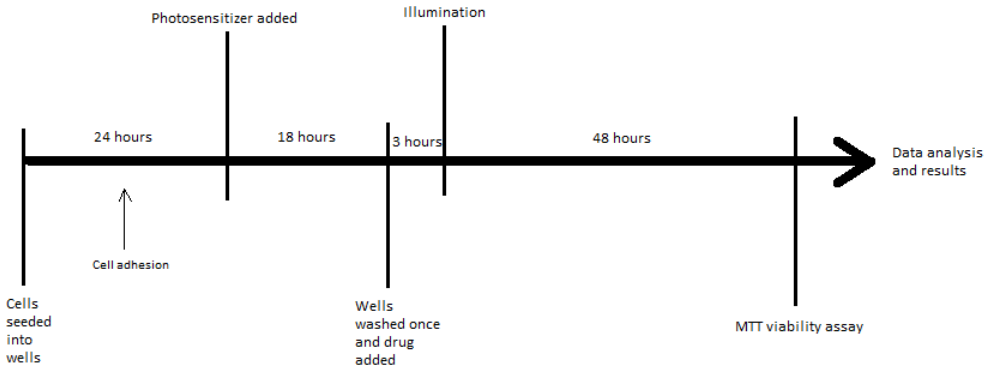

Figure 14: Timeline of a typical PCI experiment. Cells are seeded out and adhere overnight, incubated with photosensitizer for 18 hours, washed once and the drug of choice is added and incubated for 3 hours. The media is then replaced and cells are illuminated.

2.3.3 Calculation of PCI efficacy

Comparison of the quantitative effect between cell lines is often difficult due to differences in the sensitivity to PDT as well as the macromolecular drug. In cases where the cell lines display similar sensitivity towards the macromolecular drug, PCI efficacy may be assessed by the following formula:

$$\text{PCI efficacy} = \frac{LD_{50}\ (PDT)}{LD_{50}\ (PCI)}$$

where LD_{50} is the light dose, in seconds, which is responsible for killing 50% of the cells [40]. The LD_{95} can also be used to calculate PCI efficacy.

2.4 Ionizing radiation treatment of cells in culture

Cells were seeded out in Falcon ® 60 mm cell culture dishes (#353004, Corning Life Sciences, Tewksbury, MA, USA) and allowed to attach and grow overnight. Refer to Table 2 for seeding densities. The cells were irradiated 24 hours after seeding. The X-ray generator (Faxitron CP160, Tucson, AZ, USA) was used as the source of ionizing radiation in all experiments. All experiments included a nontreated control that was not given any radiation. The cell viability was assessed with the MTT assay (Procedure 2.6.1) 96 hours after irradiation treatment.

Procedure:

1. The 10-minute warm-up program was turned on for the radiation machine.
2. Culture medium was removed from the dishes using vacuum suction.

3. 2.5 ml of fresh culture medium was added to each dish.
4. Dishes were placed in the Faxitron X-ray and irradiated at selected dose. The default settings were 1 minute for 1 Gy of radiation.
5. After treatment, cells were incubated for 96 hours before the viability was measured with the MTT assay (Procedure 2.6.1).

2.5 Doxorubicin treatment of cells in culture

Chemotherapy was accomplished in 96 well plates (Nunc 96 MicroWell® with Nunclon® Delta Surface, Thermo Fisher Scientific). Refer to Table 2 for seeding densities. After seeding, the cells were incubated overnight for attachment. Doxorubicin at increasing concentrations was added and viability assessed with the MTT assay (Procedure 2.6.1) after 96 hours incubation after chemotherapy was given.

Procedure:

1. The cells were seeded in 96 well plates and left overnight for attachment.
2. The doxorubicin solutions at desired concentrations were prepared.
3. Old culture medium was removed from the plates using vacuum suction.
   100 µl of fresh culture media containing doxorubicin was added to each well.
4. Plates were incubated for 96 hours until cell viability was measured by the MTT assay (Procedure 2.6.1).

2.6 Cytotoxicity assays and viability measurements

2.6.1 THE MTT CELL VIABILITY ASSAY

The MTT (3-(4,5-dimethylthiazol-2-yl)-2,5-diphenyltetrazolium bromide) assay is a method for measurement of cell viability. The MTT reagent harbors a positive charge which allows it to enter living eukaryotic cells. Upon entering viable cells, the MTT reagent is reduced by enzymes in the mitochondria and this produces water-insoluble purple formazan crystals [59]. DMSO is added to solubilize the crystals and the intensity of the purple color is measured spectrophotometrically. MTT from Sigma-Aldrich (Cat. No. M2128) in powder-form was supplied and dissolved in PBS to create a stock solution (5 mg/ml) that was sterile filtered and stored in the refrigerator at 4 °C. The solution was also wrapped in aluminum foil to protect it from light. In all experiments, 3-4 hours of incubation with MTT (0.25 mg/ml in medium) was used on the cells; the cells were monitored closely and the MTT was removed before the cells started to detach. The cell viability was measured either 48 hours or 96 hours after treatment dependent on treatment procedure (48 hours for PDT and PCI experiments, 96 for doxorubicin and ionizing radiation experiments).

Procedure:

1. At the time of harvest, culture medium was removed from the wells using vacuum suction.
2. Media containing MTT at 0.25 mg/ml was added to the wells. MTT containing media was also added to empty wells to act as a blank.
3. The plate was incubated for 3-4 hours depending on the cell line. The plate was monitored carefully under the microscope to ensure that the cells did not detach, as well as determine if enough purple formazan crystals formed.
4. The media with MTT was removed carefully by vacuum suction to ensure that the crystals were not disturbed.
5. 100 µl of DMSO was added to each well, as well as the blank wells.
6. The plate was placed on a plate shaker (Titramax 101, Heidolph Instruments, Schwabach, Germany) for 5 minutes at 400 rpm to dissolve the crystals.
7. The plate was analyzed by PowerWave™XS2 Microplate Spectrophotometer (BioTek Instruments, Inc., Winooski, VT, USA) where the optical density was measured at 570 nm. The data was evaluated using Gen5™ Data Analysis Software (BioTek Instruments, Inc.) and Microsoft Excel.

2.6.2 CLONOGENIC ASSAY

The clonogenic assay is another way for determining cell viability. It tests the competence of a single cell to form a colony of at least 50 cells [60]. It is often used to test the efficacy of radiotherapy, but it is also used to evaluate the effect of other anticancer treatments [60, 61]. The cells were seeded at 100 and 250 cells in 6 well plates (#140675, Thermo Fisher Scientific) and incubated at 37° C for 2 weeks. The cells were then fixed with glutaraldehyde and stained with crystal violet dye. This method was attempted numerous times for both OSA/PAR and MG-63/PAR, but both cell lines were unable to form colonies. Therefore, this method was not suited for this project.

2.7 Assessment of cellular EGFR and p53 expression

Cellular EGFR and p53 expression were assessed in parental and resistant cell lines. Cellular expression of actin was used as a control.

2.7.1 CELL LYSIS AND HARVESTING

Cells were harvested by lysis from 75 cm^2 flasks which were 80% confluent. The cell lysates were distributed into 1.5 ml Eppendorf tubes and placed in a -80°C freezer for storage. Radioimmunoprecipitation assay buffer (RIPA) (1% Nonidet P-40, 0.5% sodium deocycholate, 0.1% SDS in PBS) was used as the base of the cell lysis buffer and was stored in 50 ml tubes in the refrigerator.

Immediately before cell harvesting, the full lysis buffer was prepared as followed:

- RIPA buffer (945 µl)
- Protease inhibitor cocktail P8340 (Sigma Aldrich) (10 µl)
- Phosphatase inhibitor cocktail I P2850 (Sigma Aldrich) (10 µl)
- Phosphatase inhibitor cocktail II P5726 (Sigma Aldrich) (10 µl)
- B-glycerol phosphate 2M in dH_2O (10 µl)
- Activated Na_2Vo_3 (sodium orthovanadate) 200 mM in sH_2O (5 µl)
- PMSF 200 mM in isopropanol (5 µl)
- NaF 200 mM in dH_2O (5 µl)

Procedure:

1. A Styrofoam ice box container was filled with crushed ice, sprayed down with 70 % ethanol and placed inside the lab bench.
2. Cell flasks were placed on ice inside the container.
3. Culture medium was removed using vacuum suction.
4. 2-3 ml of ice-cold PBS was added to the flasks. The flask was gently moved around to distribute the PBS evenly across the cell monolayer to wash the cells.
5. The PBS was removed from the flask using vacuum suction.
6. 0.5 ml of full lysis buffer was added to each flask. The flask was tilted and gently moved around to distribute the lysis buffer evenly across the cell monolayer every 60 seconds for 15 minutes.
7. After 15 minutes, a plastic cell scraper (#99002, Techno Plastic Products AG, Trasadingen, Switzerland) was used to collect the cell lysate. The scraper was vigorously pushed across the entire monolayer in order to collect the lysate.
8. The cell lysate was transferred to a 1.5 ml Eppendorf tube (# 72.690.001, Sarstedt AG & Co. KG, Nümbrecht, Germany).
9. The cell lysate was sonicated for 20 seconds in order to rupture DNA.
10. The cell lysate was vortexed, spun down and the supernatant was separated into 1.5 ml Eppendorf tubes containing 75 µl aliquots.
11. All aliquots were stored in a -80 °C freezer.

2.7.2 SDS-PAGE

Sodium dodecyl sulfate-polyacrylamide gel electrophoresis (SDS-PAGE) is used to separate proteins according to their molecular weight. SDS is a negatively charged detergent that binds to the protein through hydrophobic interactions and disrupts non-covalent bonds in the proteins, an event that denatures the protein. SDS also gives the proteins a negative charge which facilitates its separation in the electric field applied during gel electrophoresis. SDS-PAGE is an effective way of separating proteins from cell lysates and it can be followed up with western blot for further protein analysis.

The DC™ protein assay from Bio-Rad (#5000112, Oslo, Norway) was used to determine the protein concentration in each sample. Equal amounts of protein from each sample were then mixed with loading buffer and RIPA buffer prior to gel loading. Specifically, each well contained:

- 5 µl 5XRB loading buffer
- 20 µg cell lysate sample
- RIPA buffer to a final volume of 25 µl

Procedure:

1. Cell lysates were collected from the -80 °C freezer and thawed for 2-3 minutes at room temperature.
2. Eppendorf tubes (Sarstedt AG & Co. KG) were labeled with cell line/sample number.
3. 80 µg cell lysate sample was added to its assigned tube.
4. 20 µl of 5XRB loading buffer (Appendix A) was added to each tube.
5. RIPA buffer was added to each tube for a final volume of 100 µl.
6. All tubes were spun down for 30 seconds and boiled for 5 minutes at 95 °C in a benchtop sample boiler (QBT2, Grant Instruments, Cambridge, UK).
7. While the samples boiled, the SDS-PAGE gel was prepared (Mini-PROTEAN TGX Precast Gel 50 µl, #456-1084, Bio-Rad) and chamber was set up (Mini-PROTEAN 2D Electrophoresis Cell, #1652960, Bio-Rad).
8. The gel was inserted into the chamber so that the wells pointed inside the chamber. Plastic dummy gels were used in case of an odd number of gels.
9. Running buffer (Appendix A) was added to the chamber so that it completely covered the area between the gels, as well as the chamber itself according to whether 2 or 4 gels were being ran.
10. After boiling, all tubes were spun down again for 30 seconds.
11. Each well was washed with a pipette containing running buffer to remove any leftover polyacrylamide.
12. 5 µl of ladder was added to the outer wells. Two types of ladders were used; Precision Plus Protein™ Dual Color Standards #1610374 (Bio-Rad) and Amersham™ ECL™ Rainbow™ Marker Full Range RPN800E (Sigma-Aldrich).
13. 25 µl of the sample was added to each well and its position on the gel was noted.
14. The gel was ran at 180 V and 300 mA for 30-40 minutes.

2.7.3 Western blot

Immunostaining of western blots is a technique used to identify specific proteins from a complex mixture such as a cell lysate. Following SDS-PAGE, the proteins are transferred from the gel to membrane (western blotting) which is incubated with the primary and secondary antibodies of interest.

Procedure:

1. The Bio-Rad Trans Blot Turbo Transfer System (#1704150, Bio-Rad) was set up according to the manufacturer instructions.
2. A stack of filter paper was wet in transfer buffer (Appendix A) and placed on the bottom of the cassette. Air bubbles were carefully removed using a roller.
3. The PVDF membrane (Trans-Blot Turbo™ Mini PVDF Transfer Packs #1704156, Bio-Rad) was activated in ethanol and then equilibrated in transfer buffer. The membrane was then gently placed on top of the stack, ensuring that no damage or scratches on the membrane occurred at any time.
4. The gel, subjected to SDS-PAGE, was carefully removed from its casting frame and was placed on top of the membrane.
5. Another stack of transfer paper was wet in transfer buffer and placed on top of the stack. Air bubbles were carefully removed using a roller.
6. The cassette was sealed and placed inside the Trans Blot Turbo™.

7. The Mini size program was selected in the menus.

2.7.4 ANTIBODY INCUBATION

The primary antibodies used in this study were anti actin #A5060 produced in rabbit (Sigma Aldrich), anti EGFR #4267S produced in rabbit (Cell Signaling Technology, Leiden, The Netherlands) and anti p53 #9282S (Cell Signaling Technology) produced in rabbit. All these primary antibodies were monoclonal. The secondary antibody used was HRP linked #7074 anti-rabbit IgG from Cell Signaling Technology. The primary antibody binds to the target protein of interest, while the secondary antibody recognizes and binds to primary antibodies from the species where the primary antibody was produced. Fat free dry milk (5%) was used as the blocking agent. The blocking step reduces nonspecific binding of both primary and secondary antibodies to irrelevant proteins or to the membrane.

Primary antibody solutions:

- 5 µl anti actin, 5 ml fat free dry milk (5%) 1:1000 dilution
- 5 µl anti EGFR, 5 ml 5% BSA in TTBS 1:1000 dilution
- 5 µl anti p53, 5 ml 5% BSA in TTBS 1:1000 dilution

Secondary antibody solution:

- 15 µl anti rabbit, 15 ml fat free dry milk (5%) 1:1000 dilution

Procedure:

1. Membrane was removed from the western blot stack and placed in TTBS (Appendix A) to prevent drying out.
2. Membrane was carefully placed inside a 50 ml tube with the proteins facing inward, towards center of the tube.
3. Membrane was blocked in 5 ml of 5% fat free dry milk in TTBS for 1 hour at room temperature on a roller.
4. Primary antibody solutions were prepared according to the list above.
5. Membrane was incubated in 5 ml of the desired primary antibody solution overnight at 4 °C on a roller. If the membrane was to be incubated in BSA, the membrane was washed once with TTBS before the antibody solution was added.
6. The next day, the membranes were washed 3 times with 5 ml TTBS for 5 minutes at room temperature on a roller.
7. Secondary antibody solution was prepared according to the list above.
8. Membrane was incubated in 5 ml of the secondary antibody solution for 1 hour at room temperature on a roller.
9. The membrane was washed 3 times with 5 ml TTBS for 5 minutes at room temperature on a roller.
10. Membrane was left in TTBS to prevent drying out until protein detection.

2.7.5 PROTEIN BAND DETECTION

The SuperSignal™ West Dura Extended Duration Substrate kit (#34076) from Thermo Fisher Scientific was used for protein detection. The horseradish peroxidase (HRP)-labelled secondary antibody reacts with the HRP substrate and produces chemiluminescence that can be detected by a camera. The ChemiDoc™ XRS+ System (Bio-Rad) was used for band detection and quantification together with the ImageLab software (Bio-Rad).

Procedure:

1. Transparent copy paper was cut into appropriately sized squares.
2. 250 µl droplets of each detection solution were combined and mixed together on a piece of transparent paper. The paper was labeled with the antibody used, as well as the orientation of the membrane.
3. The membrane was placed protein side down on the transparent paper and moved around gently using tweezers, ensuring that the membrane was completely covered with the detection solution.
4. Membrane was incubated face down for 5 minutes at room temperature.
5. After incubation, the membrane was transferred protein side up to another piece of transparent paper.
6. An additional piece of transparent paper was placed on top of the membrane to make a sandwich and air bubbles were removed as needed. The orientation and antibody used was labeled once again.
7. Membrane was placed in a light-protected chamber until imaging.
8. The membrane was loaded into the ChemiDoc and imaged using 1-30 second exposure times. ImageLab software was used to examine the protein bands.

2.8 RNA isolation

RNA isolation is the process of extracting RNA from a biological sample. RNA isolation is a complicated procedure due to the presence of RNAse enzymes everywhere in the environment. Clean gloves, clean labcoat and a clean work area was maintained throughout the whole procedure to decrease the risk of contamination with RNAses. Samples were also placed on ice when not being handled to inhibit enzymatic degradation. The GenElute ™ Mammalian Total RNA Miniprep kit (Sigma Aldrich) was used for RNA isolation according to the description provided by the producer. OSA/PAR, OSA/IR, MG-63/PAR, MG-63/IR and MG-63/DR cells were seeded at 42,500 cells/well in 6-well plates one day before RNA isolation. All cell lines were 50% confluent the day after seeding. The following procedure was performed by Ane Longva in the PCI group with the student observing.

Procedure:

1. The lysis buffer (kit) was combined with β-mercaptoethanol at a ratio of 10 µl β-mercaptoethanol per 1 ml lysis buffer. B-mercaptoethanol was added in order to denature RNases by reducing disulfide bonds in the enzymes.
2. Culture medium was carefully removed using vacuum suction.

3. The cells were washed with 1 ml cold PBS. The plate was tilted to evenly distribute the PBS. PBS was carefully removed using vacuum suction.
4. 670 µl of lysis buffer+β-mercaptoethanol mix was added to each well. The solution was pipetted up and down several times. The lysis buffer breaks apart the cells so that all proteins, DNA and cell components are released.
5. The lysate (670 µl) in each well was transferred to a labeled 1.5 ml Eppendorf tube (if being stored frozen) or to a blue filtration column (supplied with the kit) (if being used for RNA-seq immediately).
6. The tube containing the blue filtration column was centrifuged for 2 minutes at 14000 rpm at room temperature. The filtration column binds to the cell membrane, cell debris and proteins. RNA and DNA flow through the column.
7. Column was discarded, and 670 µl of 70% ethanol was added to the tube.
8. The tube was vortexed and mixed with a pipette to evenly distribute the ethanol.
9. No more than 700 µl of the sample at a time was transferred to the red binding column (as to not overflow the column). The binding column selectively binds RNA via its poly-A tail.
10. The tube containing the red binding column was centrifuged for 15 seconds at 14000 rpm at RT.
11. Filtrate was discarded and the column placed back inside the tube.
12. Steps 9 and 10 were repeated until all the lysate was transferred through the red binding column.
13. 80 µl of the DNase I/Digest Buffer was added to the column and incubated for 15 minutes at RT. The DNases destroy all genomic DNA in the sample.
14. 500 µl of wash solution #1 was added to the column.
15. The tube was centrifuged for 15 seconds at 14000 rpm at room temperature.
16. Filtrate was discarded and the column was transferred to a new 2 ml tube.
17. 500 µl of wash solution #2 was added to the column.
18. The tube was centrifuged for 15 seconds at 14000 rpm at room temperature.
19. Filtrate was discarded and the column was placed back in the tube.
20. Steps 16-18 were repeated except the tube was centrifuged for 2 minutes in order to dry the column.
21. Centrifuge again for 15 seconds at 14000 rpm at room temperature to remove all of the wash solution.
22. Column was transferred to a new 2 ml tube and 50 µl elution solution was gently added to the middle of the column, ensuring that the pipette tip did not disturb the membrane. The elution solution elutes the RNA from the binding column so it can be isolated.
23. The tube was centrifuged for 1 minute at 14000 rpm at room temperature.
24. The tube containing the purified RNA was placed on ice and stored in the -20 °C freezer if being used for RNA-seq or in the 70 °C freezer if being stored for a prolonged period.

After the isolation, RNA quality was assessed using the Bioanalyzer (Agilent) to measure the RNA integrity number (RIN, 1-10). This number is calculated by comparing the detection signals from the 18S and 28S RNA fragments and background in a gel electrophoresis. The background increases with an increased amount of degraded RNA molecules, which would lead to a low RIN value. The RIN numbers indicate whether the RNA quality is sufficient for RNA sequencing.

2.9 RNA sequencing (RNA SEQ)

RNA sequencing (RNA seq) is a technology used to characterize and quantify the transcriptome of a cell [62, 63]. RNA seq has many functions: 1. Identifies all actively transcribed genes in a cell type or tissue, 2. Determines differential gene expression, 3. Identifies new transcripts, 4. Detects alternative splicing events, 5. Detects fusion transcripts, 6. Detects strand-specific measurements and 7. Analyzes any mutations or RNA editing [64]. RNA seq was here performed to evaluate expression changes in the resistant cell lines that could be utilized as molecular targets for PCI. The planned workflow in this part of the project is displayed in Figure 15.

2.9.1 SAMPLE PREPARATION

Messenger RNA (mRNA) is the type of RNA most frequently used in RNA seq as it is a coding protein to be synthesized. During sample preparation, mRNA is isolated using poly(T) oligomers that selectively hybridize with the poly-A tail of mRNA. RNA isolation was performed as described in Procedure 2.8. After the mRNA is isolated, the mRNAs are fragmented and complementary DNA (cDNA) is synthesized from the mRNA by reverse transcriptase (RTase) and DNA polymerases. This process involves random primers that anneal to the mRNA fragments that attract the RTase enzyme. The cDNA is created by the addition of deoxyuridine triphosphates (dUTPs) which contain the deoxyribose sugar instead of a ribose sugar to keep the strand information [65]. The newly established cDNA is then used in further sequencing protocols.

The paired end 2 x 76 basepair sequencing protocol was used. The software used for analysis was STAR (Aligner) Version STAR_2.5.0b, Cufflinks Version 2.2.1 and Cufflinks Assembly & DE (BaseSpace Workflow) Version 2.1.0. The RNA SEQ and analysis were done in collaboration with the Genomics Core Facility at Norwegian Radium Hospital.

2.9.2 ILLUMINA SEQUENCING

Illumina is a type of next-generation sequencing (NGS) that is considered a high-throughput method that efficiently sequences several nucleotides at high speed [66]. Illumina has made it possible to sequence complete genomes of various organisms in an affordable and convenient matter. The chemistry behind Illumina sequencing works in four steps: 1. Library preparation, 2. Cluster generation, 3. Sequencing and 4. Data analysis [66]. These steps and the detailed mechanism behind them are explained in Appendix B.

The differentially expressed genes found in each resistant cell line were further analyzed using bioinformatics tools, specifically the Ingenuity Pathway Analysis (IPA). IPA is a program that uses statistical gene-set enrichment analysis to identify pathways and biological functions correlated to the differentially expressed genes, in a way that is easier to interpret lists of genes in terms of biological systems. IPA was selected as the software of choice since it can simultaneously analyze both the upregulated and downregulated genes.

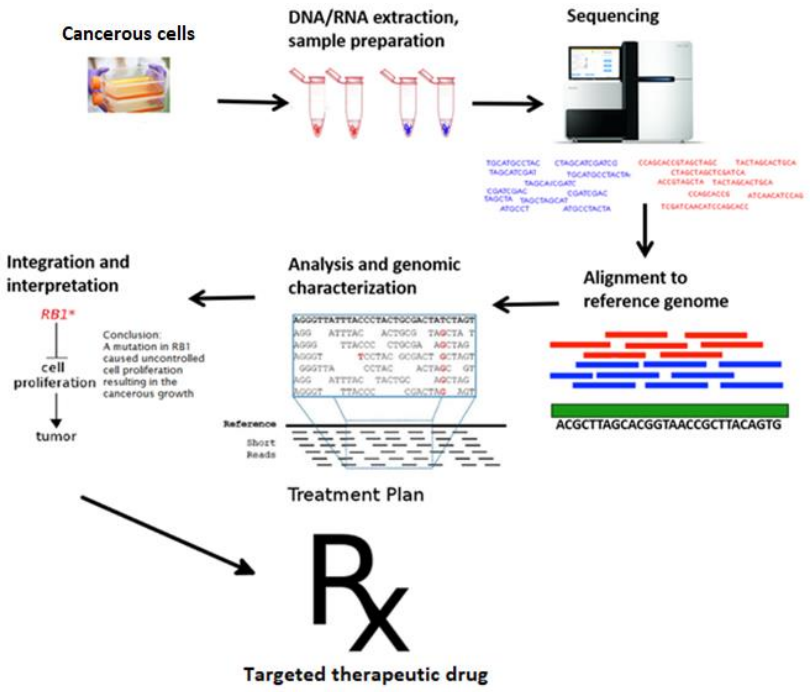

Figure 15: The planned workflow for the sequencing in this project. The cancerous cells were collected along with the normal cells for comparison. The samples are prepared where DNA is removed and mRNA is selectively isolated. The samples are sequenced and then analyzed, aligned and characterized using bioinformatic techniques. The results are interpreted, and conclusions are met to develop a treatment plan or find a molecular target for treatment. Modified from oslo.genomics.no.

2.10 Fluorescence detection

Fluorescence is the light emitted from a particle that has absorbed a photon [67]. Fluorophores are molecules that can absorb photons and emit fluorescence at different wavelengths depending on their chemical structure [67]. The fluorophore in its ground state absorbs energy, in the form of photons, and becomes excited. The energy can be released as a photon (fluorescence) at higher wavelength than the excitation wavelength. Fluorophores are used in several biological methods including flow cytometry and fluorescence microscopy applied in the present project.

2.10.1 Flow cytometry

Flow cytometry is a method that examines characteristics of a population of cells [68]. The flow cytometer is equipped with lasers that may be used to excite fluorescently-labeled cells which thereby emit light at various wavelengths also measured by the instrument [68]. There are three parts of the flow cytometer: the fluidics, the optics and the electronics. The fluidics function to carry the particles/cells within a stream of liquid to the laser. The optics consists of lasers that illuminate the particles/cells found in the stream. The particles scatter light from the laser which is detected by several lenses and filters that guide the light signals to detectors. The light signals are transformed into data

that can be read by a computer which presents information about the particles' light-scattering and fluorescent properties.

Flow cytometry was here applied to evaluate the level of non-specific endocytosis in OSA/PAR, OSA/IR, MG-63/PAR, MG-63/IR and MG-63/DR cell lines. The cells were seeded 350,000 cells/well in 6-well plates one day before flow cytometry. The cells were sub confluent on the day of flow cytometry to ensure the highest number of cells analyzed. Cellular uptake of Alexa488 labeled rGel (1.1 mg/ml, 30 kDa) (produced in the research group) was used as a measurement of non-specific endocytosis. Cells were incubated with fluorescent labeled rGel, at a concentration of 100 nM, for 4 hours before flow cytometry. Alexa488 labeled rGel was detected using a 488 nm laser for excitation with 20 mW laser power (Coherent, Santa Clara, CA, USA) and the 505 longpass and 530/30 bandpass filters for emission detection. The flow cytometer used was an LSR II SORP (Becton, Dickinson & Company, Franklin Lakes, NJ, USA) with the help of the Flow Cytometry Core Facility at Oslo University Hospital.

The cell lines were compared by subtracting the fluorescence intensity of the non-treated control cells from treated cells and averaging these values for 3 trials using Microsoft Excel. A two-sample t-Test was run between the parental and resistant cell lines in order to determine if the two populations differed significantly in their median fluorescence intensity.

Procedure:

1. Fluorescent rGel (100 nM) was added to the cells and incubated for 4 hours.
2. After 4 hours, the culture media was carefully removed with suction.
3. Cells were washed with 1 ml of pre-warmed PBS containing Ca^{2+} and Mg^{2+}. The plates were tilted to distribute the PBS evenly.
4. PBS was carefully removed with suction.
5. The cells were trypsinated (Section 2.2.1) and the plates were tilted around for 30 seconds to evenly distribute the trypsin.
6. Trypsin was carefully removed with suction.
7. 300 µl of trypsin was added to each well and the plates placed in a 37 °C incubator for approximately 6 minutes so the cells could detach.
8. After the cells detached, 1 ml of media was added to each well to neutralize the trypsin.
9. The cells were transferred into Corning™ Falcon ® 5 ml test tubes with cell strainer cap (#352235, Fisher Scientific, Loughborough, UK).
10. Tubes were centrifuged for 3 minutes at 1300 rpm with a low break at room temperature.
11. The cells were resuspended in 1 ml PBS with 1% FBS.
12. Cells were analyzed with the flow cytometer.

2.10.2 Fluorescence microscopy

In fluorescence microscopy, the sample of interest is labeled with a fluorophore that can be imaged upon excitation. A fluorescence microscope is equipped with lasers or other light sources that can activate fluorophores and a camera that can detect fluorescence. A schematic illustration of a fluorescence microscope is given in Figure 16.

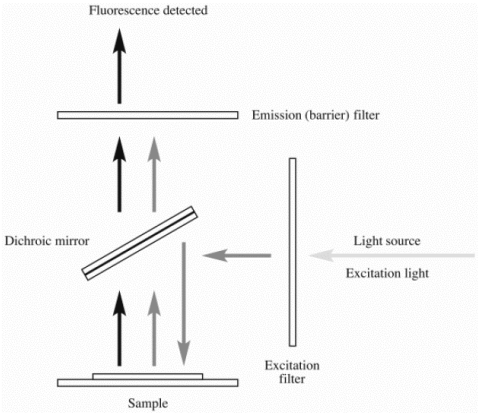

Figure 16: Arrangement of filters and light source in a fluorescence microscope. The excitation light is filtered to control the excitation wavelength. A mirror reflects the excitation light and excites the fluorophore in the sample. Fluorescence/emission light from the fluorophore is then filtered before it is detected by the camera. Retrieved from [69].

Fluorescence microscopy was here combined with conventional microscopy to evaluate the size and morphology of each cell line. The 48 well plates with Nunclon® Delta Surface (Sigma-Aldrich) were used for fluorescence microscopy. Before seeding, a round glass coverslip (10 mm diameter) was added to the bottom of each well carefully using tweezers. The cells were trypsinated and added to the 48 well plates. OSA/PAR plates contained 3000 cells/well, OSA/IR contained 7000 cells/well, MG-63/PAR contained 4500 cells/well, MG-63/IR contained 7000 cells/well, MG-63/DR contained 7000 cells/well and MES-SA contained 5500 cells/well. The cells were left to attach and grow for 48 hours. The glass coverslips were then fixated on rectangular glass microscope slides.

Hoechst 33342 dye from Thermo Fisher Scientific (# 62249) was added to each sample. Hoechst 33342 is a nucleic acid stain that emits blue fluorescence. The dye enters living cells and displays chromatin condensation due to mitosis or apoptosis. Hoechst 33342 has a maximum excitation at 350 nm and emission at 461 nm. It allows for differentiation of living vs. apoptotic cells and it helps visualize the cell cycle stage, size of cells and multinucleation. Hoechst 33342 was detected using a 359 nm excitation filter and 461 nm emission filter. Fluorescence and phase contrast images were taken using a Zeiss Axiolan 1 epi-fluorescens- and phase contrast microscope (Carl Zeiss AG, Oberkochen, Germany) and a CCD (cooled charge-coupled device)-camera (Astromed, Cambridge, UK). An objective with 63x magnification was used for all images. Axio-Vision Analysis software (Carl Zeiss) was used for image processing.

The size of the cells was calculated by measuring the length and width (in µm) of at least 10 cells on the fixated slides. The area was calculated (length x width) for all cells measured and an average area was calculated from these values. A two sample T-test was run to calculate any significant differences in size among the cell lines. All calculations were done in Microsoft Excel.

Procedure:

1. Culture medium was carefully removed with a 100 ml pipette.
2. Each well was washed twice with 400 µl PBS containing Ca^{2+} and Mg^{2+}.
3. Leftover PBS was removed with a pipette and 300 µl of PFA (paraformaldehyde) was added. PFA is a fixation agent often used in microscopy. The cells were incubated with PFA for 15 minutes at room temperature on a plate shaker.

4. PFA was removed from the wells using vacuum suction.
5. Each well was washed twice with 400 µl PBS and the PBS was left in the wells to keep the slides moist.
6. Glass coverslips were loosened carefully using a pipette tip and placed cells face up in a humid chamber consisting of steamy paper towel atop a plastic lid.
7. 100 µl of PBS was quickly added from the wells to the side of the coverslips, ensuring they were always moist. This was repeated for all coverslips.
8. The PBS on top of the coverslips was removed carefully using suction and 100 µl Hoechst 33342 dye was added to the side of the coverslip using a pipette and left to incubate for approximately 1-3 minutes.
9. Microscope slides were labeled with cell line name, date, etc. and 10 µl of ProLong™ Glass Antifade Mountant (P36980, Thermo Fisher Scientific) was added in the center of each labeled microscope slide.
10. The coverslip was washed with 1 ml PBS by pipetting carefully up and down.
11. The coverslip was lifted from the paper towel with tweezers and gently dipped up and down 10 times in a small cup of ddH_2O and dried on clean paper towel. The orientation of the coverslip was carefully noted.
12. The coverslip was placed cells face down on a drop of mounting media on the microscope slide, avoiding air bubbles.
13. The microscope slides were left to fixate overnight and analyzed with fluorescence microscopy the next day.

2.11 Data analysis

The data is displayed as means of three independent experiments ± standard deviation unless otherwise noted. Graphs were created using the scientific data analysis and graphing software SigmaPlot™ version 14.0 (Systat Software Inc., San Jose, CA, USA). Statistical analysis was accomplished using the two-sided T test in Microsoft Excel and a value of $p < 0.05$ was considered statistically significant. All experiments have been reproduced twice, unless otherwise noted.

3. Results

3.1 Growth curves and doubling times

Growth curves of OSA/PAR and MG-63/PAR were generated to verify the appropriate number of cells to be seeded in all experiments. This was to ensure that the cells were in log-phase during the experiments and did not reach confluency.

3.1.1 GROWTH CURVES OF OSA/PAR AND MG-63/PAR CELLS

The OSA/PAR and MG-63/PAR cell lines were seeded according to the PDT and PCI procedure (Procedure 2.3.2) at increasing density, grown for one week and analyzed by the MTT assay (Procedure 2.6.1). Based on the density curves (Figure 17), the optimal seeding density was determined for each cell line (Table 2). Overall, the OSA/PAR line grew faster and more aggressively compared to MG-63/PAR. Therefore, OSA/PAR was always seeded out at a lower density than MG-63/PAR.

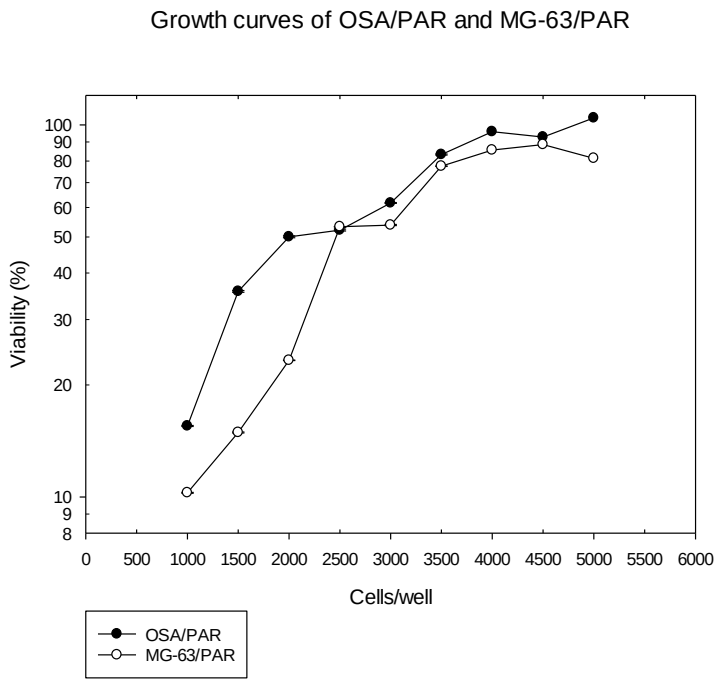

Figure 17: Growth curves of OSA/PAR and MG-63/PAR. Representative result is shown from one experiment among four independent experiments. Each point is the average of six parallels. The empirical standard deviation is pictured as vertical bars.

Table 2: Appropriate seeding densities for all six cell lines which were used in all three types of experiments. PDT and PCI experiments were accomplished in 96-well plates, ionizing radiation experiments were accomplished in 60 mm cell culture dishes and chemotherapy experiments were accomplished in 96-well plates.

Cell line:	PDT and PCI experiments:	Ionizing radiation experiments:	Chemotherapy experiments:
OSA/PAR	3000 cells/well	75000 cells/plate	3000 cells/well
MG-63/PAR	3500 cells/well	85000 cells/plate	3500 cells/well
MES-SA	6000 cells/well	90000 cells/plate	6000 cells/well
OSA/IR	4000 cells/well	85000 cells/plate	---
MG-63/IR	4000 cells/well	85000 cells/plate	---
MG-63/DR	4000 cells/well	---	4000 cells/well

3.2 Fluorescence microscopy images of all cell lines

Images were taken of each cell line to determine cellular morphology. Samples were prepared according to Procedure 2.10.2. The average size of each cell line was calculated and displayed in Figure 18 (Procedure 2.10.2). A representative image of each cell line is displayed below in Figure 19. All OSA and MG-63 cells were larger than the MES-SA cells. MES-SA cells had a somewhat uniform circular shape; there was no uniform shape noticeable among the other cell lines. In both OSA and MG-63, the resistant cells appeared larger than the parental cells, but they did not differ significantly in calculated size (Figure 18), due to large variations in size within each cell line. An increased presence of multinucleated cells was found in MG-63/IR (Figure 19E). Except from this, the morphology of the resistant cell lines was similar to that of the parental cell lines.

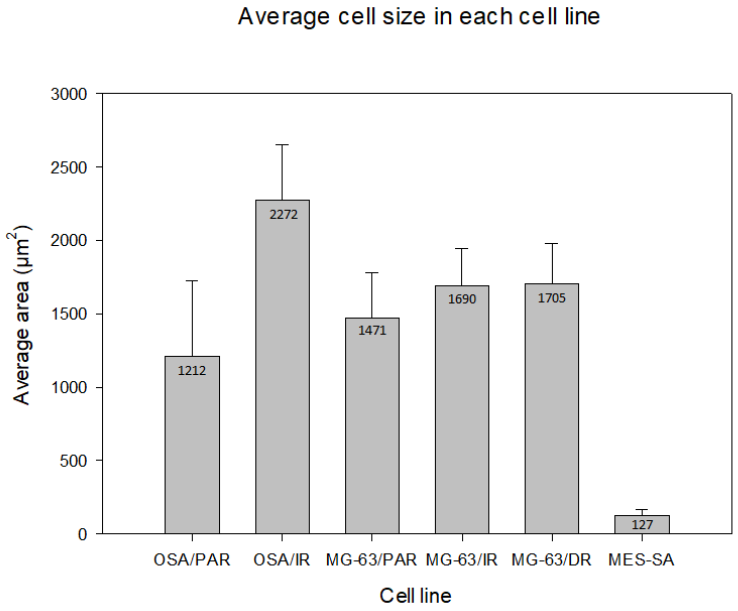

Figure 18: Average cell size of 10 cells in each cell line indicated by the average area (µm^2). No significant differences were observed in cell size between parental and resistant cell lines. Error bars: SD

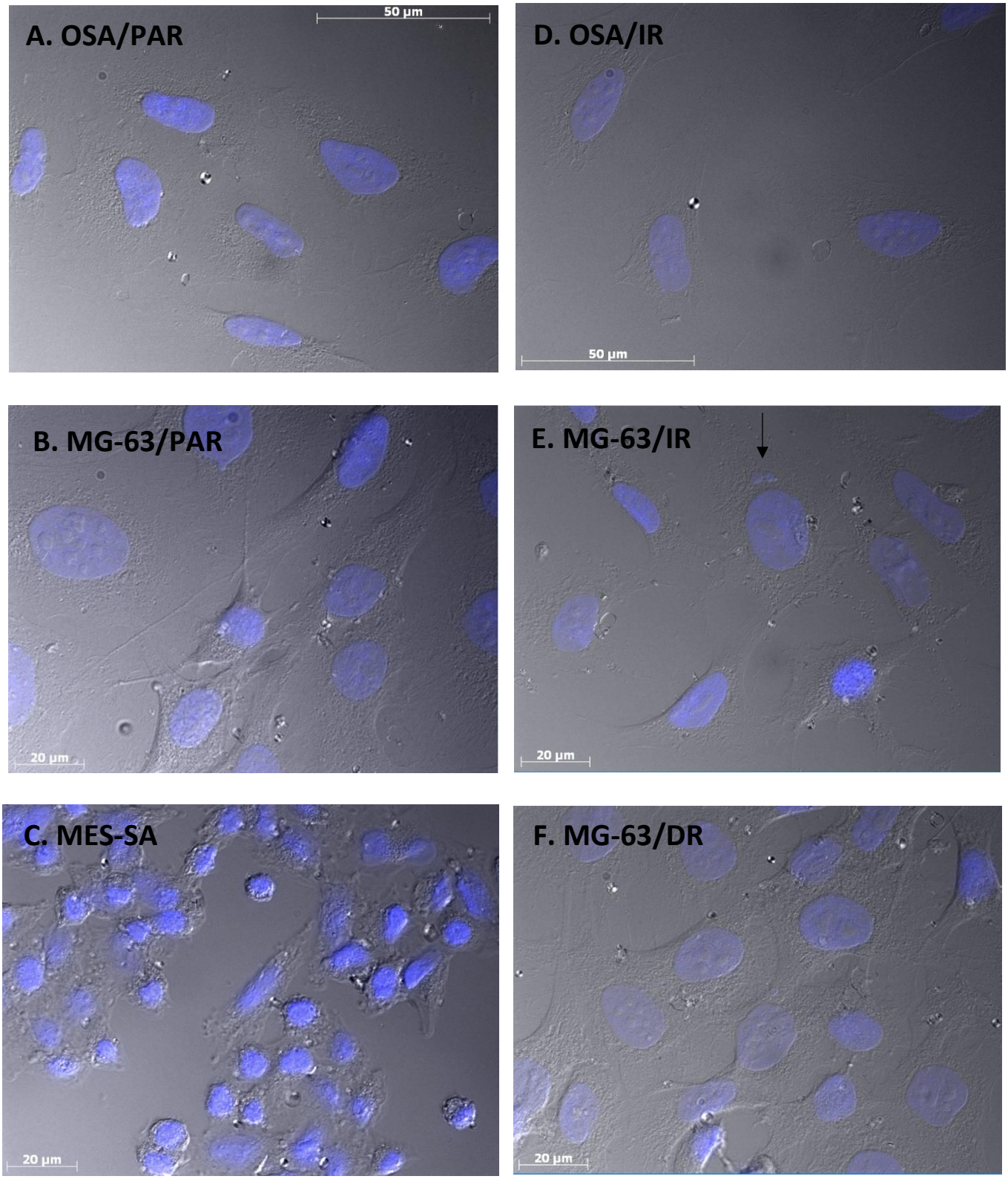

Figure 19: Morphology of all cell lines. (A) OSA/PAR, (B) MG-63/PAR, (C) MES-SA, (D) OSA/IR, (E) MG-63/IR, (F) MG-63/DR. The presence of multinucleation is pictured in E and indicated by the black arrow.

3.3 Radiosensitivity and generation of ionizing radiation resistant osteosarcoma cell lines

Two osteosarcoma cell lines, OSA and MG-63, were initially selected to develop models for IR and doxorubicin resistance.

Osteosarcoma is associated with intrinsic resistance towards radiotherapy, and sensitivity of OSA and MG-63 towards ionizing radiation was initially tested. The sarcoma cell line MES-SA, previously shown sensitive to ionizing radiation, was used as a positive control. Both OSA/PAR and MG-63/PAR were found resistant towards IR as compared to the MES-SA cell line (Figure 20). The MG-63/PAR cells were, in addition, found to be more sensitive to ionizing radiation compared to OSA/PAR (Figure 20). The LD_{50} (IR dose killing 50% of the cells) was estimated to be 4 Gy for the MES-SA cells, 5 Gy for MG-63/PAR and 7.5 Gy for OSA/PAR (Figure 20). The OSA/PAR cells were also found highly resistant at higher doses of IR, and only minor increases in cytotoxicity were found when increasing the dosage above 7.5 Gy (Figure 20A). MG-63/PAR, however, had a declining dose-response curve up to 15 Gy (Figure 20B).

The LD_{50} doses of OSA/PAR and MG-63/PAR were selected for the generation of IR-resistant cell lines as described in Section 2.1.1. Only small differences in sensitivity were found between the OSA/PAR and OSA/IR cell lines (Figure 20A). The MG-63/IR cell line was, however, less sensitive to IR as compared to MG-63/PAR (Figure 20B). Thus, successful adaptive IR-resistance was obtained in the MG-63/IR cell line, but not in the OSA/IR cell line.

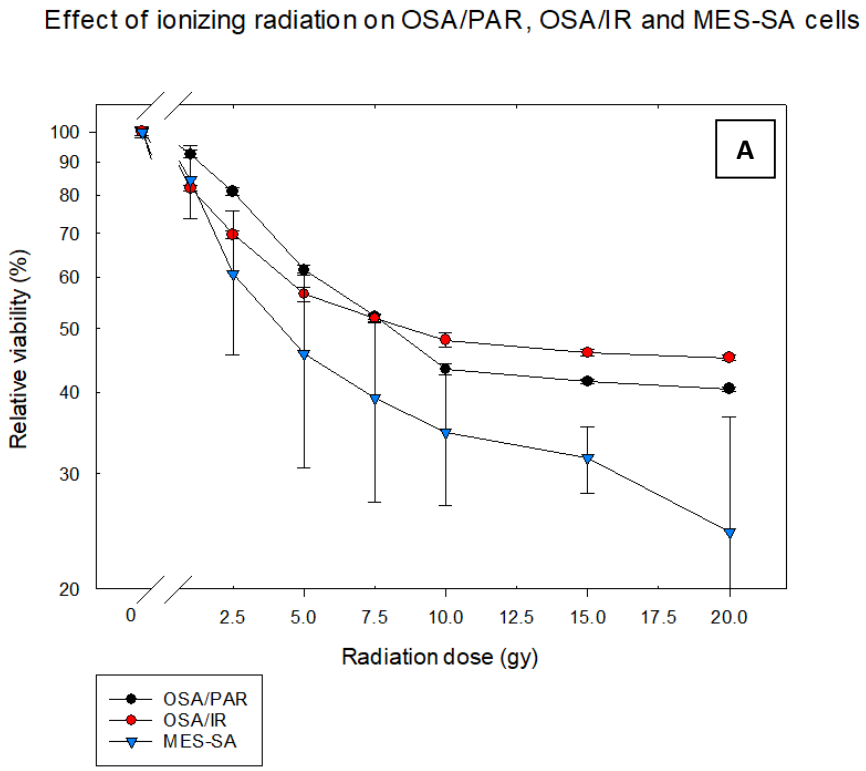

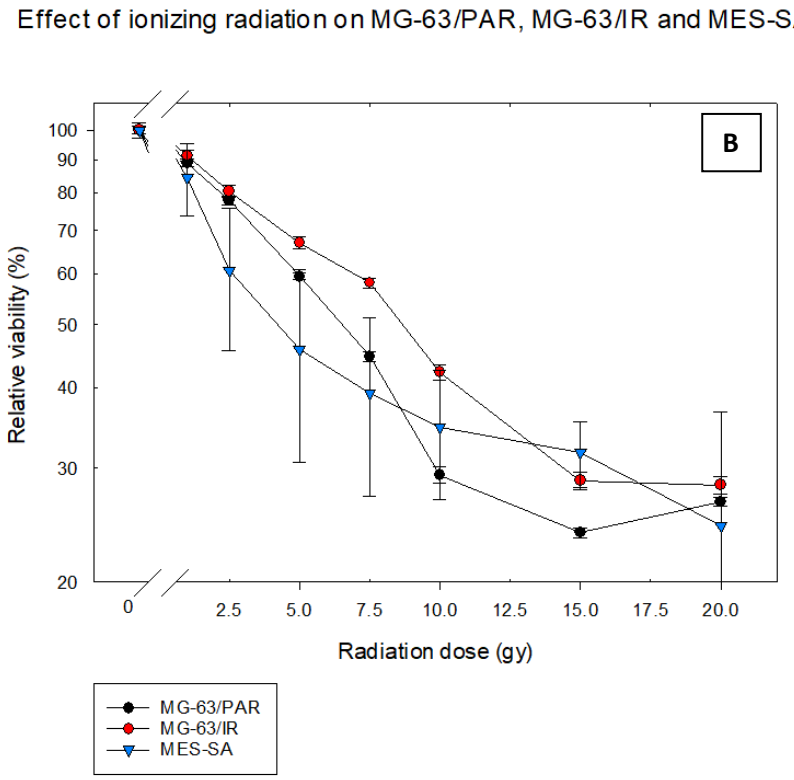

Figure 20: Sensitivity of **(A) OSA/PAR and OSA/IR and (B) MG-63/PAR and MG-63/IR** to ionizing radiation. The IR sensitive MES-SA cell line is included as a positive control. Both graphs display curves generated from an average of three independent experiments. Error bars: SD.

3.4 Doxorubicin resistance and generation of doxorubicin resistant osteosarcoma cell lines

Osteosarcoma is associated with intrinsic resistance towards chemotherapy, and sensitivity of OSA and MG-63 towards doxorubicin was initially tested. The OSA/PAR cell line was found more resistant to doxorubicin compared to MG-63/PAR at high doxorubicin dosage (Figure 21). LD_{95} (dose reducing 95% of the viability) was found at 7.5 µM doxorubicin for OSA/PAR and 5µM doxorubicin for MG-63/PAR. Similar sensitivity towards doxorubicin was, however, found between the cell lines up to ~LD_{50}.

1 µM doxorubicin was selected for the generation of resistant cell lines as described in Section 2.1.2. The OSA cell line did not survive after multiple attempts, thus the generation of an OSA/DR cell line was unsuccessful. The MG-63/DR was found less sensitive towards doxorubicin as compared to MG-63/PAR since the LD_{95} for MG-63/DR was higher than MG-63/PAR (Figure 22). The highest sensitivity towards doxorubicin was found in the MES-SA cell line, previously shown to respond to this drug [70] (Figure 22). Thus, the generation of a doxorubicin resistant MG-63 cell line, MG-63/DR was successful.

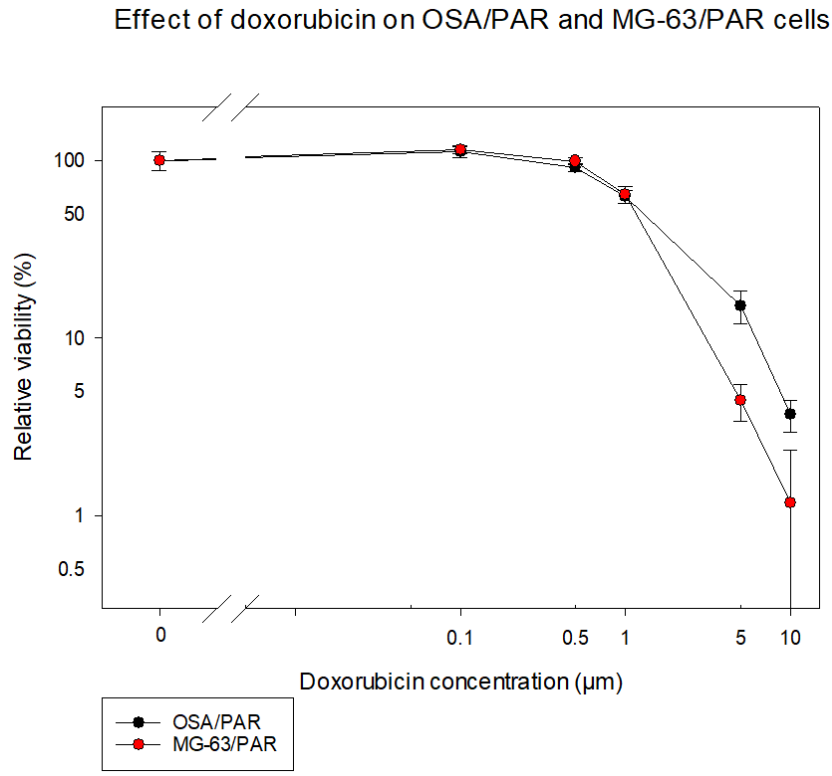

Figure 21: Sensitivity of **OSA/PAR and MG-63/PAR** to doxorubicin. Representative experiment out of three is shown. Each point is the average of six parallels. Error bars: SD.

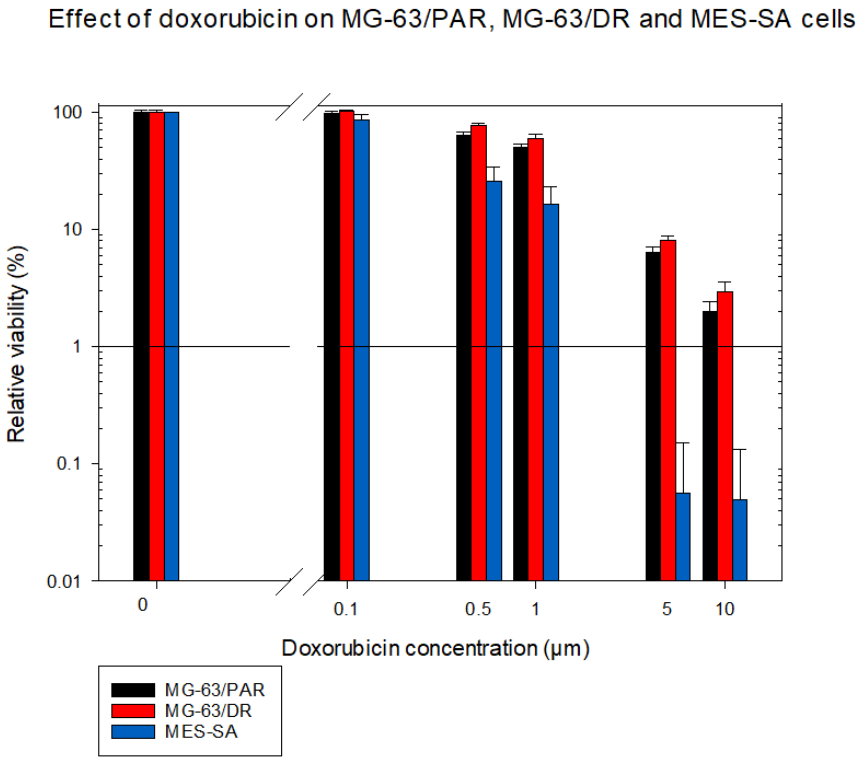

Figure 22: Sensitivity of **MG-63/PAR, MG-63/DR and MES-SA** to doxorubicin. This graph displays barrels generated from an average of three independent experiments. Error bars: SD

3.5 Cellular expression of P53 and EGFR

P53 is one of the most commonly mutated genes in sarcoma and the mutation is associated with resistance. P53 expression was assessed in the parental and resistant cell lines. The expression of EGFR was also investigated since PCI-EGF/rGel/rGel, targeted to EGFR, was one of the treatment modalities evaluated in the project.

A weak band of p53 was observed on the western blots of OSA/PAR and OSA/IR cells, while no band was detected for the MG-63/PAR, MG-63/IR or MG-63/DR cell lines (Figure 23). This is in agreement with previous results from the Department of Tumor Biology, Institute for Cancer Research, Oslo, Norway. A strong band was found for the MES-SA cell line, previously reported to have a functional p53 gene (Figure 23). A strong band of EGFR was observed for all cell lines except for MES-SA (Figure 23). This concurs with previous results showing that there is no EGFR expression in MES-SA. The cell lysates were evenly loaded, indicated by the comparable intensity of the actin bands (Figure 23).

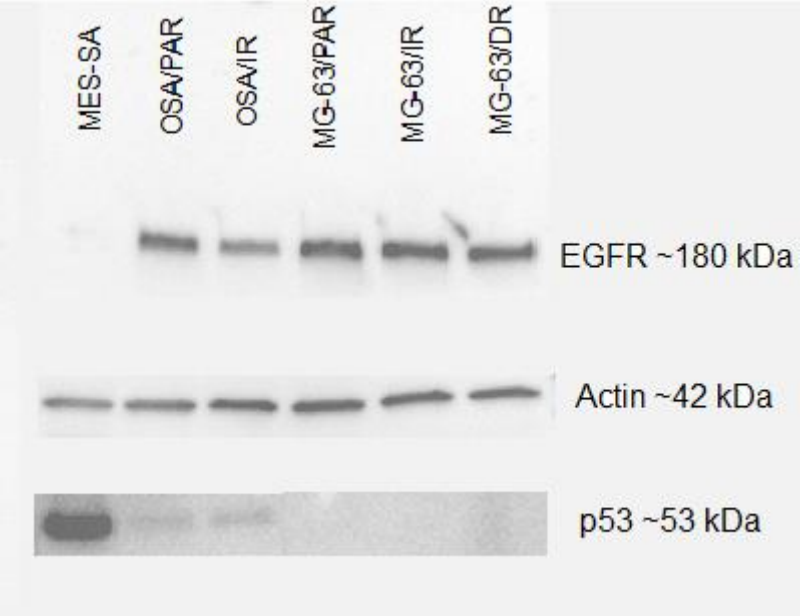

Figure 23: Western blot displaying the expression of EGFR, actin and p53 in the **MES-SA, OSA/PAR, OSA/IR, MG-63/PAR, MG-63/IR and MG-63/DR** cell lines. EGFR (MW: 180 kDa), actin (MW: 42 kDa) and p53 (MW: 53 kDa). This blot shows a representative experiment out of three.

3.6 PCI of rGel

It was evaluated if PCI could be used as a therapeutic approach to osteosarcoma, given that OSA and MG-63 show resistance towards both ionizing radiation and chemotherapy. Gelonin was selected as the macromolecule to be delivered by PCI based on previous results of rGel-PCI in resistant cell lines [35, 70, 71].

3.6.1 PDT AND PCI IN PARENTAL CELL LINES

All cells were treated according to the standard PDT and PCI procedure (Procedure 2.3.2) with 10 nM gelonin and increasing light exposure times. The light dose needed to reduce the viability to 50% with PDT was less in MES-SA compared to the other two cell lines, indicating intrinsic cross resistance in OSA/PAR and MG-63/PAR towards PDT (Figure 24). All three cell lines displayed a PCI effect with rGel, visualized by the increased effect of PCI-rGel compared to rGel and PDT monotherapies (Figure 24).

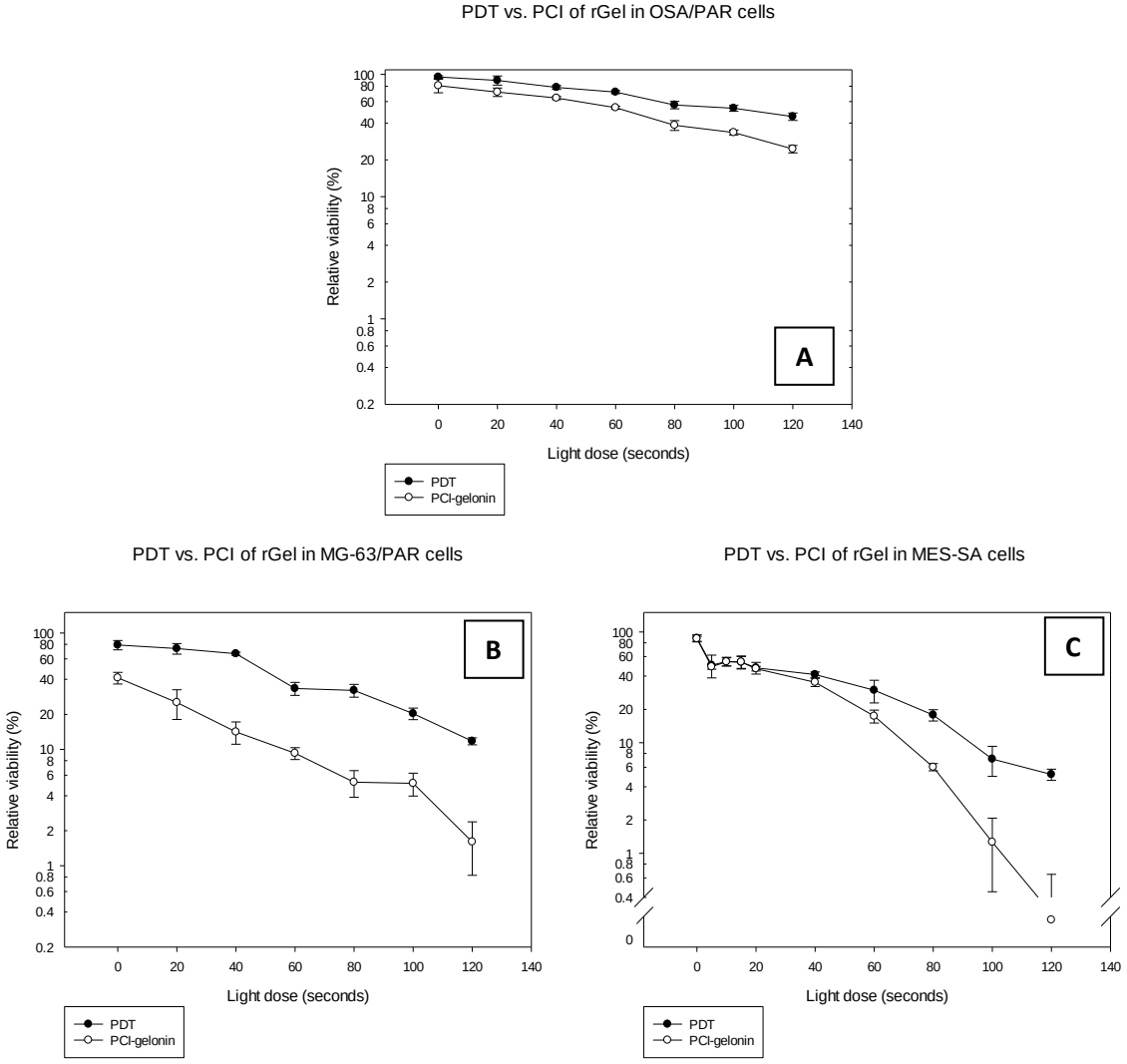

Figure 24: PDT and PCI of rGel in **(A) OSA/PAR, (B) MG-63/PAR and (C) MES-SA** cells, measured by MTT 48 hours after treatment. Representative experiment out of three is shown. Each point is the average of three parallels. Error bars: SD.

3.6.2 PDT AND PCI IN OSA/PAR AND OSA/IR

It was evaluated if the repeated IR treatment of OSA/PAR cells had any influence on PDT and PCI sensitivity. OSA/PAR and OSA/IR were subjected to PDT and PCI as described in Procedure 2.3.2 with 10 nM rGel and increasing light exposure times. A PCI effect was observed in both cell lines, visualized by the increased effect of PCI-rGel compared to rGel and PDT monotherapies (Figure 25). OSA/PAR and OSA/IR responded similarly towards PCI-rGel, indicating that the repeated IR treatment did not have an effect on PDT and PCI sensitivity in OSA cells.

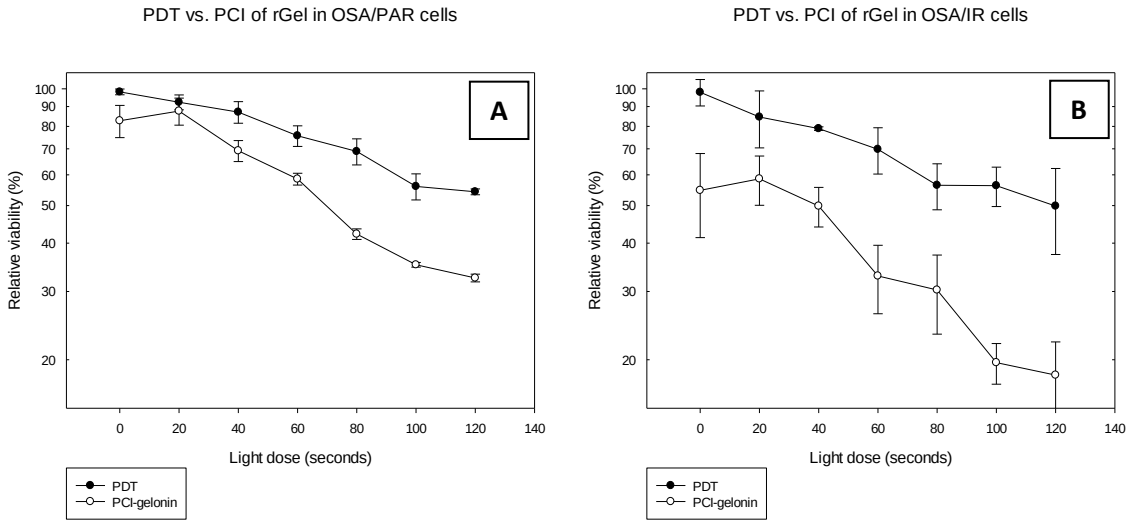

Figure 25: PDT and PCI of rGel in **(A) OSA/PAR and (B) OSA/IR** cells, measured by MTT 48 hours after treatment. Representative experiment out of three is shown. Each point is the average of three parallels. Error bars: SD.

3.6.3 PDT AND PCI IN MG-63/PAR, MG-63/IR AND MG-63/DR

It was evaluated if the repeated IR and doxorubicin treatment of MG-63/PAR cells had any influence on PDT and PCI sensitivity. MG-63/PAR, MG-63/IR and MG-63/DR were subjected to PDT and PCI as described in Procedure 2.3.2 with 10 nM rGel and increasing light exposure times. A PCI effect was observed in all cell lines, visualized by the increased effect of PCI-rGel compared to rGel and PDT monotherapies (Figure 26). MG-63/PAR and MG-63/IR responded similarly towards PCI-rGel, indicating that the repeated IR treatment did not influence PDT and PCI sensitivity (Figure 26A, B). However, MG-63/DR appeared more resistant to the treatment with PDT and PCI, indicating that doxorubicin treatment did have an effect on PDT and PCI sensitivity (Figure 26C).

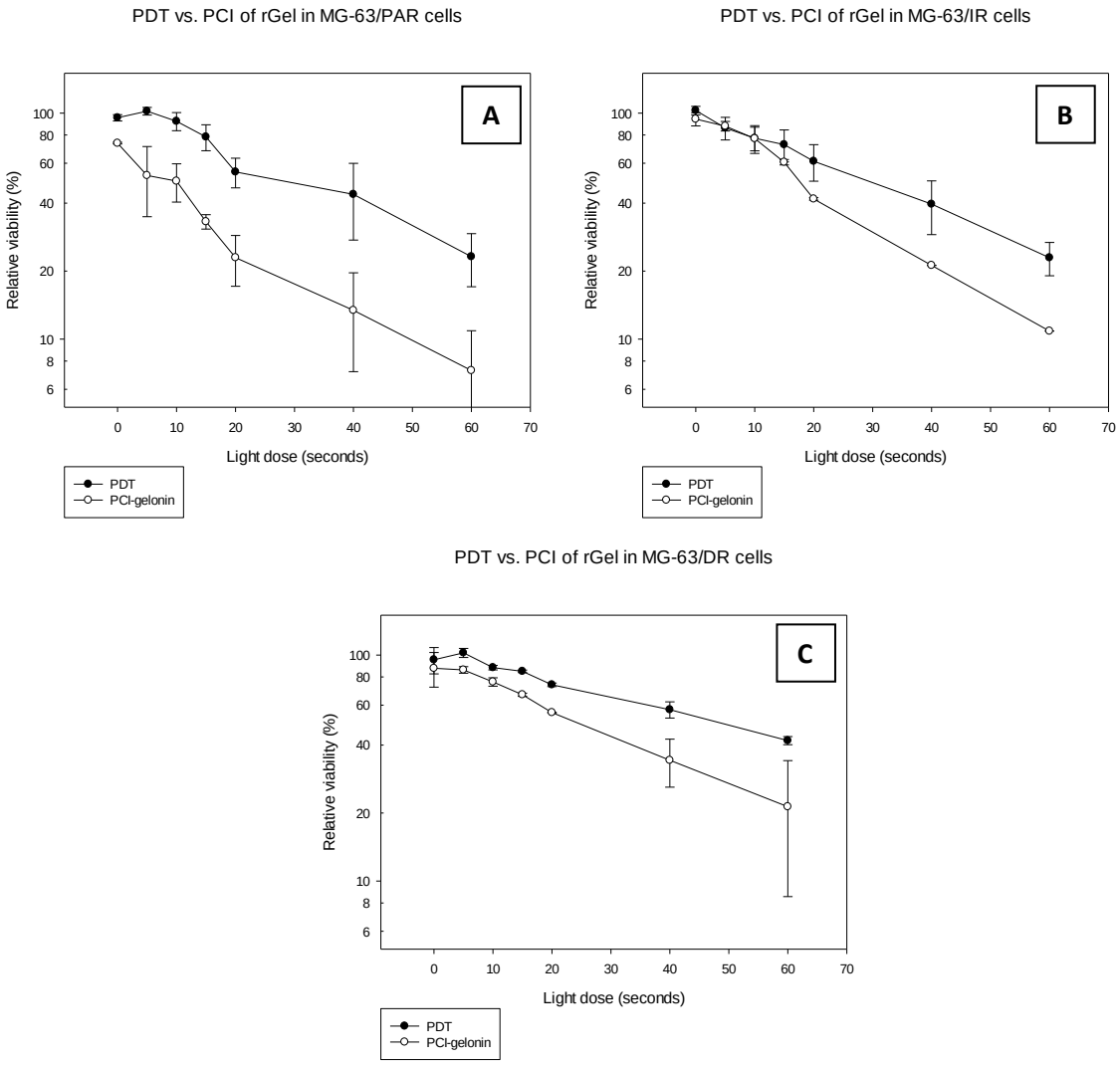

Figure 26: PDT and PCI of rGel in **(A) MG-63/PAR, (B) MG-63/IR and (C) MG-63/DR** cells, measured by MTT 48 hours after treatment. All graphs display curves generated from an average of two independent experiments. Error bars: SD.

3.6.4 PCI EFFICACY OF PARENTAL CELL LINES AND RESISTANT CELL LINES

PCI efficacy in each cell line was calculated according to Procedure 2.3.3 (Figure 27) at LD_{50}. 10 nM gelonin, as applied in the experiments shown in Figures 25-26, reduced the viability to 70-80% in each cell line. No significant differences in PCI efficacy were found between the cell lines indicating that PCI with rGel was able to circumvent the intrinsic mechanisms of resistance in OSA/PAR and MG-63/PAR compared to MES-SA, and also the adaptive mechanisms of resistance in OSA/IR, MG-63/IR and MG-63/DR.

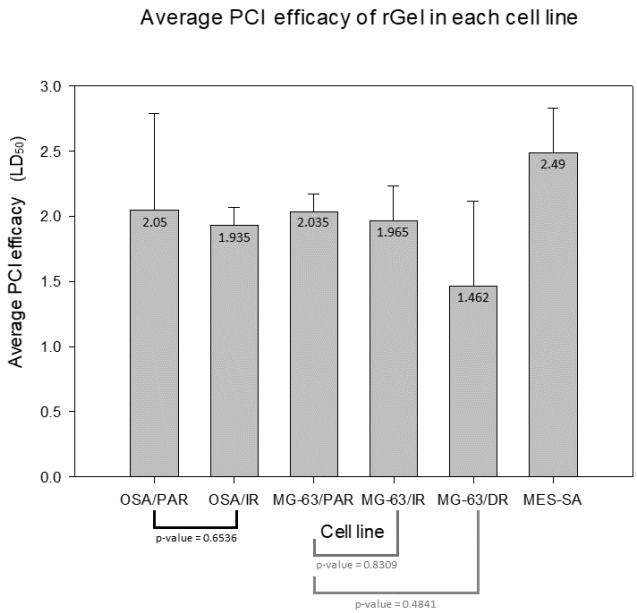

Figure 27: rGel-PCI efficacy in **OSA/PAR, OSA/IR, MG-63/PAR, MG-63/IR, MG-63/DR and MES-SA** cell lines. The barrels show the average PCI efficacy calculated at LD_{50} from three independent experiments. Error bars: SD.

3.7 PCI of EGF/rGel/rGel

Even though PCI-rGel was indicated as efficient for all cell lines, the overall response was modest (Figures 24-26). A more cancer specific and efficient utilization of the PCI technology may be obtained by the combination with targeted toxins. Many osteosarcoma cell lines have increased expression of EGFR and this is related to poor prognosis [51, 53]. PCI of the targeted toxin, EGF/rGel/rGel, designed in the project group, was therefore evaluated in all cell lines.

3.7.1 PCI EFFECT OF EGF/RGEL/RGEL IN OSA/PAR AND MG-63/PAR

All cells were treated according to the standard PCI procedure (Procedure 2.3.2) with increasing drug concentration. The cells were treated with the light dose causing 50% viability determined from preliminary experiments; OSA/PAR was illuminated for 60 seconds and MG-63/PAR was illuminated for 40 seconds.

At the highest drug concentration tested (100 nM), EGF/rGel/rGel and rGel monotherapies proved to reduce the viability to ~75% in OSA/PAR (Figure 28A). However, when combined with PCI, the viability was significantly decreased to <1% (Figure 28A). A similar pattern was observed with MG-63/PAR cells, where EGF/rGel/rGel monotherapy reduced the viability to 50% while PCI-EGF/rGel/rGel at 100 nM reduced the viability to 3% (Figure 28B). EGF/rGel/rGel exhibited a significantly stronger PCI effect as

compared to rGel (Figure 28). Thus, PCI-EGF/rGel/rGel is here indicated as a promising therapeutic approach for osteosarcoma cancers expressing EGFR.

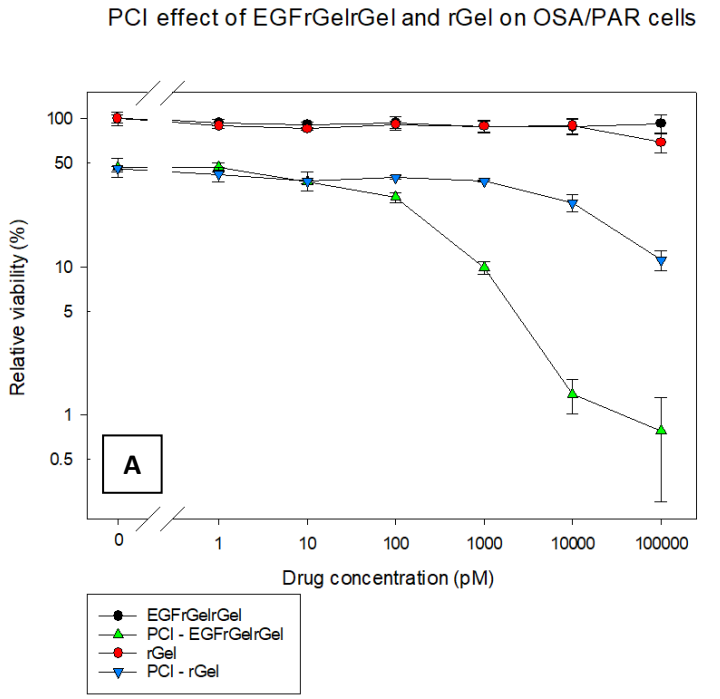

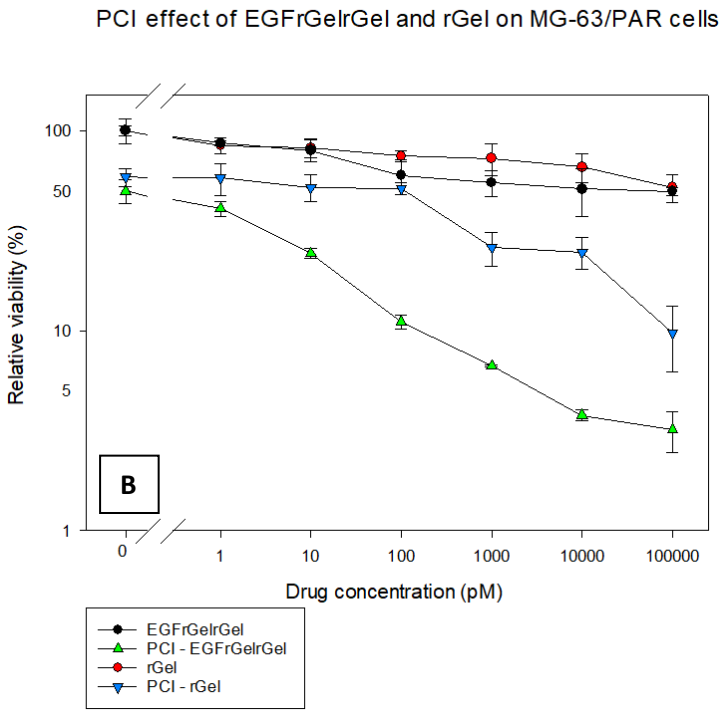

Figure 28: PCI of rGel and EGF/rGel/rGel in **(A) OSA/PAR and (B) MG-63/PAR** cells, measured by MTT 48 hours after treatment. For both cell lines, a representative experiment out of three is shown. Error bars: SD.

3.7.2 PDT AND PCI OF EGF/RGEL/RGEL IN MES-SA CELLS

The sensitivity of MES-SA towards PCI-EGF/rGel/rGel was also evaluated. All cells were treated according to the standard PDT and PCI procedure (Procedure 2.3.2) with 10 nM of rGel and EGF/rGel/rGel and increasing light exposure times.

PCI was highly effective in combination with rGel, as in agreement with Section 3.6.1 (Figure 29). However, no enhanced effect was observed with PCI of EGF/rGel/rGel compared to PCI of rGel and PCI-rGel was more effective than PCI-EGF/rGel/rGel (Figure 29). Therefore, PCI-EGF/rGel/rGel is not an effective treatment for MES-SA cells.

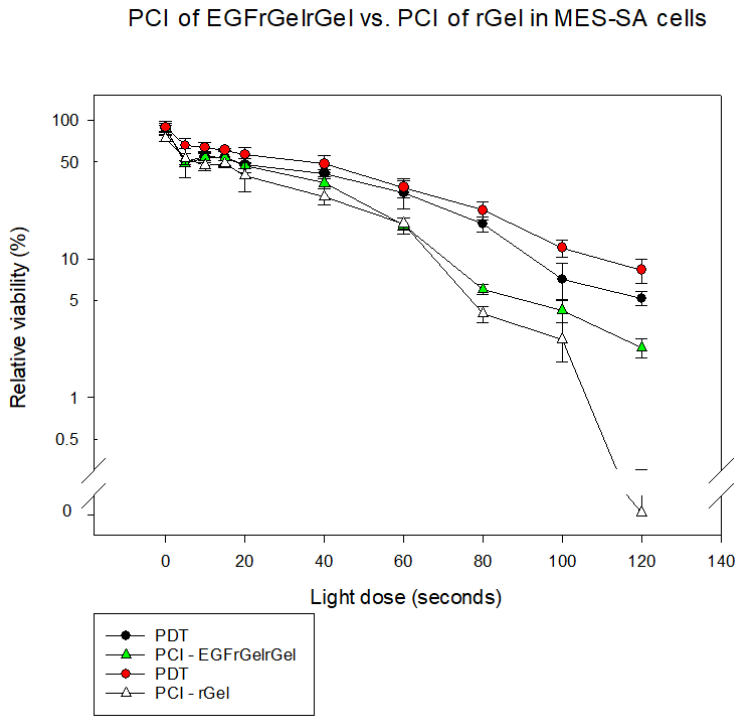

Figure 29: PDT and PCI of EGF/rGel/rGel and rGel in **MES-SA** cells, measured by MTT 48 hours after treatment. Representative experiment out of three is shown. Error bars: SD.

3.7.3 PDT AND PCI IN OSA/PAR AND OSA/IR

Our results proved that repeated IR treatment did not influence PCI-rGel sensitivity in OSA cells (Section 3.6.2). It was evaluated if there was a difference in response to PCI-EGF/rGel/rGel among the parental and resistant cell lines. OSA/PAR and OSA/IR were subjected to PDT and PCI as described in Procedure 2.3.2 with 10 nM EGF/rGel/rGel and increasing light exposure times. A PCI effect was observed in both cell lines, visualized by the synergistic effect of PCI-EGF/rGel/rGel compared to EGF/rGel/rGel and PDT monotherapies (Figure 30A and B). The PCI effect with EGF/rGel/rGel was much stronger than seen with PCI-rGel, indicating EGFR targeted PCI as an effective modality in OSA/PAR and OSA/IR.

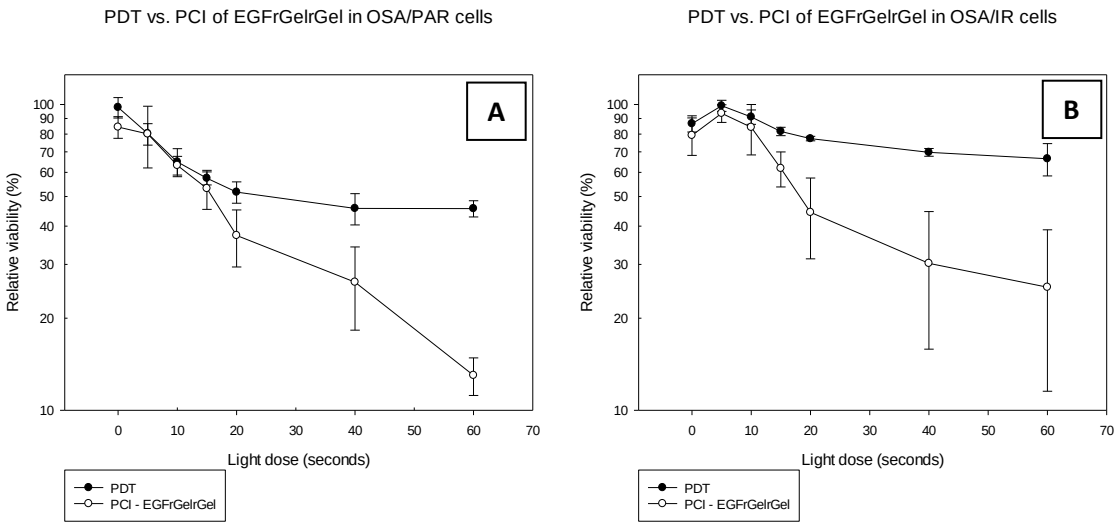

Figure 30: PDT and PCI of EGF/rGel/rGel in **(A) OSA/PAR and (B) OSA/IR** cells, measured by MTT 48 hours after treatment. Both graphs display a curve generated from an average of two independent experiments. Error bars: SD.

3.7.4 PDT AND PCI IN MG-63/PAR, MG-63/IR AND MG-63/DR

It was evaluated if there was a difference in response to PCI-EGF/rGel/rGel among the parental and resistant cell lines. MG-63/PAR, MG-63/IR and MG-63/DR were subjected to PDT and PCI as described in Procedure 2.3.2 with 10 nM EGF/rGel/rGel and increasing light exposure times. All cell lines had a strong PCI effect with EGF/rGel/rGel (Figure 31A, B and C), further indicating PCI-EGF/rGel/rGel as a possible treatment approach for EGFR expressing osteosarcoma.

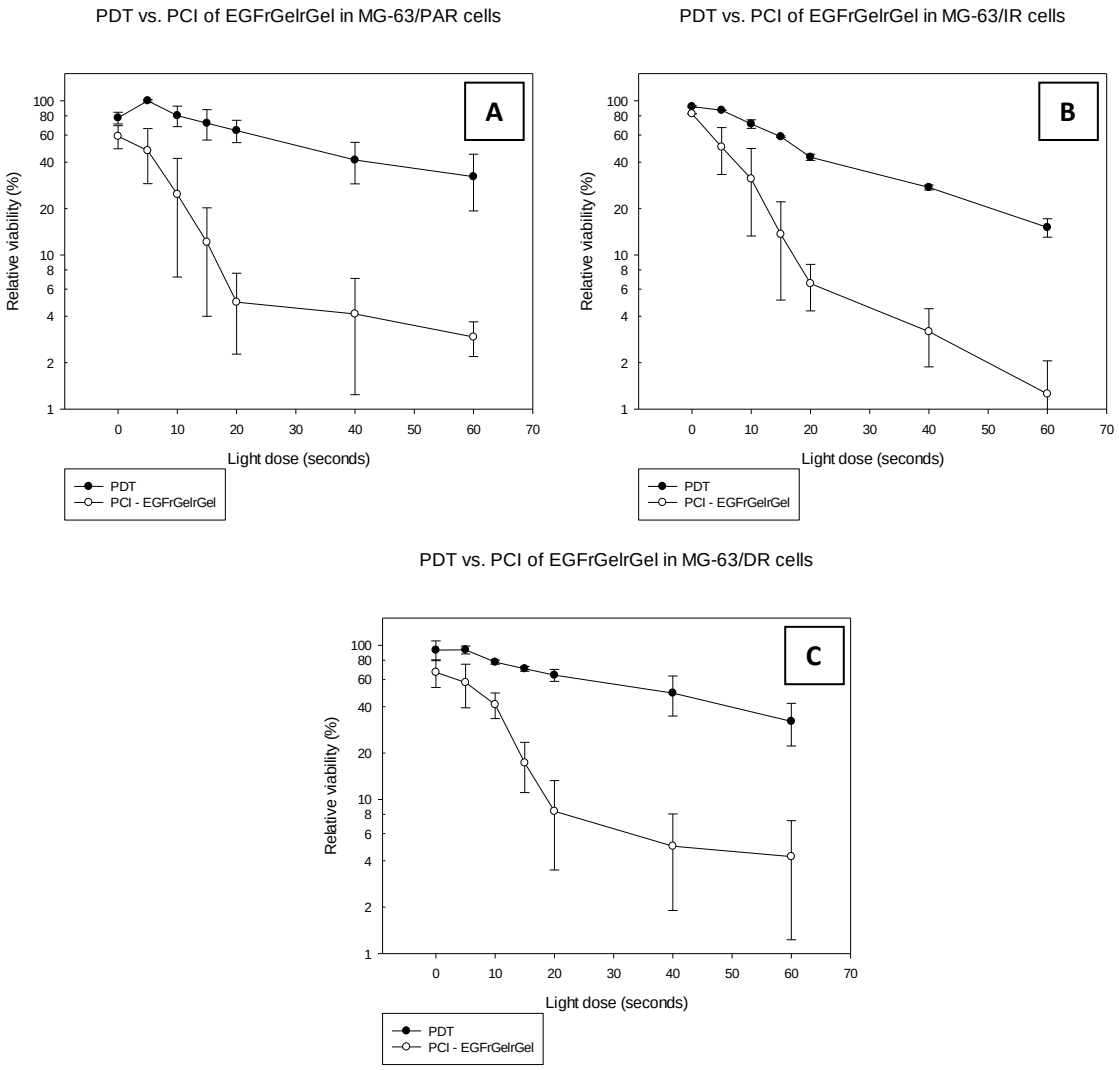

Figure 31: PDT and PCI of EGF/rGel/rGel in **(A) MG-63/PAR, (B) MG-63/IR and (C) MG-63/DR** cells, measured by MTT 48 hours after treatment. All graphs display a curve generated from an average of two independent experiments. Error bars: SD.

3.7.5 PCI EFFICACY OF PARENTAL CELL LINES AND RESISTANT CELL LINES

PCI efficacy in each cell line was calculated according to Procedure 2.3.3 at LD_{95}. 10 nM EGF/rGel/rGel, as applied in the experiments shown in Figures 29-31, reduced the viability to 80-90% in each cell line (Figure 32). The PCI efficacy for EGF/rGel/rGel was generally higher than observed for rGel in all resistant and parental OSA and MG-63 cells, indicating the intrinsic mechanisms of resistance to be circumvented by the treatment. In addition, no significant differences in PCI efficacy were presented between the OSA and MG-63 cell lines, indicating that PCI with EGF/rGel/rGel was able to also circumvent the adapted mechanisms of resistance related to repeated IR or doxorubicin treatment (Figure 32). However, there were significant differences in PCI-EGF/rGel/rGel efficacy between MES-SA and OSA/PAR ($p = 0.027$) and MES-SA and MG-63/IR ($p = 0.0413$). The PCI efficacy of EGF/rGel/rGel was also calculated at LD_{50} and these results are displayed in Appendix D.

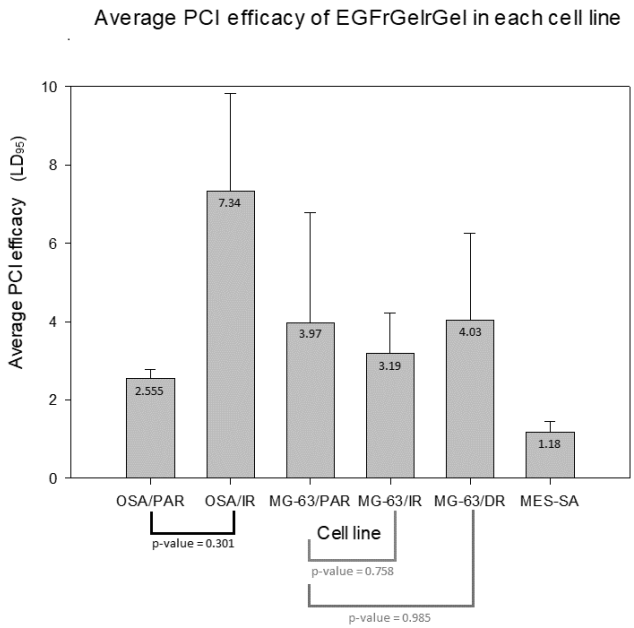

Figure 32: EGF/rGel/rGel-PCI efficacy in **OSA/PAR, OSA/IR, MG-63/PAR, MG-63/IR, MG-63/DR and MES-SA** cell lines. The barrels show the average PCI efficacy calculated at LD_{95} from three independent experiments. Error bars: SD.

3.8 Uptake of rGel in OSA/PAR, OSA/IR, MG-63/PAR, MG-63/IR AND MG-63/DR

3.8.1 FLOW CYTOMETRY ANALYSIS: UPTAKE OF FLUORESCENT RGEL

Diverse types of cancers, including resistant forms, display differences in drug uptake, and this may be reflected in their patterns of macropinocytosis [72]. Cellular uptake of gelonin is mainly through macropinocytosis. The uptake of fluorescent gelonin (rGel) in the different cell lines was here evaluated by flow cytometry. The samples were prepared according to the Procedure 2.10.1. As described in Section 3.3, no clear difference in radio-sensitivity was found between OSA/PAR and OSA/IR. The results on rGel uptake revealed, however, a significant more than 2-fold increase in rGel uptake in the OSA/IR cell line compared to the parental OSA/PAR cell line (Figure 33). No difference in rGel uptake was found between the parental and resistant MG-63 cell lines (Figure 33). The uptake of rGel in the two parental cell lines OSA/PAR and MG-63/PAR was also found similar (Figure 33).

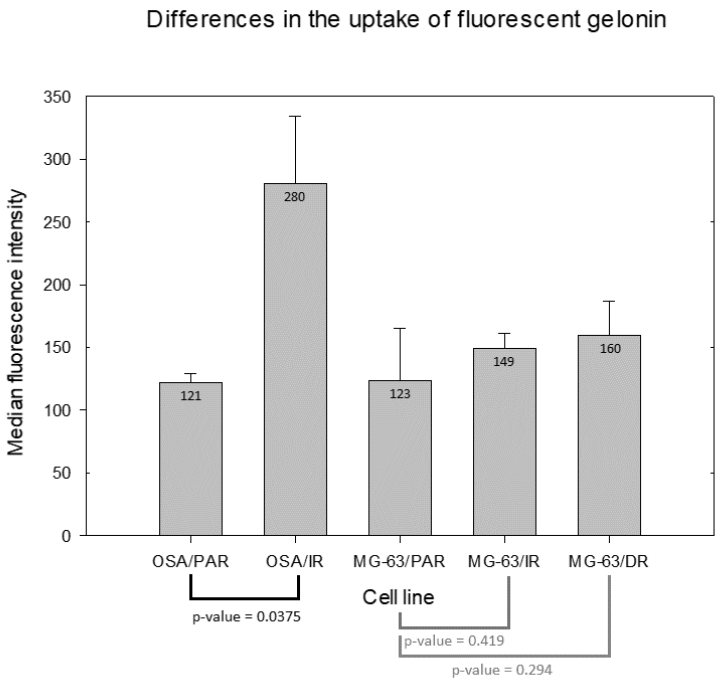

Figure 33: Uptake of fluorescent labeled rGel in **OSA/PAR, OSA/IR, MG-63/PAR, MG-63/IR and MG-63/DR**. The uptake was evaluated by flow cytometry. The medium fluorescence intensity was calculated by averaging three trial replicates. Error bars: SD.

3.9 RNA Seq of OSA/PAR, OSA/IR, MG-63/PAR, MG-63/IR AND MG-63/DR

The gene expression between the parental and resistant cell lines was compared by RNA Seq. Table 3 shows the analysis results for each cell line. The RIN was calculated according to Procedure 2.8. The read length for all samples was 76 base pairs and this refers to how many nucleotides from each end of the RNA fragments are sequenced. The number of reads displays information about the quantity of the data and refers to how many 76 bp sequences were generated. The total aligned reads act as a quality control which signifies if the alignment was proper; any percentage above 80% is recognized as sufficient quality. The reads aligned to correct strand also acts as a quality control and determines how well the reads matched up with the reference genome. The assessed gene count is how many genes were detected. The number of differentially expressed genes conveys how many genes in the resistant cell line are differentially expressed compared to the parental cell line. This number was calculated by using custom filtering parameters where the $\log_2$(fold change) > 1.2 and p-value < 0.01. These filtering parameters were determined and applied to the data by the Genomics Core Facility at Oslo University Hospital.

Table 3: RNA seq analysis for all cell lines. All values were calculated by the Genomics Core Facility at OUS.

Cell line:	RIN:	No. of Reads (2x):	Total Aligned Reads (%):	Reads aligned to correct strand (combined):	Assessed gene count (at least 10X coverage):	No. of differentially expressed genes compared to parental (PAR):
OSA/PAR	9.90	45,223,681	98.3% 98.5%	99.6%	11,408	---
OSA/IR	10	52,899,865	98.5% 98.6%	99.7%	11,816	56
MG-63/PAR	10	90,799,758	97.2% 97.6%	99.7%	11,817	---
MG-63/IR	10	76,998,724	98.6% 98.6%	99.7%	11,829	152
MG-63/DR	10	89,802,189	98.3% 98.4%	99.7%	11,961	156

Detailed maps, using the IPA program (Procedure 2.9.2), were created by Susanne Lorenz (Genomics Core Facilities, OUS) which display the significantly affected pathways or functions affected (presented in black, bold), as well as the differentially expressed genes (presented in blue) between the parental and resistant cell lines (Figures 34-36). The maps also highlight how the genes and pathways could potentially affect cancer growth and resistance (presented in red). In the figures, the p-values measure how likely the enrichment of genes for a certain pathway or function is a true result and not only a random effect; a low p-value indicates high enrichment and signifies high likelihood of a true enrichment. The z-scores are a measure of pathway activation or inhibition; a negative z-value indicates that the pathway is inhibited and a positive z-score indicates that the pathway is activated.

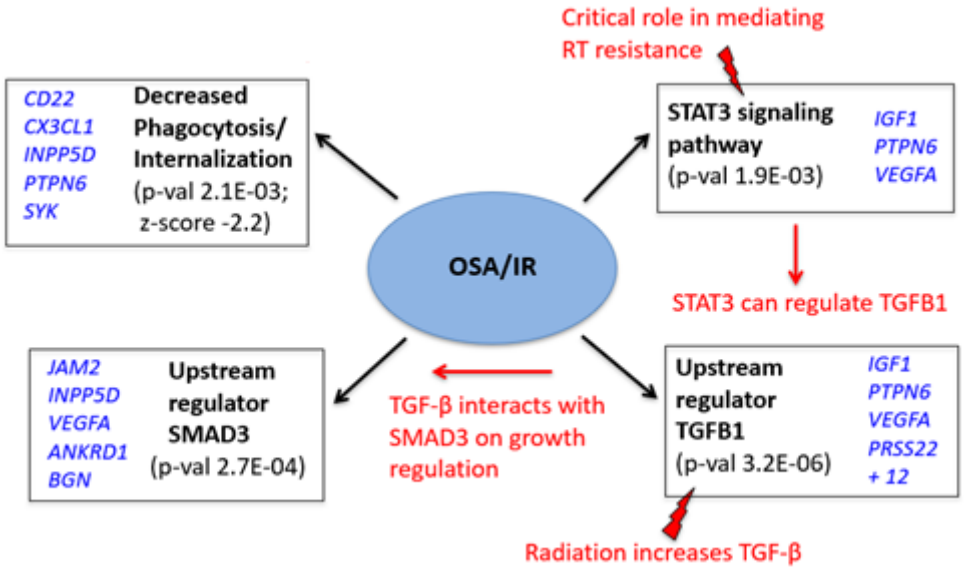

Figure 34: The differentially expressed genes in the OSA/IR cell line compared with the parental OSA/PAR cell line. The number of differentially expressed genes in total was 56 (Table 3). Displayed in the figure are the most notable pathways affected. Figure made by Susanne Lorenz (Genomics Core Facilities, OUS).

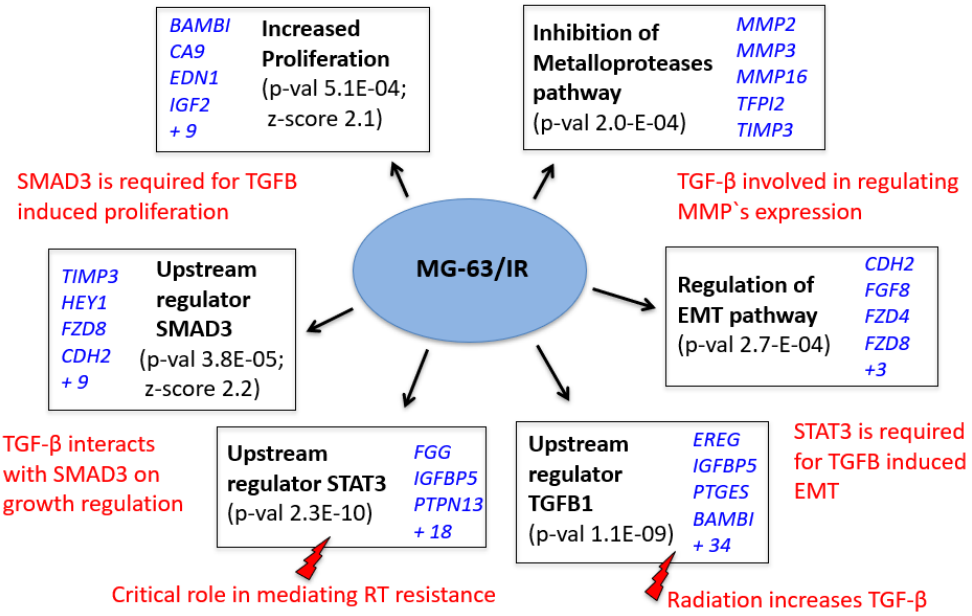

Figure 35: The differentially expressed genes in the MG-63/IR cell line compared with the parental MG-63/PAR cell line. The number of differentially expressed genes in total was 152 (Table 3). Displayed in the figure are the most notable pathways affected. Figure made by Susanne Lorenz (Genomics Core Facilities, OUS).

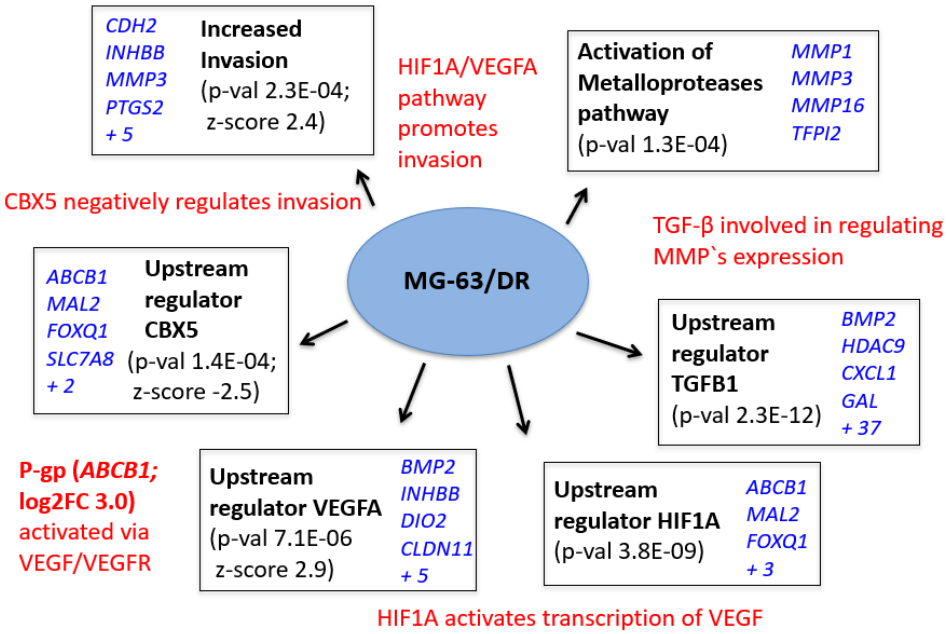

Figure 36: The differentially expressed genes in the MG-63/DR cell line compared with the parental MG-63/PAR cell line. The number of differentially expressed genes in total was 156 (Table 3). Displayed in the figure are the most notable pathways affected. Figure made by Susanne Lorenz (Genomics Core Facilities, OUS).

4. Discussion

4.1 Acquired resistance in cell lines

Intrinsic or acquired resistance to IR and chemotherapy is a major complication in cancer therapeutics today, including treatment of sarcoma. In this project, resistant cell lines to IR and doxorubicin were generated from parental OSA and MG-63 osteosarcoma cell lines. The resulting cell lines (OSA/IR, MG-63/IR and MG-63/DR) were characterized by their morphology, responses to radiation and doxorubicin, as well as their drug uptake patterns and genetic expression profile. Adapted radioresistance was acquired in only one cell line, MG-63/IR, while only minor changes in radiation sensitivity were observed in OSA/IR (Figure 20). The RNA seq as well as the evaluation of macropinocytosis did, however, show several alterations in OSA/IR as compared to the parental cell line. Several other studies have used similar methods in generating resistant cancer cell lines to IR. McDermott *et al.* [73] treated the prostate cancer cell line, 22Rv1, with a fractionated and weekly dose of 2 Gy until attainment of a cumulative dose of 60 Gy. Like our study, they grew age-matched controls alongside the irradiated cells to be used for comparison. They, however, used the clonogenic assay to determine cell viability and found that cell survival decreased at a slower rate in the resistant line (RR-22Rv1) than compared with the age-matched control (AMC-22Rv1) and the wild type 22Rv1 cell line (WT-22Rv1). They observed a significant difference in the survival of the radiation resistant cells and the age-matched and wildtype controls, proving that radioresistance was acquired successfully in RR-22Rv1. Other studies also have comparable approaches to generate IR-resistant cell lines [74, 75]. Even though we observed increased IR resistance in MG-63/IR as compared to the parental cell line, the difference here was small, compared to what has been obtained in cell lines from other origins. Overall, our results on the generation of treatment resistant cell lines likely reflects the general IR resistance of osteosarcomas.

IR is often used as palliative treatment and can be used alongside either chemotherapy or other modalities in many cancers including osteosarcoma [18] and it is estimated that 50% of all cancer patients will undergo radiation as part of their therapy [76]. The most common regime of radiation therapy is daily exposures between 1.5 Gy and 3 Gy given every weekday over several weeks [76]. Unfortunately, IR resistance is very common in osteosarcomas due to the heterogenous characteristics of the cells. Osteosarcoma can also develop after radiation therapy is given to patients with other types of cancers. Berner *et al.* [77] found that 9 out of 37 extraskeletal osteosarcoma patients developed radiation-induced sarcoma and these 9 patients were given chemotherapy or underwent amputation surgery as their main method of treatment.

Although we only obtained minor IR resistance in OSA/IR, we decided to continue evaluating this cell line throughout the project. Despite OSA/IR only showing minor resistance to IR, our results revealed that OSA/IR did differ significantly from its parental (p-value = 0.0375) in the uptake of fluorescent labeled rGel (Figure 33). Thus, even though OSA/IR is only slightly more IR-resistant, repeated IR exposure did alter the cell line compared to the parental cell lines. The increased uptake of rGel in OSA/IR was further investigated with RNA seq, but these results showed decreased phagocytosis and internalization in OSA/IR cells (Figure 34) compared to the parental cell lines. rGel has been proven to enter the cell by endocytosis [71], so it contradictory that OSA/IR has increased fluorescent rGel uptake

when it expresses genes that decrease phagocytosis and internalization. The increased uptake of rGel in OSA/IR may, however, be related to the increased size of OSA/IR compared to the other cells. Even though our calculations here did not end up significant, the OSA/IR did appear as larger in size compared to OSA/PAR (Figure 18). A larger cell will have larger plasma membrane and therefore be able to endocytose more material such as rGel.

In both OSA/IR and MG-63/IR, the viability became stagnant after the cells were exposed to around 10 Gy of IR (Figure 20) and despite the increase in dose, the cells did not experience a decrease in viability. This could be due to the MTT assay not accurately detecting the viability below a certain point, in this case 20% to 50% viability. However, this is probably not the case since the MTT assay detected as low as ~1% viability in OSA/PAR and MG-63/PAR when exposed to doxorubicin (Figure 21). Therefore, this phenomenon could be due to the cells containing heterogenous populations at the start of IR treatment. For instance, when the cells were first exposed to prolonged IR, some cells in the population were intrinsically resistant to IR and others were not. All the cells that were sensitive were killed, while the intrinsically resistant cells survived and duplicated, eventually producing a cell line more resistant to IR.

Chemoresistance was acquired in only one cell line, MG-63/DR, since the generation of OSA/DR was unsuccessful due to severe toxicity of prolonged doxorubicin treatment. In a similar project, Han *et al.* [78] exposed an osteosarcoma cell line, SOSP-9607, to stepwise concentrations of cisplatin (0.1 µg/ml – 2 µg/ml cisplatin) in medium for 12 months. Like our study, they used the MTT assay to test the chemoresistance and found that the cisplatin resistant cell line, SOSP-9607/CDDP, had a 6.24-fold increase in resistance towards cisplatin. Compared to these studies, the acquired resistance obtained in our study is minor and it is possible that a more pronounced acquired resistance would be obtained by increasing the doxorubicin exposure time to 12 months. Han *et al.* [78] also investigated the morphology between the parental and resistant cell lines and reported that the resistant cells were larger than the parental cells, with an irregular shape and an enlarged nucleus and/or multinucleation in agreement with the indications in our study. In addition, they tested cross-resistance and found that the SOSP-9607/CDDP cells were resistant to adriamycin (doxorubicin). McDermott *et al.* [73] studied cross-resistance with chemotherapy and found that the RR-22Rv1 cell line (IR-resistant) was more sensitive to Docetaxel than WT-22Rv1. Our study did not test cross-resistance between chemotherapy and IR, but the changes detected from RNA seq indicate a more resistant cell line was generated in MG-63/DR. Du *et al.* [79] generated an adriamycin resistant MG-63 cell line, MG-63/ADR, in a very similar manner. Other studies have used analogous methods for testing chemoresistance and successfully obtained chemoresistant cell lines using similar methods to our study [80-82].

The low sensitivity of OSA and MG-63 towards IR and chemotherapy may be due to their lack of functional p53 protein [25, 83] (Figure 23). P53 has been proven to have a major role in IR response and also many of the other important pathways that contribute to cancer like the DNA damage response, DNA repair and induction of apoptosis [83]. Mutations in the p53 protein are common in osteosarcomas; Isfort *et al.* [84] analyzed the modifications of various oncogenes and tumor suppressor genes in human osteosarcoma cell lines and found that p53 was altered in five out of the six osteosarcoma cell lines tested. Ye *et al.* [85] transfected two osteosarcoma cell lines, U-2OSR2 and KHOSR2, with a wildtype p53 protein and found that it causes increased chemosensitivity in the cells. They also claim that p53 is mutated in 22% of osteosarcomas. Both Chen *et al.* [86] and Lorenz *et al.* [87] showed that there is a higher frequency of p53 aberrations found in osteosarcoma, present in both patient samples and cell

lines. Taking this into consideration, another sarcoma cell line, MES-SA, was used in comparison since it contains a functional p53 protein. It has been shown in past experiments that MES-SA is sensitive to doxorubicin and IR [88, 89], which concurs with our results (Figure 20, 22). Our results also indicate MES-SA to be more sensitive to both IR and doxorubicin, compared to MG-63 and OSA (Figure 20, 22). The difference in IR and doxorubicin sensitivity between MES-SA and OSA and MG-63 parental cell lines may be related to p53 expression.

Past studies have shown that treatment-resistant variants of human cancers often express different genes than the non-resistant variants [90, 91]. RNA seq was accomplished in order to determine any differences in gene expression between the acquired IR and doxorubicin resistant cell lines generated in this project. Generation of an IR resistant line was successful in the case of MG-63/IR. The IR response of OSA/IR was, however, similar to OSA/PAR. However, we decided to sequence OSA/IR in addition since it did display a significant difference in drug uptake in comparison to OSA/PAR (Figure 33). Generation of an acquired doxorubicin resistant line was successful in MG-63 (MG-63/DR). Thus, the genomes of OSA/IR, MG-63/IR and MG-63/DR were sequenced with RNA seq as well as the parental cell lines OSA/PAR and MG-63/PAR. OSA/IR differentially expressed 56 genes in comparison to OSA/PAR (Table 3). MG-63/IR and MG-63/DR differentially expressed 152 and 156, respectively, in comparison to MG-63/PAR (Table 3). The low count of differentially expressed genes for OSA/IR is in agreement with the minor increase in IR resistance and may reflect high capacity of DNA repair in this cell line, or other resistance mechanisms such as high levels of ROS scavengers.

The RNA seq data indicates alterations in four different features/pathways in OSA/IR (Figure 34); (i) phagocytosis/internalization, (ii) STAT3 signaling, (iii) TGFB1 regulated pathways, and (iv) SMAD3 regulated pathways. The RNA seq results indicated a decrease in phagocytosis/internalization in OSA/IR and many genes apart of the STAT3 pathway were found to be differentially expressed in OSA/IR (Figure 34). It is known that the STAT3 pathway has a role in mediating radiation therapy resistance, as shown by Wu *et al.* [92] where they found that inhibiting STAT3, which is activated in pancreatic CSCs, decreased pancreatic tumor growth and sensitized the cells to radiotherapy. STAT3 also regulates transforming growth factor-beta 1 (TGFB1), which was also shown to be differentially expressed in OSA/IR (Figure 34). TGFB1 has been found to promote tumorigenesis, metastasis and chemoresistance in several cancers [93, 94]. TGFB1 is an upstream regulator of the SMAD pathway, specifically acting on SMAD3 during growth and regulation [95]. SMAD3 was also found to be differentially expressed in OSA/IR (Figure 34), confirming that the SMAD pathway is compromised when cancer cells are repeatedly exposed to IR. These results prove that the STAT3 and SMAD3 pathways are altered in OSA/IR and are connected by the differing expression of TGFB1. Despite OSA/IR showing a moderate increase in IR resistance, the repeated treatments of IR led to changes in the gene expression of OSA/IR, causing it to develop a more aggressive phenotype.

The RNA seq data indicates alterations in six different pathways in MG-63/IR (Figure 35); (i) metalloprotease pathway, (ii) EMT pathway, (iii) TGFB1 regulated pathways, (iv) STAT 3 signaling, (v) SMAD3 regulated pathways and (vi) increased proliferation. The data showed an inhibition of the metalloproteases pathway, regulated by TGFB1, which contributes to increased invasion, metastasis, growth and survival in cancer cells [96]. The epithelial-mesenchymal transition pathway (EMT pathway) was also differentially expressed in MG-63/IR (Figure 35), which involves the degradation of the extracellular matrix, by matrix metalloproteases, that leads to cancer cell invasion and metastasis [97,

98]. Like OSA/IR, the expression of TGFB1 also differed in MG-63/IR (Figure 35), confirming that prolonged IR exposure affects the expression of TGFB1 in osteosarcomas. Like OSA/IR, STAT3 and SMAD3 were also differentially expressed in MG-63/IR (Figure 35), proving once again that the STAT and SMAD pathways are affected by repeated IR exposure in osteosarcomas. The positive z-score of 2.2 indicates that SMAD3 is upregulated in MG-63/IR cells (Figure 35), but the data could not prove if this was the case in OSA/IR as well due to the absence of the z-score. Genes linked to cell proliferation were also upregulated in MG-63/IR, induced by SMAD3 and TGFB1 (Figure 35). Overall, these results prove that repeated IR exposure leads to a more aggressive phenotype in osteosarcomas, linked to increased metastasis, proliferation and survival.

The RNA seq data indicates alternations in six different pathways in MG-63/DR (Figure 36); (i) metalloprotease pathway, (ii) TGFB1 regulated pathways, (iii) hypoxia pathways, (iv) vascular endothelial growth factor regulated pathways, (v) epigenesis and (vi) increased invasion. In contrast to MG-63/IR, the data reports an activation of the metalloproteases pathway in MG-63/DR which contributes to increased metastasis, growth and survival (Figure 36). Similar to both OSA/IR and MG-63/IR, TGFB1 was differentially expressed in MG-63/DR (Figure 36), signifying that TGFB1 could play a role in osteosarcoma IR and doxorubicin resistance. Hypoxia-inducible factor 1 alpha (HIF1A) was also found to be differentially expressed in MG-63/DR (Figure 36), in agreement with Roncuzzi *et al.* [99]. HIF1A improves cells' survival in hypoxic environments, a feature necessary in tumor cells [100]. HIF1A activates the transcription of vascular endothelial growth factor A (VEGFA) which was found to be upregulated in MG-63/DR (Figure 36). VEGFA contributes to tumor angiogenesis, vascularization and growth in cancers [101]. Chromobox protein homolog 5 (CBX5) was found to be downregulated in MG-63/DR (Figure 36). CBX5 is involved in epigenetic suppression where it binds to histone tails in the heterochromatin [102]. It also negatively regulates invasion, which was another pathway upregulated in MG-63/DR (Figure 36). The deregulation of CBX5 and upregulation of genes contributing to invasion indicate that MG-63/DR is more invasive and aggressive than its parental cell line. It is also important to note that the ABCB1 gene, encoding multidrug resistance protein 1, also known as P-glycoprotein 1 (P-gp), was differentially expressed in MG-63/DR (Figure 36). P-gp is a drug efflux pump that is linked to decreased drug uptake in MDR cancer cells [103]. P-gp is activated by VEGFA which is upregulated in MG-63/DR, contributing to increased MDR in MG-63/DR.

4.2 PCI of treatment resistant osteosarcoma

Since our results revealed that OSA and MG-63 cells were intrinsically resistant towards IR and doxorubicin, and MES-SA cells were not, their responses towards PDT and PCI-rGel were evaluated. It was found that both OSA/PAR and MG-63/PAR were less sensitive to PDT as compared to MES-SA (Figure 24). MES-SA showed a strong PCI effect with rGel, in agreement with other studies [35, 70] while a minor effect of PCI-rGel was observed in both OSA/PAR and MG-63/PAR. PCI-rGel has, to our knowledge, not previously been tested on OSA or MG-63 parental cells. However, other studies have tested PCI-rGel in other sarcoma cell lines. Dietze *et al.* [104] tested two human synovial sarcoma cell lines, SW 982 and CME-1, using $TPPS_{2a}$ and PCI-rGel. In both cell lines, they found that the sensitivity towards PCI-gelonin increased four-fold and that gelonin monotherapy had no significant effect on cell

survival or protein synthesis. The MG-63/PAR and OSA/PAR cell lines used here seem less sensitive to PCI-rGel as compared to this report. Another study by Berg *et al.* [105] evaluated PCI-gelonin in 16 cell lines and found that the photosensitizers $TPPS_{2a}$ and $AlPcS_{2a}$ increased the toxicity of gelonin significantly when combined with PCI. However, in the human osteosarcoma cell line OHS, increased toxicity only occurred in the presence of ammonium chloride (NH_4Cl) or chloroquine, also interfering with the endo/lysosomal biology. The present data indicate OSA/PAR and MG-63/PAR not only to be resistant to PCI-rGel, but also to PDT. It is therefore likely that the PCI-rGel resistance is related to resistance towards the treatment with photosensitizer and light. The mechanisms for PDT/PCI-rGel-resistance were not addressed in detail here, but may be related to e.g. decreased uptake of photosensitizer, decreased generation of ROS upon light exposure (increased ROS scavengers), decreased level of membrane associated cholesterol or decreased death signaling pathways [35, 40, 106, 107].

The sensitivity of PCI-rGel was further evaluated in the resistant cell lines, OSA/IR, MG-63/IR and MG-63/DR, to determine if repeated IR or doxorubicin exposure did influence the sensitivity towards PCI-rGel. All cell lines tested showed a minor PCI effect with rGel (Figures 25-26), and no difference in PCI-rGel sensitivity was found between parental and resistant cell lines (Figure 25-26). Since OSA/IR was shown to accumulate more fluorescent rGel than OSA/PAR (Figure 33), increased sensitivity towards PCI-rGel could be expected. A study by Selbo *et al.* [70] showed that PCI-gelonin toxicity was greater in the MDR MES-SA/Dx5 cells (resistant to doxorubicin) than in the parental MES-SA cells. The MES-SA/Dx5 cells were also generated by prolonged exposure to doxorubicin and the results in increased PCI-rGel sensitivity are therefore in contrast to the doxorubicin resistant MG-63 cell line generated here.

Since the PCI-rGel effect was moderate on all cell lines except MES-SA, a more cancer specific and efficient utilization of the PCI technology was executed by using a targeted toxin in combination with PCI. Many osteosarcoma cell lines have increased expression of EGFR [108], so the targeted toxin EGF/rGel/rGel was tested in combination with PCI on all cell lines. EGF/rGel/rGel consists of the EGF protein genetically fused to two molecules of recombinant gelonin. EGF/rGel/rGel is transported into the cell via receptor-mediated endocytosis [109]. Refer to Appendix C for a detailed explanation of this process. The two molecules of rGel exert their cytotoxic effects when the cell is illuminated and they are released into the cytosol where they bind to the ribosomes and inhibit protein synthesis. Indeed, PCI-EGF/rGel/rGel was more effective than PCI-rGel in parental and resistant OSA and MG-63 cell lines (Figure 28, 30-31). PCI-EGFrGelrGel on MES-SA cells was, however, not effective, in agreement with the western blots showing low EGFR expression (Figure 23, 29). This is in agreement with Yip *et al.* [110] who evaluated the effect of PCI of cetuximab-saporin and found only minor effects in MES-SA cells. The present study is the first to test EGF/rGel/rGel on cancer cell lines. PCI of EGF/rGel/rGel is here indicated as a highly EGFR selective and effective approach for the treatment of EGFR positive osteosarcomas and will be recognized by the PCI research group as a very promising drug for future experimentation.

Our results have shown that MES-SA responds much differently to all treatments used, compared to OSA and MG-63 cells. The MES-SA was shown to have the highest PCI efficacy for PCI-rGel (Figure 27) and the lowest efficacy for PCI-EGF/rGel/rGel (Figure 32) compared to all other cell lines. There were no significant differences of rGel efficacy in MES-SA compared to OSA/PAR, MG-63/PAR or any of the resistant cell lines (Figure 27). There were also no significant differences of PCI-rGel efficacy between the parental and resistant cells (Figure 27). The efficacy of PCI-EGF/rGel/rGel was also evaluated on all cell lines and the results showed that there were no significant differences in efficacy between the

parental and resistant cell lines (Figure 32). There were, however, significant differences in PCI-EGF/rGel/rGel between MES-SA and OSA/PAR as well as MES-SA and MG-63/IR.

EGFR has been proven as a successful target in many studies and there are several clinically approved EGFR-targeting drugs being used today such as cetuximab and gefitinib [109]. Several other studies have focused on EGFR targeted therapy for resistant cancer. Sette *et al.* [111] successfully tested an EGFR inhibitor (gefitinib) on leiomyosarcoma stem-like cells that were chemoresistant. Their results showed that treatment with gefitinib reversed the chemoresistance and the cells became sensitive to chemotherapy. Song *et al.* [112] found that EGFR is highly expressed in chondrosarcoma and this overexpression of EGFR contributes to cisplatin resistance. They tested an EGFR inhibitor (erlotinib) in combination with cisplatin and the chemoresistance to cisplatin was reversed in the cells and they underwent apoptosis. Pahl *et al.* [113] found that 12 out of 12 osteosarcoma cell lines expressed EGFR on their cell membranes. The OSA cell line was one of the lines tested by Pahl *et al.* [113] and it was one of the top 3 cell lines they tested that contained the highest expression of EGFR, in agreement with our results (Figure 23). They also found that cetuximab promotes cytolysis of chemoresistant osteosarcoma cells by activating natural killer cells. Clearly, EGFR targeted therapy has proven to be very successful in osteosarcoma and this is in agreement with our results. Compared to EGFR-targeted tyrosine kinase inhibitors, such as gefitinib and monoclonal antibodies like cetuximab, EGF/rGel/rGel uses EGFR as a portal to transport gelonin into the cell and cytotoxicity is provided by ribosomal inhibition. Also, EGF/rGel/rGel is dependent on PCI activation in order to avoid lysosomal degradation and is minimally toxic without PCI, which can be localized specifically on the cancerous area, instead of the entire body.

There have been many studies that combine EGFR targeted therapy with PCI. Weyergang *et al.* [36] tested the PCI effect of EGF-saporin on A-431 cells (epidermoid carcinoma) and found a synergistic effect with EGF-saporin combined with PCI that remarkably decreased cell viability in comparison with PDT. Oliveira *et al.* [114] found that combining PCI with an anti-EGFR siRNA molecule caused a 10-fold increased efficiency in silencing the EGFR protein than siRNA monotherapy. The study that is most similar to ours is one of Berstad *et al.* [115] which involved a drug called rGel/EGF in combination with PCI. rGel/EGF is designed with EGF at the N-terminal of the protein and only one molecule of gelonin, compared to EGF/rGel/rGel with EGF at the N-terminal and two molecules of gelonin. However, the mechanism of uptake and cytotoxicity should be similar for these two drugs. The study showed that PCI of rGel/EGF was highly effective against EGFR-expressing cell line A-431 in comparison to PCI-rGel, in concordance with our results. Furthermore, the PCI effect of rGel/EGF on EGFR-negative cell line, MES-SA did not differ from PCI-rGel, also in agreement with our results. To our knowledge, the present thesis represents the first findings on EGFR targeted PCI as a treatment modality for sarcoma, and these results warrant further evaluations in preclinical models to develop this concept towards clinical utilization.

4.3 Future perspectives

Several aspects of the present study should be further evaluated. The RNA seq data should be evaluated with respect to identification of new molecular targets that can be utilized for the development of targeted toxins for PCI-mediated delivery. There were numerous amounts of differentially expressed genes that have been arduously studied in other types of cancers, and these alterations may cause the expression of possible targets in combination with PCI. Even though our results indicate PCI-EGF/rGel/rGel as an effective treatment approach in intrinsic as well as acquired resistant sarcoma, the models of acquired resistance could be improved to include IR and doxorubicin resistant cell lines that are drastically more treatment-resistant. This could be done by using the same procedure used in this study, but increasing the duration exposed and the doses used, or by including other cell lines known to acquire resistance upon exposure. Cross-resistance between IR and doxorubicin should also be tested, i.e. testing the sensitivity of MG-63/IR with other types of chemotherapeutic drugs in addition to doxorubicin and vice versa. More microscopic experiments could be accomplished to determine the uptake and localization of the drugs and see if this differs between resistant and parental cells. Another goal could be to further study the efficacy of PCI on other p53-mutated cancers including osteosarcoma, as this seems to be a phenomenon very related to our study. An idea would be to genetically introduce a functional p53 protein into the osteosarcoma cells and repeating all experiments to see if these cells would be more sensitive to the treatments when harboring an intact p53. Other sarcoma cell lines should also be included and tested with PCI-rGel and PCI-EGF/rGel/rGel to determine the general efficacy of the suggested treatment for this indication. We could also test PCI-EGF/rGel/rGel in animal models to see if it is as successful in vivo. Osteosarcoma-derived cells can then be implanted into the animal to replicate osteosarcoma in a human.

5. Conclusion

The present study has aimed to establish models for treatment resistance in osteosarcoma, a highly aggressive form of cancer typically affecting children and adolescents. IR and doxorubicin resistant osteosarcoma cell lines were established, but the resistance, however, was only moderate. The study has provided a proof-of-principle that osteosarcoma cell lines expressing EGFR can be treated successfully in vitro with PCI-EGF/rGel/rGel, and that the treatment efficacy circumvents both intrinsic as well as acquired mechanisms of resistance. Furthermore, the study is the first to test the targeted toxin EGF/rGel/rGel, which currently is recognized as one of the most promising drugs for future development of PCI of targeted toxins by the PCI research group.

The present study established an important basis for future PCI-based therapy of osteosarcoma. An important limitation is the lack of evidence explaining the role of p53 status in osteosarcoma and how it plays a role in resistance. Thus, further studies are warranted to conclude here. Another limitation is the moderate increase in resistance among the generated resistant cell lines compared to the parental cell lines.

Appendix

A. Recipes for protein analysis

5XRB loading buffer:

- 250 mM Tris pH 6.8
- 10% SDS
- 30% glycerol
- 5 % β-mercaptoethanol
- 0.02% bromophenol blue

Running buffer recipe:

- 100 ml 10x TGS (#161-0772, Bio-Rad)
- 900 ml ddH_2O

1X transfer buffer recipe:

- 200 ml 5X transfer buffer (#10026938, Bio-Rad)
- 200 ml absolute ethanol
- 600 ml ddH_2O

TTBS recipe:

- 100 ml 10x TBS (12.11 g Trizma, 98.66 g NaCl, 1000 ml ddH_2O)
- 10 ml 10% Tween 20
- 890 ml ddH_2O

5% BSA in TTBS recipe:

- 1.25 g BSA powder (#0332-100G, VWR Life Science, Radnor, PA, USA)
- 25 ml TTBS

B. Illumina sequencing overview

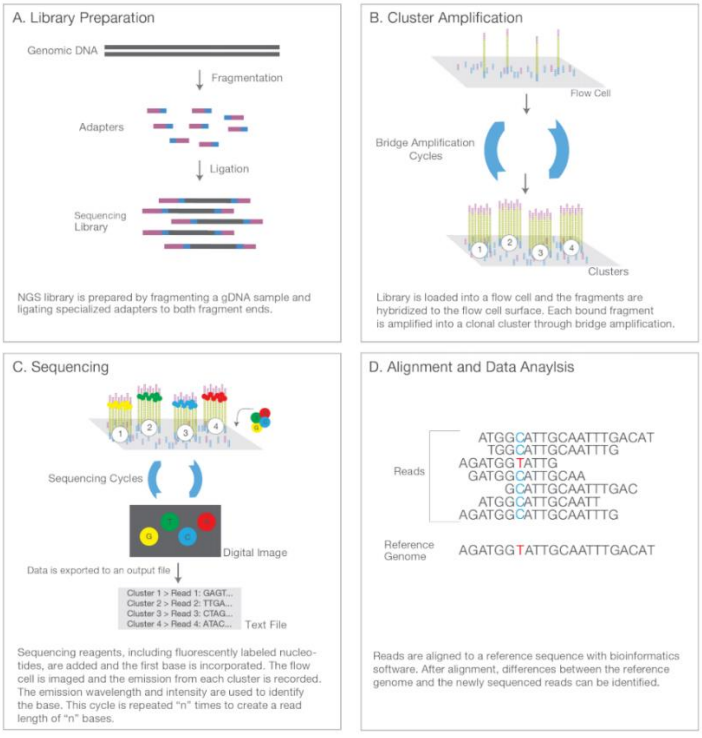

Illumina sequencing chemistry overview. Illumina NGS includes four steps: (A) library preparation, (B) cluster amplification, (C) sequencing and (D) alignment and data analysis.

A. **Library preparation:** The complementary (cDNA) or genomic DNA (gDNA) sample is randomly fragmented and 5' to 3' adaptors are ligated to each fragment. These adaptors act as reference points during amplification, sequencing and analysis. These adaptor-ligated fragments are then amplified with the polymerase chain reaction (PCR).
B. **Cluster amplification:** The library is transferred to a flow cell that is comprised of a sheath of oligonucleotides bound to the surface of the flow cell. These oligonucleotides are complimentary to the adaptors, so the fragments attach directly to the surface of the flow cell. Each fragment is amplified via bridge amplification and clonal clusters of identical fragments are synthesized.
C. **Sequencing:** The four different nucleotides each contain a unique fluorescent label that emits a specific color when incorporated onto the cluster. The Illumina method uses a technology where only one nucleotide can be added at a time. Therefore, the sequence of the fragments is displayed through the emission of the different colors, base by base.
D. **Data analysis:** The sequence reads are aligned to a reference genome using bioinformatics tools. The differences between the sequenced reads and the reference genome are noted and researchers can use this information to come to conclusions.
Retrieved from [66].

C. Receptor mediated endocytosis of EGFrGelrGel

A. Binding of EGFrGelrGel promotes EGFR receptor dimerization, cross phosphorylation and internalization of the EGFrGelrGel-EGFR receptor complex. The complex enters the endocytic pathway with EGFrGelrGel located in the lumen of the endocytic vesicles, while the photosensitizer ($TPCS_{2a}$) sits within the membrane of the vesicles. When visible light illuminates the cell, $TPCS_{2a}$ is activated and ROS is generated. The endocytic vesicles rupture and EGFrGelrGel is released into the cytoplasm and can exert its cytotoxic effects by inhibiting ribosomal function.
B. Without PCI, EGFrGelrGel remains in the endocytic vesicles and is eventually degraded by lysosomes.
Retrieved from [115].

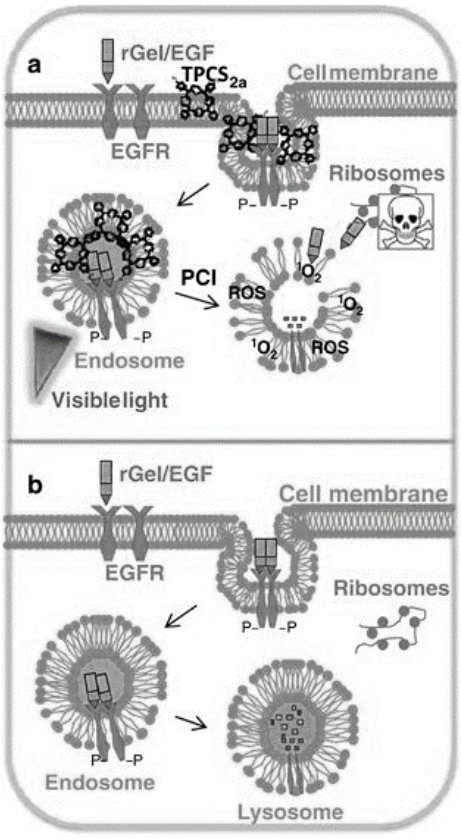

D. PCI efficacy of EGF/rGel/rGel at LD_{50} in all cell lines

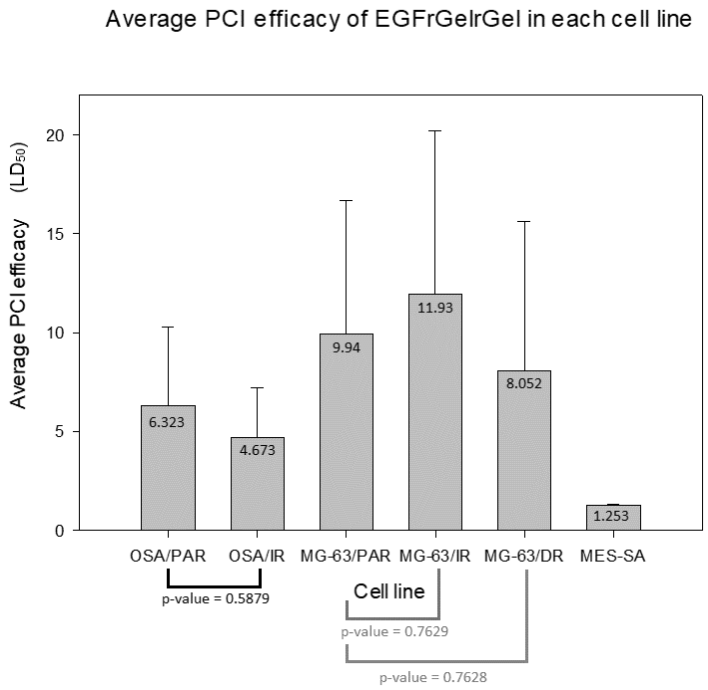

Appendix D: EGF/rGel/rGel-PCI efficacy in **OSA/PAR, OSA/IR, MG-63/PAR, MG-63/IR, MG-63/DR and MES-SA** cell lines. The barrels show the average PCI efficacy calculated at LD_{50} from three independent experiments. Error bars: SD.

References

1. Dodd, R.D., J.K. Mito, and D.G. Kirsch, *Animal models of soft-tissue sarcoma.* Dis Model Mech, 2010. **3**(9-10): p. 557-66.
2. Borden, E.C., et al., *Soft tissue sarcomas of adults: state of the translational science.* Clin Cancer Res, 2003. **9**(6): p. 1941-56.
3. *Cancer incidence, mortality, survival and prevalence in Norway*. Cancer Registry of Norway. Cancer in Norway 2016 2017; Available from: https://www.kreftregisteret.no/globalassets/cancer-in-norway/2016/cin-2106.pdf.
4. Spiguel, A., *Soft tissue sarcomas.* Cancer Treat Res, 2014. **162**: p. 203-23.
5. Moore, D.D. and H.H. Luu, *Osteosarcoma.* Cancer Treat Res, 2014. **162**: p. 65-92.
6. Bernardini, G., et al., *Proteomics of osteosarcoma.* Expert Rev Proteomics, 2014. **11**(3): p. 331-43.
7. *Survival Rates for Osteosarcoma*. 2019; Available from: https://www.cancer.org/cancer/osteosarcoma/detection-diagnosis-staging/survival-rates.html#written_by.
8. Zhou, W., et al., *Advances in targeted therapy for osteosarcoma.* Discov Med, 2014. **17**(96): p. 301-7.
9. Hanahan, D. and R.A. Weinberg, *Hallmarks of cancer: the next generation.* Cell, 2011. **144**(5): p. 646-74.
10. Pan, S.T., et al., *Molecular mechanisms for tumour resistance to chemotherapy.* Clin Exp Pharmacol Physiol, 2016. **43**(8): p. 723-37.
11. *Cancer Cells and Chemotherapy*. 2019; Available from: http://chemocare.com/chemotherapy/what-is-chemotherapy/cancer-cells-chemotherapy.aspx.
12. Botter, S.M., D. Neri, and B. Fuchs, *Recent advances in osteosarcoma.* Curr Opin Pharmacol, 2014. **16**: p. 15-23.
13. Thorn, C.F., et al., *Doxorubicin pathways: pharmacodynamics and adverse effects.* Pharmacogenet Genomics, 2011. **21**(7): p. 440-6.
14. Lal, S., et al., *Pharmacogenetics of target genes across doxorubicin disposition pathway: a review.* Curr Drug Metab, 2010. **11**(1): p. 115-28.
15. Carvalho, C., et al., *Doxorubicin: the good, the bad and the ugly effect.* Curr Med Chem, 2009. **16**(25): p. 3267-85.
16. *DNA topoisomerase II, eukaryotic-type (IPR001154)*. 2019; Available from: http://www.ebi.ac.uk/interpro/entry/IPR001154.
17. Santivasi, W.L. and F. Xia, *Ionizing radiation-induced DNA damage, response, and repair.* Antioxid Redox Signal, 2014. **21**(2): p. 251-9.
18. Berdis, A.J., *Current and emerging strategies to increase the efficacy of ionizing radiation in the treatment of cancer.* Expert Opin Drug Discov, 2014. **9**(2): p. 167-81.
19. Gladstone, M. and T.T. Su, *Radiation responses and resistance.* Int Rev Cell Mol Biol, 2012. **299**: p. 235-53.
20. D'Adamo, D.R., *Appraising the current role of chemotherapy for the treatment of sarcoma.* Semin Oncol, 2011. **38 Suppl 3**: p. S19-29.
21. Rheingold SR, N.A., Meadows AT, *Therapy-Related Secondary Cancers*, in *Holland-Frei Cancer Medicine*, P.R. Kufe DW, Weichselbaum RR, et al., Editor. 2003, BC Decker: Hamilton, ON.
22. McColl, N., et al., *European Code against Cancer 4th Edition: Ionising and non-ionising radiation and cancer.* Cancer Epidemiol, 2015. **39 Suppl 1**: p. S93-100.
23. Kim, B.M., et al., *Therapeutic Implications for Overcoming Radiation Resistance in Cancer Therapy.* Int J Mol Sci, 2015. **16**(11): p. 26880-913.

24. Hein, A.L., M.M. Ouellette, and Y. Yan, *Radiation-induced signaling pathways that promote cancer cell survival (review).* Int J Oncol, 2014. **45**(5): p. 1813-9.
25. Mirzayans, R., et al., *Ionizing radiation-induced responses in human cells with differing TP53 status.* Int J Mol Sci, 2013. **14**(11): p. 22409-35.
26. Shiotani, B. and L. Zou, *ATR signaling at a glance.* Journal of Cell Science, 2009. **122**(3): p. 301-304.
27. Agostinis, P., et al., *Photodynamic therapy of cancer: an update.* CA Cancer J Clin, 2011. **61**(4): p. 250-81.
28. Weishaupt, K.R., C.J. Gomer, and T.J. Dougherty, *Identification of Singlet Oxygen as the Cytotoxic Agent in Photo-inactivation of a Murine Tumor.* Cancer Research, 1976. **36**(7 Part 1): p. 2326-2329.
29. *Photodynamic Therapy*. 2015; Available from: https://www.cancer.org/treatment/treatments-and-side-effects/treatment-types/photodynamic-therapy.html.
30. Kushibiki, T., et al., *Responses of cancer cells induced by photodynamic therapy.* J Healthc Eng, 2013. **4**(1): p. 87-108.
31. Allison, R.R., *Photodynamic therapy: oncologic horizons.* Future Oncol, 2014. **10**(1): p. 123-4.
32. Selbo, P.K., et al., *Photochemical internalisation, a minimally invasive strategy for light-controlled endosomal escape of cancer stem cell-targeting therapeutics.* Photochem Photobiol Sci, 2015. **14**(8): p. 1433-50.
33. Weyergang, A., et al., *Photochemical internalization augments tumor vascular cytotoxicity and specificity of VEGF(121)/rGel fusion toxin.* J Control Release, 2014. **180**: p. 1-9.
34. Berg, K., et al., *Photochemical internalization (PCI)--a novel technology for release of macromolecules from endocytic vesicles.* Oftalmologia, 2003. **56**(1): p. 67-71.
35. Olsen, C.E., et al., *Circumvention of resistance to photodynamic therapy in doxorubicin-resistant sarcoma by photochemical internalization of gelonin.* Free Radic Biol Med, 2013. **65**: p. 1300-1309.
36. Weyergang, A., et al., *Photochemical internalization of tumor-targeted protein toxins.* Lasers Surg Med, 2011. **43**(7): p. 721-33.
37. Berg, K., et al., *Disulfonated tetraphenyl chlorin (TPCS2a), a novel photosensitizer developed for clinical utilization of photochemical internalization.* Photochem Photobiol Sci, 2011. **10**(10): p. 1637-51.
38. Berstad, M.B., A. Weyergang, and K. Berg, *Photochemical internalization (PCI) of HER2-targeted toxins: synergy is dependent on the treatment sequence.* Biochim Biophys Acta, 2012. **1820**(12): p. 1849-58.
39. Berg, K., et al., *Photochemical internalization (PCI): a technology for drug delivery.* Methods Mol Biol, 2010. **635**: p. 133-45.
40. Weyergang, A., et al., *Photochemical activation of drugs for the treatment of therapy-resistant cancers.* Photochem Photobiol Sci, 2015. **14**(8): p. 1465-75.
41. Wang, J.T., et al., *Photophysical and photobiological properties of a sulfonated chlorin photosensitiser TPCS(2a) for photochemical internalisation (PCI).* Photochem Photobiol Sci, 2013. **12**(3): p. 519-26.
42. Gillet, J.P. and M.M. Gottesman, *Mechanisms of multidrug resistance in cancer.* Methods Mol Biol, 2010. **596**: p. 47-76.
43. Kibria, G., H. Hatakeyama, and H. Harashima, *Cancer multidrug resistance: mechanisms involved and strategies for circumvention using a drug delivery system.* Arch Pharm Res, 2014. **37**(1): p. 4-15.
44. Impicciatore, G., et al., *Nutlins and ionizing radiation in cancer therapy.* Curr Pharm Des, 2010. **16**(12): p. 1427-42.
45. Baudino, T.A., *Targeted Cancer Therapy: The Next Generation of Cancer Treatment.* Curr Drug Discov Technol, 2015. **12**(1): p. 3-20.
46. Sevelda, F., et al., *EGFR is not a major driver for osteosarcoma cell growth in vitro but contributes to starvation and chemotherapy resistance.* J Exp Clin Cancer Res, 2015. **34**: p. 134.

47. Rajaram, P., et al., *Epidermal growth factor receptor: Role in human cancer.* Indian J Dent Res, 2017. **28**(6): p. 687-694.
48. Mitsudomi, T. and Y. Yatabe, *Epidermal growth factor receptor in relation to tumor development: EGFR gene and cancer.* Febs j, 2010. **277**(2): p. 301-8.
49. Do, S.I., et al., *The expression of epidermal growth factor receptor and its downstream signaling molecules in osteosarcoma.* Int J Oncol, 2009. **34**(3): p. 797-803.
50. Normanno, N., et al., *Epidermal growth factor receptor (EGFR) signaling in cancer.* Gene, 2006. **366**(1): p. 2-16.
51. Wang, Z., *ErbB Receptors and Cancer.* Methods Mol Biol, 2017. **1652**: p. 3-35.
52. Arteaga, C.L. and J.A. Engelman, *ERBB receptors: from oncogene discovery to basic science to mechanism-based cancer therapeutics.* Cancer Cell, 2014. **25**(3): p. 282-303.
53. Mortus, J.R., Y. Zhang, and D.P. Hughes, *Developmental pathways hijacked by osteosarcoma.* Adv Exp Med Biol, 2014. **804**: p. 93-118.
54. Movva, S., et al., *Multi-platform profiling of over 2000 sarcomas: identification of biomarkers and novel therapeutic targets.* Oncotarget, 2015. **6**(14): p. 12234-47.
55. *SJSA-1 (ATCC® CRL-2098™)*. 2019; Available from: https://www.atcc.org/Products/All/CRL-2098.aspx#characteristics.
56. *MG-63 (ATCC® CRL-1427™)*. 2019; Available from: https://www.atcc.org/Products/All/CRL-1427.aspx#characteristics.
57. *MES-SA (ATCC® CRL-1976™)*. 2019; Available from: https://www.atcc.org/products/all/CRL-1976.aspx#characteristics.
58. *LumiSource - novel light source for 'in vitro' research*. 2019; Available from: http://pcibiotech.no/lumisource-novel-light-source-for-in-vitro-research/.
59. Riss TL, M.R., Niles AL, et al., *Cell Viability Assays*, in *Assay Guided Manual [Internet]*, C.N. Sittamplam GS, Brimacombe K, et al., Editor. 2013, Eli Lilly & Company and the National Center for Advancing Translational Sciences: Bethesda (MD).
60. Franken, N.A., et al., *Clonogenic assay of cells in vitro.* Nat Protoc, 2006. **1**(5): p. 2315-9.
61. Munshi, A., M. Hobbs, and R.E. Meyn, *Clonogenic cell survival assay.* Methods Mol Med, 2005. **110**: p. 21-8.
62. Wang, Z., M. Gerstein, and M. Snyder, *RNA-Seq: a revolutionary tool for transcriptomics.* Nat Rev Genet, 2009. **10**(1): p. 57-63.
63. Yang, I.S. and S. Kim, *Analysis of Whole Transcriptome Sequencing Data: Workflow and Software.* Genomics Inform, 2015. **13**(4): p. 119-25.
64. Nishikura, K., *Functions and regulation of RNA editing by ADAR deaminases.* Annu Rev Biochem, 2010. **79**: p. 321-49.
65. PubChem. *Deoxyuridine-5'-triphosphate*. 2019; Available from: https://pubchem.ncbi.nlm.nih.gov/compound/dUTP.
66. *An introduction to Next-Generation Sequencing Technology*. 2015; Available from: https://www.illumina.com/documents/products/illumina_sequencing_introduction.pdf.
67. Lichtman, J.W. and J.A. Conchello, *Fluorescence microscopy.* Nat Methods, 2005. **2**(12): p. 910-9.
68. Robertson, S. *What is Flow Cytometry?* 2018, August 23; Available from: https://www.news-medical.net/life-sciences/What-is-Flow-Cytometry.aspx.
69. Wong, J.J.W., *Photochemical internalization (PCI) of sunitinib: efficacy and impact on sunitinib resistance*, in *Department of Pharmacy*. 2016, University of Oslo: Oslo.
70. Selbo, P.K., et al., *Photochemical internalization of therapeutic macromolecular agents: a novel strategy to kill multidrug-resistant cancer cells.* J Pharmacol Exp Ther, 2006. **319**(2): p. 604-12.
71. Selbo, P.K., et al., *Photochemical internalization provides time- and space-controlled endolysosomal escape of therapeutic molecules.* J Control Release, 2010. **148**(1): p. 2-12.
72. Ha, K.D., S.M. Bidlingmaier, and B. Liu, *Macropinocytosis Exploitation by Cancers and Cancer Therapeutics.* Front Physiol, 2016. **7**: p. 381.

73. McDermott, N., et al., *Fractionated radiation exposure amplifies the radioresistant nature of prostate cancer cells.* Sci Rep, 2016. **6**: p. 34796.
74. Gray, M., et al., *Development and characterisation of acquired radioresistant breast cancer cell lines.* Radiation Oncology, 2019. **14**(1): p. 64.
75. Wei, Q.C., et al., *Isolation and characterization of radiation-resistant lung cancer D6-R cell line.* Biomed Environ Sci, 2008. **21**(4): p. 339-44.
76. Baskar, R., et al., *Cancer and radiation therapy: current advances and future directions.* Int J Med Sci, 2012. **9**(3): p. 193-9.
77. Berner, K., et al., *Extraskeletal osteosarcoma in Norway, between 1975 and 2009, and a brief review of the literature.* Anticancer Res, 2015. **35**(4): p. 2129-40.
78. Han, T., et al., *Establishment and characterization of a cisplatinresistant human osteosarcoma cell line.* Oncol Rep, 2014. **32**(3): p. 1133-9.
79. Du, M.D., et al., *Adriamycin resistance-associated prohibitin gene inhibits proliferation of human osteosarcoma MG63 cells by interacting with oncogenes and tumor suppressor genes.* Oncol Lett, 2016. **12**(3): p. 1994-2000.
80. Barr, M.P., et al., *Generation and characterisation of cisplatin-resistant non-small cell lung cancer cell lines displaying a stem-like signature.* PLoS One, 2013. **8**(1): p. e54193.
81. Huang, L., et al., *Induction of acquired drug resistance in endothelial cells and its involvement in anticancer therapy.* J Hematol Oncol, 2013. **6**: p. 49.
82. Asada, N., et al., *Establishment and characterization of an acquired cisplatin-resistant subline in a human osteosarcoma cell line.* Anticancer Res, 1998. **18**(3a): p. 1765-8.
83. Cuddihy, A.R. and R.G. Bristow, *The p53 protein family and radiation sensitivity: Yes or no?* Cancer Metastasis Rev, 2004. **23**(3-4): p. 237-57.
84. Isfort, R.J., et al., *Analysis of oncogenes, tumor suppressor genes, autocrine growth-factor production, and differentiation state of human osteosarcoma cell lines.* Mol Carcinog, 1995. **14**(3): p. 170-8.
85. Ye, S., et al., *p53 overexpression increases chemosensitivity in multidrug-resistant osteosarcoma cell lines.* Cancer Chemother Pharmacol, 2016. **77**(2): p. 349-56.
86. Chen, X., et al., *Recurrent somatic structural variations contribute to tumorigenesis in pediatric osteosarcoma.* Cell Rep, 2014. **7**(1): p. 104-12.
87. Lorenz, S., et al., *Unscrambling the genomic chaos of osteosarcoma reveals extensive transcript fusion, recurrent rearrangements and frequent novel TP53 aberrations.* Oncotarget, 2016. **7**(5): p. 5273-88.
88. Harker, W.G., F.R. MacKintosh, and B.I. Sikic, *Development and characterization of a human sarcoma cell line, MES-SA, sensitive to multiple drugs.* Cancer Res, 1983. **43**(10): p. 4943-50.
89. Magda, D., et al., *Redox cycling by motexafin gadolinium enhances cellular response to ionizing radiation by forming reactive oxygen species.* Int J Radiat Oncol Biol Phys, 2001. **51**(4): p. 1025-36.
90. Horbach, L., et al., *Gene expression changes associated with chemotherapy resistance in Ewing sarcoma cells.* Mol Clin Oncol, 2018. **8**(6): p. 719-724.
91. Sherman-Baust, C.A., et al., *Gene expression and pathway analysis of ovarian cancer cells selected for resistance to cisplatin, paclitaxel, or doxorubicin.* J Ovarian Res, 2011. **4**(1): p. 21.
92. Wu, X., et al., *Overcoming chemo/radio-resistance of pancreatic cancer by inhibiting STAT3 signaling.* Oncotarget, 2016. **7**(10): p. 11708-23.
93. Colak, S. and P. Ten Dijke, *Targeting TGF-beta Signaling in Cancer.* Trends Cancer, 2017. **3**(1): p. 56-71.
94. Samanta, D. and P.K. Datta, *Alterations in the Smad pathway in human cancers.* Front Biosci (Landmark Ed), 2012. **17**: p. 1281-93.
95. Wrana, J.L. and L. Attisano, *The Smad pathway.* Cytokine Growth Factor Rev, 2000. **11**(1-2): p. 5-13.

96. Turunen, S.P., O. Tatti-Bugaeva, and K. Lehti, *Membrane-type matrix metalloproteases as diverse effectors of cancer progression.* Biochim Biophys Acta Mol Cell Res, 2017. **1864**(11 Pt A): p. 1974-1988.
97. Kessenbrock, K., C.Y. Wang, and Z. Werb, *Matrix metalloproteinases in stem cell regulation and cancer.* Matrix Biol, 2015. **44-46**: p. 184-90.
98. Hadler-Olsen, E., J.O. Winberg, and L. Uhlin-Hansen, *Matrix metalloproteinases in cancer: their value as diagnostic and prognostic markers and therapeutic targets.* Tumour Biol, 2013. **34**(4): p. 2041-51.
99. Roncuzzi, L., F. Pancotti, and N. Baldini, *Involvement of HIF-1alpha activation in the doxorubicin resistance of human osteosarcoma cells.* Oncol Rep, 2014. **32**(1): p. 389-94.
100. Ajdukovic, J., *HIF-1--a big chapter in the cancer tale.* Exp Oncol, 2016. **38**(1): p. 9-12.
101. Claesson-Welsh, L. and M. Welsh, *VEGFA and tumour angiogenesis.* J Intern Med, 2013. **273**(2): p. 114-27.
102. *UniProtKB - P45973 (CBX5_HUMAN)*. 2019; Available from: https://www.uniprot.org/uniprot/P45973.
103. *UniProtKB - P08183 (MDR1_HUMAN)*. 2019; Available from: https://www.uniprot.org/uniprot/P08183.
104. Dietze, A., et al., *Photochemical internalization enhances the cytotoxic effect of the protein toxin gelonin and transgene expression in sarcoma cells.* Photochem Photobiol, 2003. **78**(3): p. 283-9.
105. Berg, K., et al., *Photochemical internalization: a novel technology for delivery of macromolecules into cytosol.* Cancer Res, 1999. **59**(6): p. 1180-3.
106. Olsen, C.E., et al., *Development of resistance to photodynamic therapy (PDT) in human breast cancer cells is photosensitizer-dependent: Possible mechanisms and approaches for overcoming PDT-resistance.* Biochem Pharmacol, 2017. **144**: p. 63-77.
107. Weyergang, A., et al., *Light-enhanced VEGF121/rGel: A tumor targeted modality with vascular and immune-mediated efficacy.* J Control Release, 2018. **288**: p. 161-172.
108. Chen, H., et al., *Targeting protein kinases to reverse multidrug resistance in sarcoma.* Cancer Treat Rev, 2016. **43**: p. 8-18.
109. Tomas, A., C.E. Futter, and E.R. Eden, *EGF receptor trafficking: consequences for signaling and cancer.* Trends Cell Biol, 2014. **24**(1): p. 26-34.
110. Yip, W.L., et al., *Targeted delivery and enhanced cytotoxicity of cetuximab-saporin by photochemical internalization in EGFR-positive cancer cells.* Mol Pharm, 2007. **4**(2): p. 241-51.
111. Sette, G., et al., *EGFR inhibition abrogates leiomyosarcoma cell chemoresistance through inactivation of survival pathways and impairment of CSC potential.* PLoS One, 2012. **7**(10): p. e46891.
112. Song, Y.D., et al., *Inhibition of EGFR-induced glucose metabolism sensitizes chondrosarcoma cells to cisplatin.* Tumour Biol, 2014. **35**(7): p. 7017-24.
113. Pahl, J.H.W., et al., *Anti-EGFR Antibody Cetuximab Enhances the Cytolytic Activity of Natural Killer Cells toward Osteosarcoma.* Clinical Cancer Research, 2012. **18**(2): p. 432-441.
114. Oliveira, S., et al., *Photochemical internalization enhances silencing of epidermal growth factor receptor through improved endosomal escape of siRNA.* Biochim Biophys Acta, 2007. **1768**(5): p. 1211-7.
115. Berstad, M.B., et al., *Design of an EGFR-targeting toxin for photochemical delivery: in vitro and in vivo selectivity and efficacy.* Oncogene, 2015. **34**(44): p. 5582-92.